Development of Graphene Oxide Based Membrane as a Pretreatment Step in Thermal Seawater Desalination

BY

Bassel Alaa Awad Taha Abdelkader

A Thesis Presented to the

DEANSHIP OF GRADUATE STUDIES

KING FAHD UNIVERSITY OF PETROLEUM & MINERALS

DHAHRAN, SAUDI ARABIA

In Partial Fulfillment of the

Requirements for the Degree of

MASTER OF SCIENCE

In

Mechanical Engineering

May 2017

KING FAHD UNIVERSITY OF PETROLEUM & MINERALS

DHAHRAN- 31261, SAUDI ARABIA

DEANSHIP OF GRADUATE STUDIES

This thesis, written by **Bassel Alaa Awad Taha Abdelkader** under the direction of his thesis advisor and approved by his thesis committee, has been presented and accepted by the Dean of Graduate Studies, in partial fulfillment of the requirements for the degree of **MASTER OF SCIENCE IN MECHANICAL ENGINEERING.**

Dr. Mohamed A. Antar
(Advisor)

Dr. Zuhair Mattoug Gasem
Department Chairman

Dr. Zafarullah Khan
(Member)

Dr. Salam A. Zummo
Dean of Graduate Studies

Dr. Tahar Laoui
(Member)

8/6/17

Date

© Bassel Alaa Awad Taha Abdelkader

2017

This Dissertation is

Dedicated to

My Beloved Parents

for their prayers and encouragement

ACKNOWLEDGMENTS

I thank Allah for giving me the strength to complete my thesis. I acknowledge and appreciate my advisor Mohammed A. Antar for his valuable guidance, dedication to my work, and for providing the needed support and information in the thesis work. I appreciate his kindness while being my advisor. I would also like to thank, Dr. Zafarullah Khan, Dr. Tahar Laoui for their motivation and valuable time and effort that they dedicated on my research. I wish to express my gratitude to Dr. Ahmed A. Ibrahim for his valuable help and guidance.

Special thanks to the Centre of Nanotechnology, Dr. Zain Yamani and Dr. Abbas Hakim for allowing me to do SEM analysis. Special thanks are forwarded to Geoscience department, Dr. Bassam S. Al Tawabini and Mr. Tajudeen M. Iwalewa for their effort during ionic chromatography.

Deep gratitude is also due to my distinguished friends in KFUPM, Omar Alnoor, Mahmoud Samir, Sherif Rashwan, Ahmed Abd El-Monem, Ahmad El-Rashidi, Mahmed S. Mahrous and Abd El-Rahman Etman.

Acknowledgment is due to King Fahd University of Petroleum & Minerals for supporting this research.

Finally, I must express my very profound gratitude to my family, especially my parents for providing me with unfailing support and continuous encouragement throughout my years of study and through the process of researching and writing this thesis. This accomplishment would not have been possible without them.

Table of Contents

ACKNOWLEDGMENTS v
Table of Contents vi
LIST OF TABLES ix
LIST OF FIGURES x
Nomenclature xii
ABSTRACT xiii
ملخص الرسالة Abstract (Arabic) xiv
CHAPTER 1 INTRODUCTION 1
1.1 Background 1
1.2 Thermal Desalination Process 2
1.2.1 MSF 3
1.2.2 MED 3
1.3 Challenges of Thermal Water Desalination 3
1.4 Hydrated Diameter 5
1.5 Nanofiltration 6
1.6 Graphene Oxide 7
1.7 Thesis Objective 9
1.8 Thesis Outlines 9
CHAPTER 2 LITERATURE REVIEW 11
2.1 Introduction 11
2.2 Performance of NF membranes 12
2.3 Performance of NF membranes in integrated systems 23
2.3.1 UF-NF 23
2.3.2 NF and ion exchange 24
2.3.3 FO-NF 24
2.3.4 NF-SWRO 25
2.3.5 NF-SWRO-MD 26
2.3.6 NF-MSF 26
2.3.7 NF and salt production 30
2.4 Other methods used as pretreatments 31

2.4.1 FO-MSF 31
2.4.2 Salt precipitation and MSF 32
2.5 Modeling of the NF membrane 32
2.5.1 Spiegler–Kedem model 33
2.5.2 Extended Nernst–Planck equation 34
2.5.3 NF transport mechanisms 36
2.6 Membrane fouling 41
2.6.1 Effect of pressure 43
2.6.2 Effect of feed flow rate 43
2.6.3 Effect of temperature 43
2.6.4 Effect of surface roughness 44
2.7 Graphene Oxide 44
2.8 Concluding remarks 45
CHAPTER 3 METHODOLOGY AND EXPERIMENTAL SETUP 48
3.1 Objective and Methodology 48
3.2 Synthesize of the membrane 49
3.2.1 Material 49
3.2.2 Methods of preparation 49
3.2.3 Characterization 53
3.3 Membrane performance 53
3.3.1 Diffusion test 53
3.3.2 Cross flow test 55
CHAPTER 4 RESULTS & DISCUSSION 58
4.1 Optimization 58
4.1.1 Effect of polyelectrolyte 58
4.1.2 GO 60
4.1.3 Graphene oxide and reduced graphene oxide 62
4.1.4 Effect of coating method 65
4.1.5 Deposition method 66
4.1.6 Effect of number of layers 68
4.1.7 Effect of reduction time and the HI solution temperature 69
4.2 Summary 73
CHAPTER 5 CROSS FLOW TEST 75

5.1 Introduction 75
5.2 Tested Membranes 75
5.3 Cross flow test for $MgSO_4$ and $CaSO_4$ 76
5.3.1 Effect of pressure 76
5.3.2 Effect of inlet flow rate 79
5.4 Cross flow test for seawater 81
5.4.1 Effect of pressure 82
5.4.2 Effect of inlet flow rate 84
5.5 Characterization of the 2rGO/PAM-PES membrane surface 86
5.6 Top Brine Temperature (TBT) 88
5.6.1 PhreeQC 88
5.6.2 Saturation index 89
5.6.3 TBT for the testes membrane 90
CHAPTER 6 CONCLUSION AND FUTURE WORK 93
Reference 95
Vitae 113

LIST OF TABLES

Table 1-1:Typical composition of seawater with salinity of 36,000 ppm.[2] 5
Table 1-2: Hydrated daimeter for different ions in seawater. 6
Table 2-1: Performance of commercial NF membranes 22
Table 2-2: Properties of commercial NF membranes 23
Table 2-3: Comparison between different methods used as pretreatment for the thermal desalination process 32
Table 2-4: Performance of graphene oxide membranes 45
Table 3-1: Solutions prepared 50
Table 3-2: Procedure of developing GO/PAM-PES and rGO/PAM-PES 52
Table 4-1: Cross flow test results for GO membranes. 61
Table 4-2: Comparsion between 2GO/PAM-PES and 2rGO/PAM-PES membrane using cross flow test. 64
Table 4-3: Comparison between spin coating, dead end and dip coating using cross flow test 66
Table 4-4: Comparsion between LBL and one layer PAM using cross flow test 68
Table 4-5: Effect of number of layers on rejection and flux using cross flow test. 69
Table 5-1: Composition of Used seawater 82

LIST OF FIGURES

Figure 1-1: Chemical relations of scale deposition in thermal seawater desalination [5]. . 5
Figure 1-2: Transport of ions and molecules in polymer membrane. 8
Figure 1-3: Transport of ions and molecules in GO membrane [20]. 8
Figure 2-1: AFM pictures of the studied NF membranes: (a) NF270; (b) NF200; (c) NF90; (d) ESNA 1-LF2; (e) K-SR2; (f) NF99HF [26]. 14
Figure 2-2: SEM images of an NF270 membrane [30]. 17
Figure 2-3: Effect of feed pressure on ion rejection [33]. 18
Figure 2-4: Effect of feed pressure on water flux [34]. 19
Figure 2-5: Effect of water temperature on ion rejection [33]. 20
Figure 2-6: Schematic diagram of the hybrid FO-NF system for seawater desalination [64]. 25
Figure 2-7: Schematic diagram of the hybrid NF-RO-MD seawater desalination process [71]. 26
Figure 2-8: Schematic diagram of the dihybrid NF/MSF desalination system [46]. 28
Figure 2-9: Schematic diagram of the trihybrid NF/RO/MSF desalination system [49].. 28
Figure 2-10: Effect of NF on sulfate scale potential in a BR-MSF plant [38]. 29
Figure 2-11: Shifting the maximum TBT by NF [38]. 30
Figure 2-12: Schematic flow diagram of the FO-MSF hybrid system [79]. 31
Figure 2-13: Effect of membrane charge density on the contributions of different transport mechanisms [91]. 37
Figure 2-14: Effect of membrane pore size on the contributions of different transport mechanisms [91]. 38
Figure 2-15: Effect of flux on the contributions of different transport mechanisms [91]. 39
Figure 2-16: Effect of the membrane thickness-to-porosity ratio on the contributions of different transport mechanisms [91]. 40
Figure 3-1: Milli-Q integral water purification system for ultrapure water. 50
Figure 3-2: SCS G3 Spin Coater series. 51
Figure 3-3: Procedure of developing GO/PAM-PES and rGO/PAM-PES. 52
Figure 3-4: Diffusion cell [128]. 55
Figure 3-5: Schymatic diagram of the cross flow test 56
Figure 3-6: Cross flow permeation test system. 57
Figure 4-1: Detachments of GO layer from PES a) GO-PES, b)GO/PAM-PES. 59
Figure 4-2: optical micrsocpe image for a) rGO/PAM-PES, b) rGO/PEI-PES. 59
Figure 4-3: chemical structure a) GO/PAM-PES, b) GO/PEI-PES 60
Figure 4-4: Diffusion test results for GO membranes. 61
Figure 4-5: SEM results for GO/PAM membranes a) 3GO/PAM-PES, b) 5GO/PAM-PES, c) 7GO/PAM-PES. 62

Figure 4-6: Graphene oxide and reduced graphene oxide 63
Figure 4-7: Comparsion between 2GO/PAM-PES and 2rGO/PAM-PES membrane using diffusion test. 64
Figure 4-8 : SEM images for a) 2GO/PAM-PES b) 2rGO/PAM-PES 65
Figure 4-9: 2rGO/PAM-PES and 2rGO/2PAM-PES..... 67
Figure 4-10: Comparsion between LBL and one layer PAM using diffusion test 67
Figure 4-11: Effect of number of layers on rejection using diffuion test. 69
Figure 4-12: Effect of reduction time and HI temperature at low concentration using diffusion test a) 25C, b) 80C. 71
Figure 4-13: Effect of reduction time and HI temperature at High concentration using diffusion test a) 25C, b) 80C. 72
Figure 4-14: Effect of reduction time on water contact angle for 2rGO/PAM-PES membrane reduced at HI temperature 80^{o}C. 73
Figure 4-15: Effect of GO concentration, reduction time and the HI solution temperature a) 25^{O}C, b) 80^{O}C on ion rejection. 74
Figure 5-1: Effect of pressure using $MgSo_4$ solution on the a) rejection, b) permeate flux..... 78
Figure 5-2: Effect of pressure using $CaSo_4$ solution on the a) rejection, b) permeate flux..... 79
Figure 5-3: Effect of inlet flow rate using $MgSo_4$ solution on the a) rejection, b) permeate flux. 81
Figure 5-4: Effect of inlet flow rate using $CaSO_4$ solution on the a) rejection, b) permeate flux 81
Figure 5-5: Effect of pressure using seawater on the rejection a) NF270, b) NF-GO, c) 2rGO/PAM-PES. 84
Figure 5-6: Effect of inlet flow rate using seawater on the rejection a) NF270, b) NF-GO, c) 2rGO/PAM-PES. 86
Figure 5-7: SEM results for 2rGO/PAM-PES membranes a) before cross flow test, b) after cross flow test..... 88
Figure 5-8: Effect of pressure on the saturation index a) NF270, b) NF-GO, c) 2rGO/PAM-PES. 92
Figure 5-9: Effect of pressure on top brine temperature 92

Nomenclature

C	Concentration, (mol/m^3)
D	Solute diffusivity (m^2 /s)
F	Faraday's constant
j_w	Solvent permeation flux, (m/s)
j_v	volume flux, (m/s)
j	Solute flux, (mol/m^2-s)
K	Mass transfer coefficient in feed channel, (m/s)
P	permeability (m/s)
R	Universal gas constant, (J /mol-K)
T	Temperature, (K)
X	distance normal to membrane, (m)
Z	Valence of species
ψ	Membrane potential
σ	Reflection coefficient
IAP	Ion Activity Product
K	Equilibrium Constant

Subscripts

i	Solute species
Pore	Inside pore
c	Convective
s	Solute

ABSTRACT

Full Name : Bassel Alaa Awad Taha Abdelkader

Thesis Title : Development of graphene oxide based membrane as a pretreatment step in thermal seawater desalination

Major Field : Mechanical Engineering

Date of Degree : May 2017

One of the main applications of nanofiltration (NF) is the pretreatment stage of seawater desalination. NF has high rejection rates for divalent ions and could eliminate the scaling species that pose serious fouling problems in seawater desalination. This thesis comprehensively examines the synthesis of graphene oxide (GO)/ polyacrylamide (PAM) over polyether sulfone (PES) membranes as a substrate to be used as a pretreatment step for thermal seawater desalination application. GO/PAM-PES membranes were prepared by spin coating technique then reduced to rGO/PAM-PES by subjecting the membrane to hydrogen iodide (HI). The effects of HI temperature and reduction time on the ion rejection and permeate flux were investigated using diffusion test and cross flow test with $MgSO_4$, $CaSO_4$ and seawater. The use of positively charged polyacrylamide (PAM) as an adhesive layer on PES membrane surface had further improved GO and rGO stability on PES membrane surface compared to polyethylenimine (PEI). It is shown that using reduced graphene oxide (rGO) instead of GO increases ion rejection. Increasing pressure increases both the rejection and the permeate flux. Using seawater, rGO/PAM-PES yields the highest rejection for Mg and Ca ions compared with commercial Nanofiltration membrane (NF270).

ملخص الرسالة **Abstract (Arabic)**

الاسم الكامل: باسل علاء عوض طه عبد القادر

عنوان الرسالة: تطوير غشاء أكسيد الجرافين كخطوة المعالجة في تحلية الحرارية لمياه البحر

التخصص: الهندسة الميكانيكية

تاريخ الدرجة العلمية: مايو 2017

واحدة من التطبيقات الرئيسية للفلترة النانوية هي مرحلة المعالجة الأولية لتحلية مياه البحر. الفلترة النانوية لديها معدلات رفض عالية للأيونات ثنائي التكافؤ ويمكن القضاء على الأنواع التحجيم التي تشكل مشاكل في تحلية مياه البحر. هذه الأطروحة تبحث بشكل شامل في تركيب أوكسيد الجرافين / بولي أكريلاميد على أغشية البولي سلفون لاستخدامها كخطوة معالجة أولية لتطبيق تحلية مياه البحر بالطرق الحرارية. تم إعداد أغشية أوكسيد الجرافين / بولي أكريلاميد عن طريق استخدمنا لاسلوب الطبقة بقرب الطبقة بواسطة تقنية النسج بالدوران. ثم خفضت إلى أوكسيد الجرافين المختزل / بولي أكريلاميد عن طريق إخضاع الغشاء إلى يوديد الهيدروجين. تم دراسة تأثير درجات الحرارة و الوقت على معدل انتقال الايونات خلال أغشية أكسيد الجرافين. وقد أدى استخدام بولي أكريلاميد موجبة الشحنة كطبقة لاصقة على سطح غشاء بيس مزيد من تحسين غو والاستقرار رغ على سطح بيس غشاء مقارنة مع البولي إثيلينيمين. وقد تبين أن استخدام انخفاض أكسيد الجرافين المختزل بدلا من أكسيد الجرافين زيادة رفض الأيونات. زيادة الضغط سوف تزيد من كل من رفض وتدفق المياه المعالجة. باستخدام مياه البحر، أوكسيد الجرافين المختزل / بولي أكريلاميد ينتج أعلى رفض لأيونات المغنيسيوم والكالسيوم مقارنة مع غشاء الترشيح النانوي التجاري

CHAPTER 1

INTRODUCTION

1.1 Background

Due to continuous increase in the population, higher living standards and needs, and the expansion of industrial and agricultural activities, there is always a continual and rapid increase in the global demand for clean water. The scarcity of clean water is recognized as a global threat to domestic, agricultural and industrial activities and thus to the existence of society. Urgent measures are needed to avoid this threat. To meet these increased demands for clean water, there has been extensive research on desalination technologies that convert vast, available yet unusable water resources, such as sea and brackish water, to usable forms. The mineral composition of the water is significantly altered and then partially reconstituted to achieve a stable product that can be distributed in pipes. This water differs from natural waters in the sense that its composition is controllable whereas natural waters vary over a very wide range of compositions that is a matter of geology. Per the International Desalination Association, in June 2015, 18,426 desalination plants operate worldwide, producing 86.8 million cubic meters per day, providing water for 300 million people. This number increased from 78.4 million cubic meters in 2013, a 57% increase in just 2 years [1].

One major impediment to the widespread application of seawater desalination technology (thermal-based or membrane-based) is its relatively high production costs. However, many recent advancements in seawater desalination technology have led to appreciable declines in water production costs. One such advancement is the application of nanofiltration (NF) as a pretreatment technique for both thermal and membrane based processes. NF targets the removal of scale-forming agents (mainly sulfates) that adversely affect desalting processes. Sulfate scaling represents an inherent problem to all forms of desalination processes (either thermal or membrane type) as it could lead to their precipitation on the desalination equipment, e.g., tubes or membranes. Accordingly, the production cost and energy consumption of desalination processes increase and, in the worst scenario, it may ruin the plant leaving only one alternative for the plant operator; re-tubing for thermal plants or changing the membranes for membrane type of desalination. Hence, the continued development of NF membranes technology in the view of sulfate rejection from seawater for desalination plants pretreatment is a promising technique that could offer significant benefits by optimum elimination of sulfate ions. This would indeed; help in minimizing sulfate scale formation on equipment involved in desalination processes.

1.2 Thermal Desalination Process

Large scale thermal desalination systems include Multistage Flash (MSF) distillation and Multiple Effect Distillation (MED).

1.2.1 MSF

MSF plants are major contributors to desalting capacity in the middle east. The principle of MSF distillation is that heated water boils rapidly (flash) when the pressure of the vapor is rapidly reduced below the vapor pressure of the liquid at a given temperature. The formed vapor is condensed on surfaces that are in contact with feed water, thus heating it prior to its introduction into the brine heater. This will recover some of the heat of vaporization. Approximately 25 to 50% of the flow is recovered as fresh water in multistage plants. Characteristics of MSF plants include high feed water volume and flow, corrosion and scaling in the plant, and high rates of use of treatment chemicals [2].

1.2.2 MED

Several configurations of MED plants exist including vertical and horizontal tubes. In all cases steam is condensed inside a tube causing evaporation of saline water on its outer surface. Pressure is reduced sequentially in each effect (stage) as the temperature declines, and additional heat is provided in each stage to improve performance. The vapor formed in one effect provides this additional heat to the next effect through its condensation. Scale formation and removal seem to be less problematic in vertical tube vs. horizontal tube units [2]. However, a limit of the top brine temperature is set to no more than 70^{o}C to avoid scaling since seawater is sprayed on tube outer side where ball cleaning (usually used in MSF Plants) cannot be used in MED systems.

1.3 Challenges of Thermal Water Desalination

As shown in Figure 1-1, brine temperature limitations in thermal seawater desalination techniques (e.g., MSF and MED) are dependent on the presence and

concentrations of divalent ions. Scaling occurs under supersaturation conditions and proceeds with nucleation, crystal growth, and precipitation [3]. Temperature, pH, total dissolved salts (TDS), and ion concentrations influence the rate of scale formation. NF can eliminate the scaling species in thermal seawater desalination plants, which helps to increase the top brine temperature (TBT) and hence increase the number of stages in MSF or MED technologies, thereby increasing the gain output ratio (GOR) [2]. At present, scaling is controlled by the addition of anti-scaling chemicals. There are two types of scalants in MSF and MED technologies: alkaline scales caused by calcium carbonate and magnesium hydroxide and non-alkaline scales caused by calcium sulfate [4]. The TBT is generally less than approximately 112°C in MSF and 66°C in MED. Studies have considered using NF membrane softening to remove divalent ions as a possible pretreatment for distillation processes. This step would allow operation under a higher TBT of 170°C for thermal desalination units.

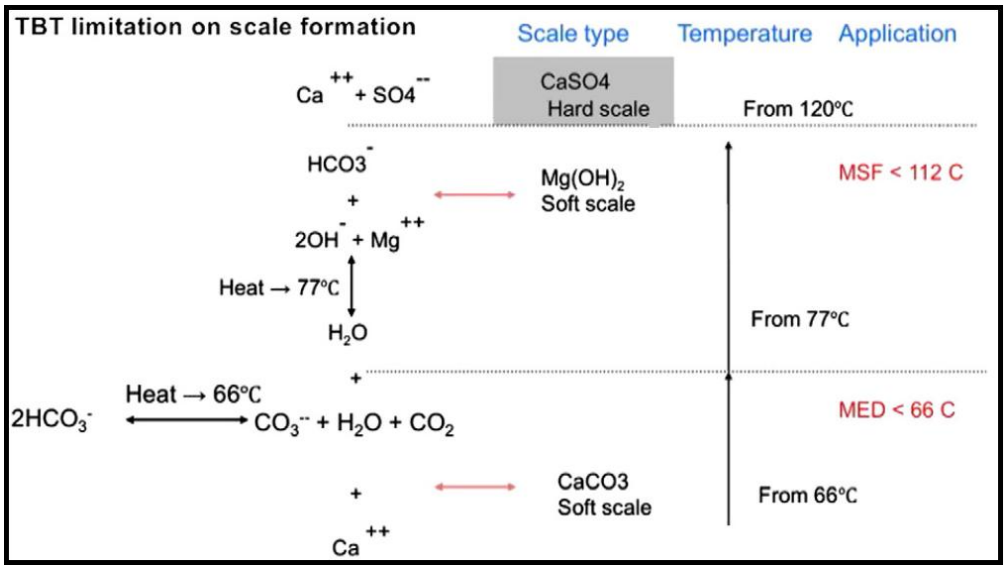

Figure 1-1: Chemical relations of scale deposition in thermal seawater desalination [5].

1.4 Hydrated Diameter

Table 1-1 represents the composition of seawater with salinity of 36,000ppm, monovalent ions represent almost 87%, whereas the divalent ions 13%. To increase TBT, all divalent ions (calcium, sulfate, magnesium) should be removed from seawater. Hydrated diameter for these ions are presented in Table 1-2, where the smallest diameter of divalent ion (sulfate) is 0.758nm, and the biggest diameter of monovalent ion (sodium) is 0.716nm.

Table 1-1:Typical composition of seawater with salinity of 36,000 ppm.[2]

Compound	Composition	Mass Percent	ppm
Chloride	Cl^-	55.03	19810.8
Sodium	Na^+	30.61	11019.6
Sulfate	SO_4^{2-}	7.68	2764.8
Magnesium	Mg^{2+}	3.69	1328.4

Calcium	Ca^{2+}	1.16	417.6
Potassium	K^{+}	1.16	417.6
Carbonic Acid	CO_3^{2-}	0.41	147.6
Bromine	Br^{-}	0.19	68.4
Boric Acid	$H_3BO_3^{-}$	0.07	25.2
Strontium	Sr^{2+}	0.04	14.4
Total			36000

Table 1-2: Hydrated daimeter for different ions in seawater.

Ion	Ca^{2+}	Mg^{2+}	SO_4^{2-}	Na^{+}	K^{+}	Cl^{-}	Reference
Hydrated Diameter [nm]	-	-	-	0.716	0.602	0.582	[6]
	0.824	0.856	-	0.716	0.662	0.664	[7]
	0.824	-	0.758	-	0.662	0.664	[8]
	0.82	0.86	-	0.72	0.66	0.66	[9]
	0.824	0.856	-	0.716	0.662	0.664	[10]

1.5 Nanofiltration

A semi permeable membrane is a selective barrier to some elements while allowing others to pass through its pores. The membrane performance can be described by its selectivity and permeated flux. NF membranes typically achieve divalent ion rejection of 75-99%, whereas monovalent ion rejection is typically in the range of 30-50% [11]. For this reason, NF alone is insufficient in reducing the total dissolved salts (TDS) content to the permissible limit of <500 ppm set by the World Health Organization [12]. To optimize ion rejection while taking energy efficiency into account, NF should be integrated with other major desalination processes, such as pretreatment in seawater reverse osmosis (NF-

SWRO), multistage flash distillation (NF-MSF), multi-effect distillation (NF-MED), and NF-SWRO-$_{reject}$-MSF desalting technologies. Finally, NF has high rejection rate for divalent ions, and thus has the potential of eliminating the scaling species, which poses serious fouling problems in seawater desalination. Therefore, NF has the potential of eliminating the scaling species in thermal seawater desalination plants, which will help in increasing the top brine temperature (TBT), thus, increasing number of stages in MSF or MED (flashing range), which increases the gain output ratio, GOR [2].

1.6 Graphene Oxide

Graphene oxide (GO) is very thin; only one carbon atom thick, thus has low permeation resistance which increases the flux [13]. GO layers also have good mechanical properties[14], chemical and thermal stability [15][16] with unique antifouling and antibacterial properties due to its hydrophilic nature [17]. Thus, it can be designed to be permeable to either water or water vapor and to reject other unwanted molecular species [18]. GO is an oxygen, hydrogen and carbon compound at different proportions (between 2.2 - 2.9 C:O ratio) [19]. It is a single layer of graphite oxide with a thickness of around 1.1 ± 0.2 nm.

Thin film composite membranes that are used today are polymer membrane where the active layer that rejects ions is typically made of polyamide which is non-porous membrane as it does not have well defined channels for water to pass. Thus, ions are rejected by membrane and water molecules first wet the membrane then diffuse through it as shown in Figure 1-2. In contrast, GO coated membrane is basically GO flakes implied over each other. The water passes between these flakes as shown in Figure 1-3. The interlayer spacing

value between GO layers was found to be higher than interlayer spacing of graphite. This could be related to the introduced oxygen functional groups after the oxidation process. Therefore, by using reduced graphene oxide (rGO), the interlayer spacing can be controlled, so if we can reduce these inter layer spacing less than 0.75nm which is sulfate hydrated diameter we will be able to eliminate most of the divalent ions which are the reason for brine temperature limitation in thermal desalination process.

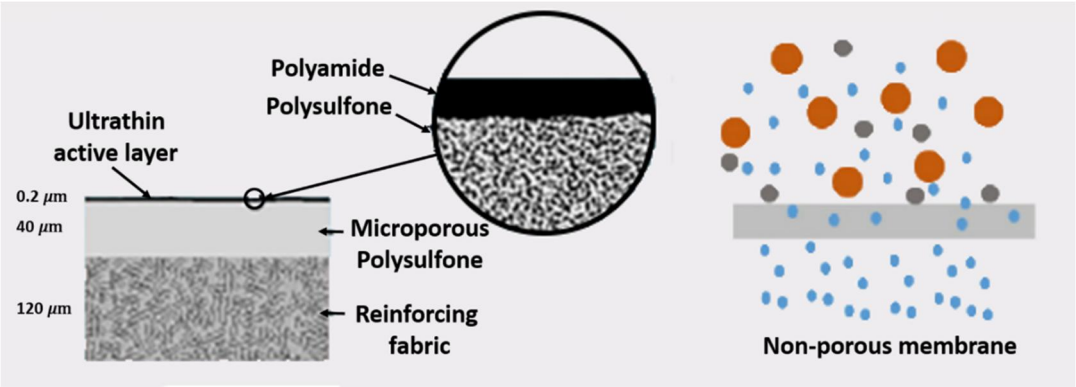

Figure 1-2: Transport of ions and molecules in polymer membrane.

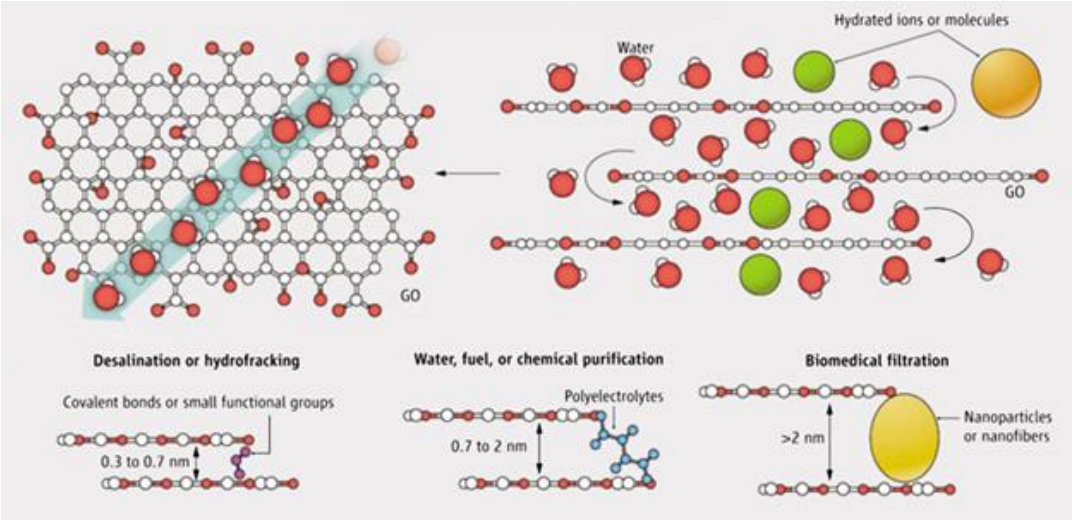

Figure 1-3: Transport of ions and molecules in GO membrane [20].

1.7 Thesis Objective

The objective of this work is to develop a membrane then investigate its performance as a pretreatment step for seawater desalination. The specific objectives are as follows:

- Develop a membrane composed of polyether-sulfone as a support coated with graphene oxide.
- Investigate the performance of developed membrane with MgSO4, CaSO4 solution and seawater.
- Study the effect of the operating pressure on the rejection of divalent ions and permeate flux.
- Compare the performance of the developed membrane with commercial NF membrane.

1.8 Thesis Outlines

- Chapter 1 is an introduction for thermal desalination scaling problems, NF and GO membranes.
- Chapter 2 includes literature review of NF and other methods used as pretreatment for thermal seawater desalination.
- Chapter 3 has a description of the material used and experimental setup.
- Chapter 4 contains the results and the discussion; developing the GO membrane and evaluate the performance of the prepared membrane using diffusion test.

- Chapter 5 presents the results and the discussion; for the performance of the prepared membrane and compare it with commercial NF membrane in a cross flow test.
- Chapter 6 includes the conclusion and recommendations for future work.

CHAPTER 2

LITERATURE REVIEW

2.1 Introduction

With ever-increasing population and rise in their living standards and needs, together with the expansion of industrial and agricultural activities, there is a continual and rapid increase in the demand for clean water throughout the world. The clean water scarcity is being recognized as a global threat to domestic, agricultural and industrial activities and thus to the very existence of human society. Urgent measures are needed to avoid this looming threat. To meet this rise in demand for clean water, the development of technologies for converting the vastly available yet un-useable water resources such as sea and brackish water to useable form by desalination is also on a steep rise.

However, one of the major impediments in the wide spread application of seawater desalination technology (whether thermal-based, or membrane-based), is the relatively high production costs of the current state of the art desalination processes. Recently, many advances have been made in seawater desalination technology, which lead to appreciable decline in water production cost. One advance is the breakthrough application of nanofiltration (NF) as the water pretreatment technique for both thermal and membrane based processes. Nanofiltration targets the removal of scale forming agents (mainly sulfates), which is one of main problems that adversely affect the desalting process.

Several literature reviews [21]–[25] on NF membranes have been published. The use of NF membranes for pretreatment in different desalination processes, membrane fouling, measurements of membrane pore size and roughness, membrane performance, and modeling have been discussed. Hilal et al. [21] discussed the use of NF membranes as a pretreatment step in seawater desalination. The authors reported that NF membranes were able to remove microorganisms, turbidity and a fraction of dissolved salts. However, the NF membranes encounter a major problem of fouling, which resulted in high-energy demand and reduced lifetimes.

Mohammad et al. [22] reported on the fabrication of NF membranes by interfacial polymerization and discussed the transport of ionic species through NF membranes based on the Nernst–Planck equation. The authors also addressed the prevention and mitigation of NF membrane fouling. Bruggen et al. [23] reviewed the drawbacks of NF, discussed the problems and mitigation of membrane fouling, and examined solute transport models and simulations. Luo et al. [24] discussed the effects of pH and salt concentration on NF membrane flux, rejection and fouling and found that the presence of salt and high pH resulted in increased permeability.

2.2 Performance of NF membranes

Llenas et al. [26], [27] experimentally investigated six commercial NF membranes using synthetic and real seawater to identify the optimum membranes and operating conditions for the removal of various ionic species that result in the buildup of scale in SWRO, such as $CaSO_4$, $Mg(OH)_2$, and $CaCO_3$. The authors measured the membrane surface roughness and pore sizes. Membrane pore sizes were obtained based on the rejection of neutral

solutes, i.e., glycerin, glucose, and 2-propanol. Membrane roughness was measured using atomic force microscopy (AFM), as shown in Figure 2-1. Ion chromatography, total carbon analysis and inductively coupled plasma mass spectrometry were used to measure anion (Cl^-, SO_4^{2-}, and Br^-), cation (Na^+, K^+, Ca^{2+}, and Mg^{2+}), inorganic carbon, boron and strontium concentrations. The operating pressures varied between 2 and 20 bars. The results showed that the rejection of the scale-forming divalent ions was high in all tested membranes. Furthermore, the rejection of scale-forming ions was nearly the same for all membranes, whereas the rejection of monovalent ions was lower for real seawater than for synthetic seawater.

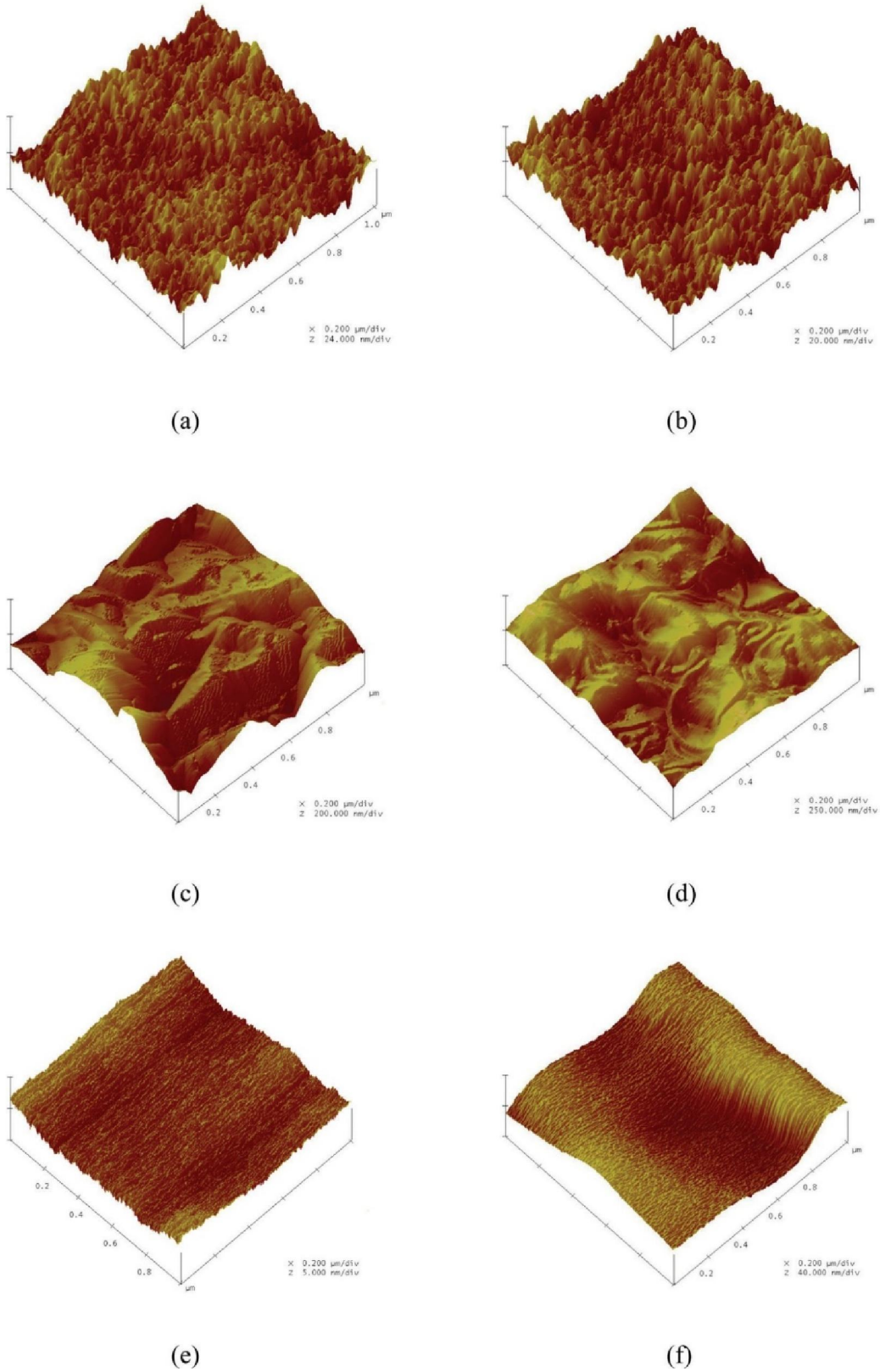

Figure 2-1: AFM pictures of the studied NF membranes: (a) NF270; (b) NF200; (c) NF90; (d) ESNA 1-LF2; (e) K-SR2; (f) NF99HF [26].

Hilal et al. [28] studied NF membrane performance for both seawater and brackish water. They used three commercial NF membranes (NF270, NF90, NF30) to treat salt solution (NaCl) at concentrations of up to 25,000 ppm. They determined the pore size and pore size distribution of the membranes using AFM. The NF90 membrane had the smallest pore size and highest roughness, the NF270 membrane had the largest pore size, and the NF30 membrane had the lowest roughness. The applied pressures varied between 2 and 9 bars in the membrane tests. For all tested membranes, salt rejection and permeation flux increased with increasing pressure and decreasing salt concentration. NF90 had the highest rejection of up to 95%, whereas NF30 had the lowest rejection of 6% at a salinity of 5,000 ppm. At 25,000 ppm salinity, the salt rejection of the NF90 membrane dropped to 41%, whereas that of the NF30 membrane dropped to 3%. The salt rejection of the NF270 membrane was 11-29%. The NF270 membrane showed the highest flux, whereas the NF30 membrane had the lowest flux.

Ryabchikov et al. [29] investigated the performance of three different types of NF membranes (NF90, ERN, and SR90) in seawater desalination using a cross flow arrangement. The operation pressures were 8-18 atm. The concentrations of Cl^-, SO_4^{2-}, Ca^{2+}, and Mg^{2+} and the temperature and pH of the solution were measured. Membrane permeability and salt rejection increased with increasing applied pressure. The total salt rejection was 30-40%, whereas the rejection of the salts influencing water hardness (Ca^{2+} and Mg^{2+}) was 90-95%.

González et al. [30] investigated the rejection of sulfates and chlorides in highly concentrated saline water using NF270 membranes. The thickness of the membrane's effective layer was 0.7±0.27 μm, as determined by scanning electron microscopy (SEM)

(Figure 2-2). Sulfate rejection reached 96%, whereas chloride rejection reached only 11%. The authors reported that sulfate rejection decreased with increasing chloride concentration.

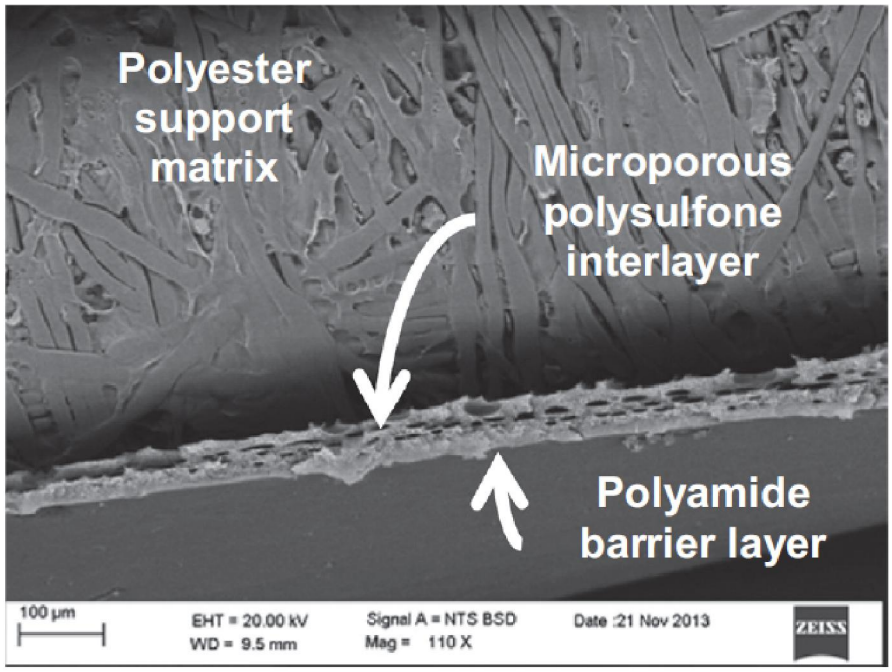

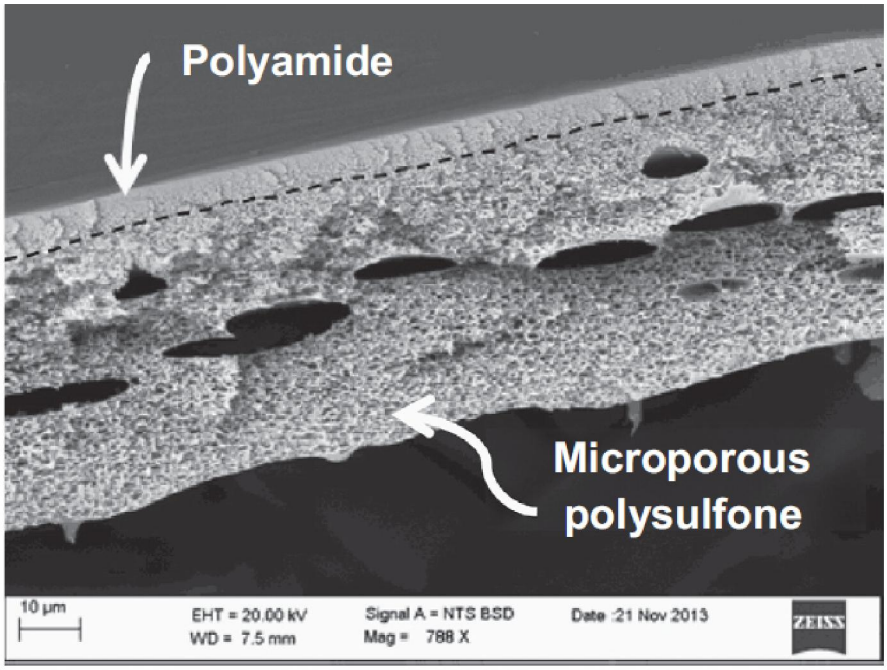

Figure 2-2: SEM images of an NF270 membrane [30].

Izadpanah et al. [31] studied the ability of NE4040-90 NF membranes to remove ions from seawater at operating pressures of 4-10 bars. The rejections of Ca^{2+}, Mg^{2+}, and total hardness were 96-98%, whereas the TDS was 79-89%. These rejection levels increased with increasing pressure. However, the rejection decreased slightly at considerably higher pressures. The salt rejection and permeate flux for the NF membranes increased with increasing pressure, as shown in Figure 2-3 and Figure 2-4. Transport through NF membranes can be explained in terms of diffusion and convection [21]: as the pressure increases, the contribution of convection overcomes diffusion due to high water flux; therefore, the rejection increases. However, at extremely high pressures [32], the rejection decreases with increasing pressure for certain salts. Both the flux and polarization modulus increased with increasing pressure. At extremely high pressures (e.g., 34 bar), an increased polarization modulus overcomes the increased flux effect and thus results in decreased rejection.

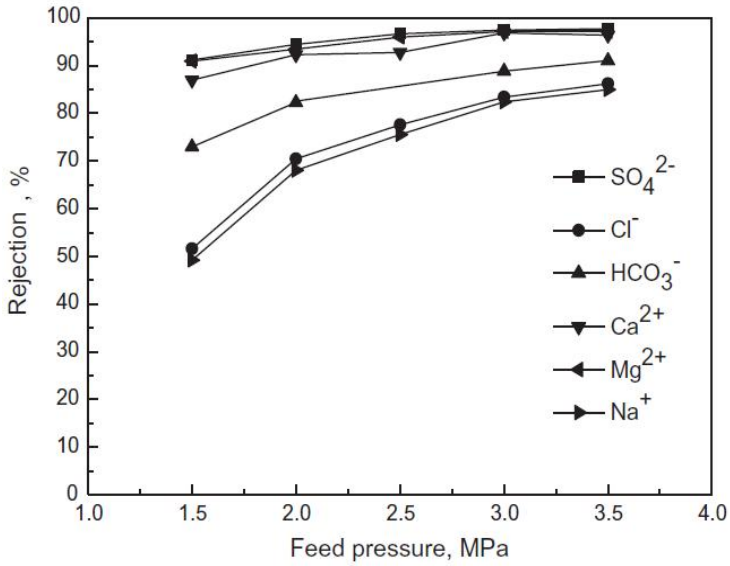

Figure 2-3: Effect of feed pressure on ion rejection [33].

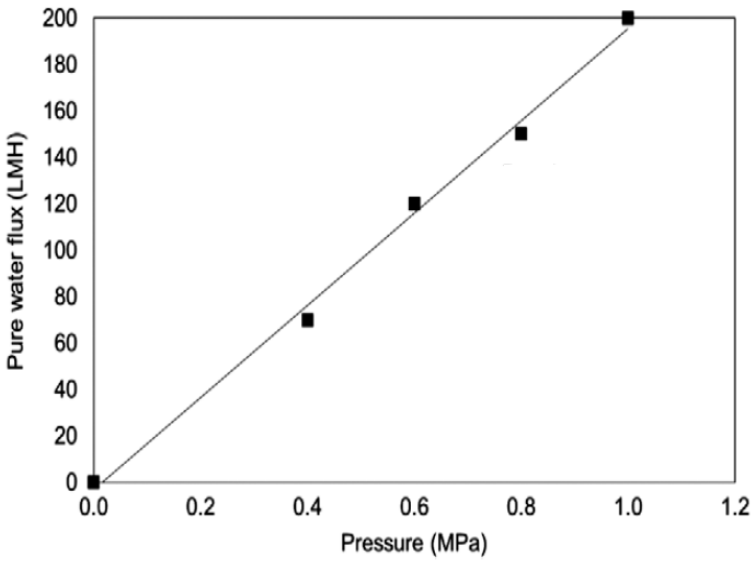

Figure 2-4: Effect of feed pressure on water flux [34].

Kaewsuk et al. [34] studied the effects of ion compositions on NF rejection. The overall ion rejection is high at high cation concentrations. However, the flux decreased as the cation concentrations increased. Similarly, for increasing anion concentrations, the flux decreased (except for HCO_3^- for which the flux increased). Chloride ions had stronger effects on the rejection of magnesium ions than on the rejection of calcium ions. The electrostatic repulsion between sulfate and bicarbonate ions and the NF membrane was strong at low concentrations. Temperature impacted the membrane properties by altering the diffusion of water and ions and the polymer separation layer [33]. At high temperatures, the polymer chain in the separation layer increased and became more effective, resulting in increased membrane pore sizes. The diffusion of water and ions also improved at high temperatures, as shown in Figure 2-5. Thus, the permeate flux increased with increasing temperature. At the same time, the rejection of most ions increased slightly, whereas that for Na and Cl ions slightly decreased. This trend occurred because Na and Cl ions have

relatively smaller sizes than other ions, which enables them to easily penetrate the NF membrane.

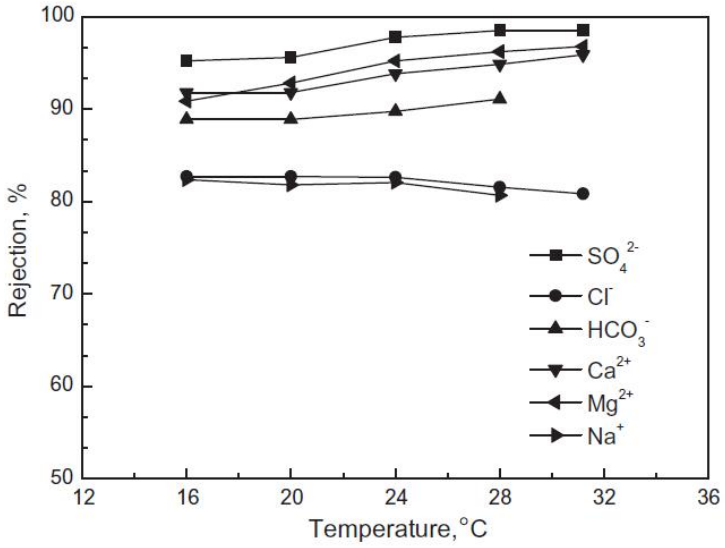

Figure 2-5: Effect of water temperature on ion rejection [33].

Many studies have investigated the performance of dual-stage NF-NF membranes [32], [33], [35]–[37]. Liu et al. [33] examined the performance of a dual-stage NF system, in which the first stage was operated at 35 bar and the second stage was operated at 20 bar. The TDS, ion rejection and permeate flux increased with increasing pressure. Temperature and feed flow rate had weaker effects than pressure. Scaling was likely in the first stage, whereas the scaling index was lower in the second stage because the majority of the scaling ions were removed in the first stage. Harrison et al. [32] investigated the performance of dual-stage NF membranes for seawater desalination. Three types of membranes (NF90, NE-90, and TS-80) were used to investigate water flux, ion rejection, and fouling. The operating pressure varied from 10 to 40 bar. The results showed that dual-stage NF membranes desalinated the seawater. Vuong et al. [37] studied a two-stage NF system for seawater desalination. The first-stage permeate served as the feed for the second stage. The

operating pressures in the first and second stages were 36 and 20 bar, respectively. The rejection of divalent ions was greater than that of monovalent ions.

A portion of the data available for NF membranes is presented shown in Table 2-1. The rejection percentages of the NF membranes were highly dependent on the operating conditions, ion compositions and membrane characteristics (Table 2-1 and

Table 2-2).

Table 2-1: Performance of commercial NF membranes

Description			Pressure (bar)	Permeate flow (L/m^2hr)	Rejection (%)										Reference
					Ca^{2+}	HCO^-	Mg^{2+}	SO^{2-}	Na^+	K^+	CO^{2-}	Sr^{2+}	Cl^-	Total hardness	TDS	
Seawater	NF270		to 20 bar	15-120	37-63	37-60	65-82	97-98	10-22	18-28		48-74	17-27			[26]
	NF200			15-65	32-63	37-68	62-85	98-99	8-25	4-22		44-79	4-22			
	NF90			1-15	95-98	55-88	94-99	95-98	37-70	22-47		94-99	60-88			
	NF99HF			15-115	43-72	22-72	69-86	99	8-20	0-18		58-80	25-42			
	ESNA 1-LF2			25-140	25-40	15-38	38-48	65-75	38-42	15-25	-	23-40	17-23	-	-	
	K-SR2			30-130	45-62	15-42	72-82	98	3-10	8-12		60-78	10-15			
Real seawater	NF270		From 2 to 20 bar	20-120	43-70	35-58	65-85	95-98	5-30	12-28			5-15			[27]
	NF200			15-80	38-70	32-67	67-90	98-99.5	5-38	10-28			10-25			
	NF90 NF99HF			10-25	83-95	65-87	87-95	90-96	25-60	18-53			30-65			
				18-120	35-68	28-58	63-86	95-98	0-15	5-20			8-25			
	ESNA 1-LF2			50-280	15-17	10-38	22-23	47-67	8-12	5-15	-	-	5-12	-	-	
	K-SR2			30-190	38-60	22-40	55-75	97-98	5-8	4-10			0-12			
solution up to 25000 ppm	NF90	c=5000 ppm	to 10 bar	2-40	-	-	-	-	-	-	-	-	-	-	40-95	[28]
		c=10,000		2-25											27-75	
		c=15,000		0.5-8											10-70	
		c=20,000		0.5-4.2											7-52	
		c=25,000		0.3-3											2-40	
	NF270	c=5000 ppm		20-110											11-29	
		c=10,000		15-90											6-21	
		c=15,000		15-78											5-16	
		c=20,000		15-75											3-14	
		c=25,000		10-60											3-11	
	NF30	c=5000 ppm		5-23											2-6	
		c=10,000		4-21											0.5-5	
		c=15,000		3.5-19											0.5-4.2	
		c=20,000		3-17											0-3.7	
		c=25,000		2.5-15											0-3	
$CaCl_2$ 500 mg/L $MgSO_4$ 2000 mg/L NaCl 2000 mg/L	NF90-4040		From 8 to 18 bar	29.05 38.38	82.5-84.9	-	94.8-96	99.6-99.8	-	-	-	-	20-29	-	-	[29]
	SR90-4040			60.70 51.88	64-71		87.2-89.8	97.7-99.1	17-25				25-29			
	ERN KP-100-1016			64.29	94.2-96.8		97.8-98.5	99-99.3	-				45-59			
Ca=254 mg/L Mg =345 mg/L	NE 4040-90		4	-	97.0588	-	96.3333	-	-	-	-	-	-	96.5957	82.3541	[31]
			6		98.2353		98.3333							98.2979	89.3964	
			8		97.6471		98							97.8723	89.2555	
			9		97.0833		97.9798							97.6871	82.1128	
			10		97.9167		97.1717							97.415	82.2359	
IMS design program	ESNA1-LF2	R=60%	32.8 bar	-	70.5	62.5	82.4	87.7	29	3.3	91.7	76	33.6	-	38	[38]
UF-NF	ESNA3 4040		20.3 bar		34.71883		65.48263	98.96104	17.17797				16.61161	60.44234	24.46682	[39]
Real seawater	NF90-2540		30 bar	19	97.5	54.4	98.8	98.8	15.4	17.4			21.9		19.5	[40]
	NF270-2540			65.8	95.5	76	96.9	99.2	50	48.9			56.3		51.7	
ESNA3	R=Q /Qf	10	From 7 to 20 bar	From 14.2 to 44.3	20	-	38	93	-	-	75	-	-	42	-	[41]
		15			25		45	93			76			41.5		
		20			26		50	94			77			41		
		20			30		52	95			77			40.5		
		30			34		55	96			78			40		
		35			35		57	97			79			40		
4 to 8 NF elements	SR90 400		From 2 to 14 bar	-	23	86	76	98	10	14	-	-	4	-	-	[42]
5 NF modules			18	-	80.9	63.3	88	93.3	26.7	-	-	-	26.7	87	37.3	[43]–[49]
			22		89.6	76.6	94	97.8	46.3				46.3	93.3	54.1	
			31		89.2	81.3	91.1	92.8	57.7				57.7	90.8	62.8	

Table 2-2: Properties of commercial NF membranes

	Membrane name	Manufacturer	Membrane type	Roughness (nm)	Pore size (nm)	Maximum operating temperature (°C)	Maximum operating pressure (bar)	Maximum feed flow (m^3/h)	Reference
1	NF90-2540	Dow Chemical Company	Polyamide Thin-film Composite	103.3	0.34	45	41	1.4	[26], [50]
2	NF270-2540			5.35	0.5			1.4	[26], [50]
3	NF200			7.39	0.46			-	[26], [50]
4	SR90			-	-	45	41.6	17	[50]
5	K-SR2	Koch Membrane Systems	-	0.76	0.69	-	-	-	[26], [51]
6	ESNA1-LF2	Hydranautics NITTO DENKO Company	Composite polyamide	49.07	0.49	45	41.6	17	[38], [52]
7	ESNA3 4040			-	1	45	40	53.5	[41], [52]
8	NF99HF	Alfa Laval	Polyamide Thin-film Composite	12.29	0.46	50	55	-	[26], [53]
9	NF30	MICRODYN-NADIR Gmbh	Polyethersulfone	1.45	0.61	-	-	-	[28]
10	NE4040-90	CSM Company	Polyamide	-	-	45	41	4.09	[31], [54]

2.3 Performance of NF membranes in integrated systems

2.3.1 UF-NF

Song et al. [39] investigated the performance of NF membranes in seawater desalination pretreatment by operating an integrated membrane system (UF-NF) for 500 hours. There were two cleaning periods (after 280 h and 440 h). The operating pressure was 20.3 bar and increased to 20.5 bar in the second period (after the first cleaning). The pressure increased to 20.6 bar in the third period (after the second cleaning). The increased operating pressure indicated that fouling occurred. Membrane fouling is difficult to chemically clean. The salt rejection and permeate flux decreased with time before the chemical cleaning and decreased more sharply after the chemical cleaning. Su et al. [55] studied the performance

of a UF-dual-stage, NF-integrated system. The UF filtrate turbidity was nearly zero. For the dual-stage NF, the permeate flux decreased and energy consumption increased with decreasing feed temperature. Salt rejection and energy consumption increased with increasing operating temperature. The rejection of divalent ions exceeded 95%.

2.3.2 NF and ion exchange

Al-Rawajfeh et al. [56], [57] studied the effects of NF and salt precipitation as pretreatment processes on scale formation in MSF and RO desalination processes. They used four different configurations. The results showed that sulfate scaling was significant in the MSF process, whereas carbonate scaling was significant in the RO process. Furthermore, the authors showed that NF efficiently removed sulfate ions. The performance of the hybrid ion-exchange (IX) and NF process in desalinating brackish water and seawater was also investigated [58]–[63]. The ion-exchange-treated water served as the feed to the NF membrane. IX converted more than 95% of the chloride ions to sulfate ions. The NF process exhibited high sulfate rejection (greater than 99%). The NF retentate was rich in sulfate and could be used to regenerate the exhausted IX resin.

2.3.3 FO-NF

Tan et al. [64] studied a hybrid forward osmosis and NF (FO-NF) system for seawater desalination. The FO draw solution was circulated into a two-stage NF membrane at pressures up to 43 bar. The results showed that the second-stage NF was necessary to desalinate seawater. A hybrid FO-NF system for brackish water was studied. This system required a lower hydraulic pressure than RO and had less flux decline caused by membrane fouling and no pretreatment requirements [65], [66]. Altaee and Hilal [67] studied a multistage NF-FO-RO system for brackish water. The system recovery rate exceeded 90%.

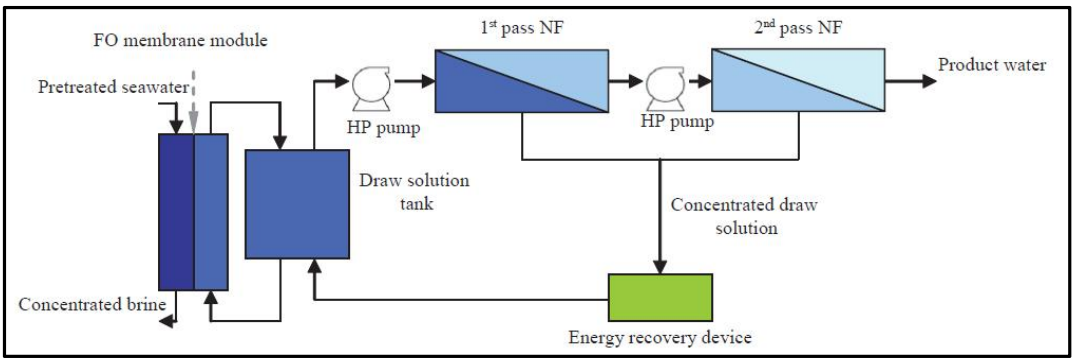

Figure 2-6: Schematic diagram of the hybrid FO-NF system for seawater desalination [64].

2.3.4 NF-SWRO

Kaya et al. [40] investigated the use of NF as a pretreatment stage for reverse osmosis in seawater desalination. They examined the performance of a single NF (NF90 and NF270) in SWRO and an integrated system (NF+RO). The NF membranes were individually employed in closed loops at 30 bars. For the integrated system study, the NF permeate served as the feed for the SWRO membrane. The permeate recovery of the NF90 membrane was less than that of the NF270 membrane. The salt rejection of the NF90 membrane was greater than that of the NF270 membrane. Al-Hajouri et al. [68] investigated the performance of NF membranes in pretreatment processes for SWRO with respect to conductivity and feed pressure over a period of eight years. The feed pressure varied from 18 to 38 bars. The initial permeability was high. However, a decrease in NF salt rejection was observed due to fouling. Chemical cleaning was conducted every nine months. Song et al. [41] investigated the performance of NF membranes to evaluate the scaling potential of NF-SWRO. The NF membrane rejected sulfate ions at 10-15 bars and produced permeate with a lower scaling potential in thermal desalination. AlTaee et al. [36] simulated dual-stage NF-NF, NF-RO and single-stage RO membrane processes using ROSA software [69] to compare performances, energy requirements, specific power

consumption, and overall costs. The results showed that the NF-NF process had the lowest cost and lowest specific power consumption, whereas the RO process had the highest specific power consumption.

2.3.5 NF-SWRO-MD

Drioli et al. [70] investigated the performance of integrated membrane systems and found that the integrated systems had higher recovery factors than the RO unit alone. The production was nearly double that of the RO unit. El-Zanati et al. [71] investigated the performance of an integrated NF-SWRO-MD membrane system. NF was used in a pretreatment step for the RO system. The rejected brine from the SWRO and NF systems was used as feed for the MD process. The NF and RO feed pressures were 31 and 34.2 bar, respectively. The permeate flow rate was 42 m^3/d. The brine flow rates for NF and RO were 30 and 28 m^3/d, respectively. The MD feed rate was 58 m^3/d at 35°C.

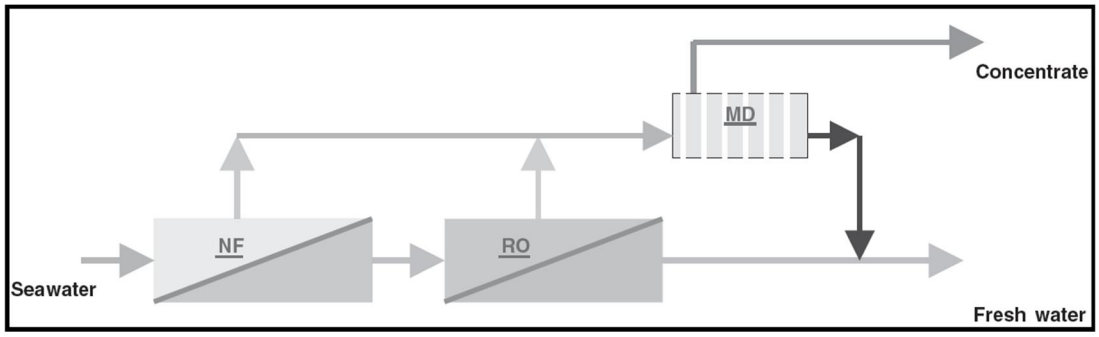

Figure 2-7: Schematic diagram of the hybrid NF-RO-MD seawater desalination process [71].

2.3.6 NF-MSF

Mabrouk et al. [72] compared the results of numerical simulations and experiments of using an NF membrane as a pretreatment for an MSF pilot unit driven by solar energy. Four solar concentrator modules with tracking systems were connected in series. Oil was

thermally heated by solar energy as it passed through a shell and tube heat exchanger opposite the NF permeate. The system was tested under a TBT of 100°C. The GOR was 15. The predicted GOR was 18 at a TBT of 130°C.

Awerbuch [42] used NF as a pretreatment for MSF to increase the TBT. The performance of the SR90 membrane was studied. He reported that the use of NF reduced fouling and increased the percentage of NF permeate used in the MSF, which thereby increased the TBT. The performance of the NF membrane as a pretreatment for MSF and RO desalination processes was also studied by another group from SWCC [43]–[49]. Three integrated systems were prepared and tested (NF-RO, NF-MSF, and NF-RO_{reject}-MSF). NF permeate was used in the MSF. The feed pressure was varied from 20 to 40 bar. For the first 34 days, the MSF was operated at a TBT of 120°C without using anti-scalants. The results indicated that no scale formation occurred. However, the fouling factor increased with increases in the recovery ratio. The MSF was then operated for 50 days at a TBT of 130°C with 35 ppm acid. No scaling issues were observed. In the trihybrid system, the NF permeate was used as the SWRO feed, and the SWRO retentate was used as the MSF feed. Due to the low concentrations of calcium and sulfate ions in the NF permeate, the MSF was operated at a TBT of 130°C. The NF feed temperature was varied from 24 to 34°C, and the pressure varied from 24 to 28 kg/cm^2. The NF recovery rate increased with increased temperature and pressure.

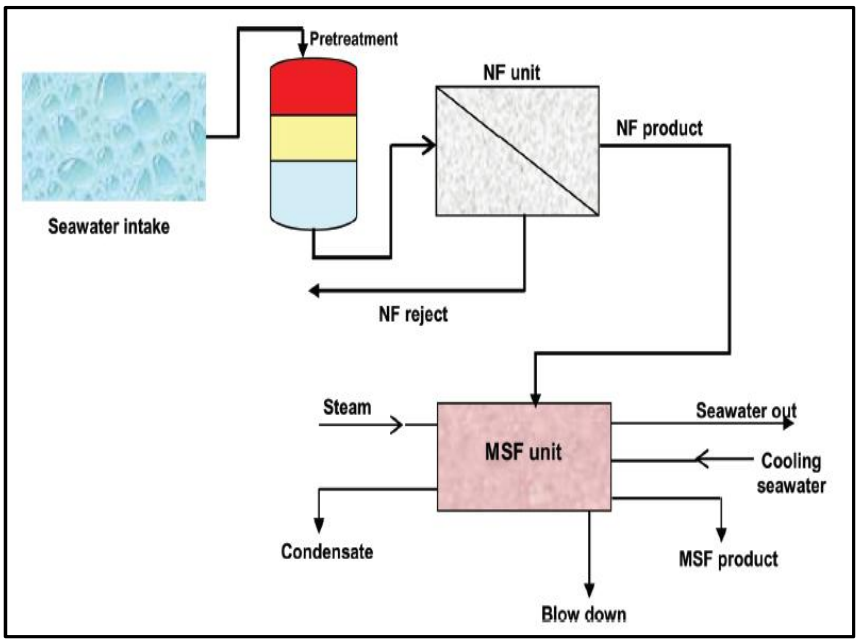

Figure 2-8: Schematic diagram of the dihybrid NF/MSF desalination system [46].

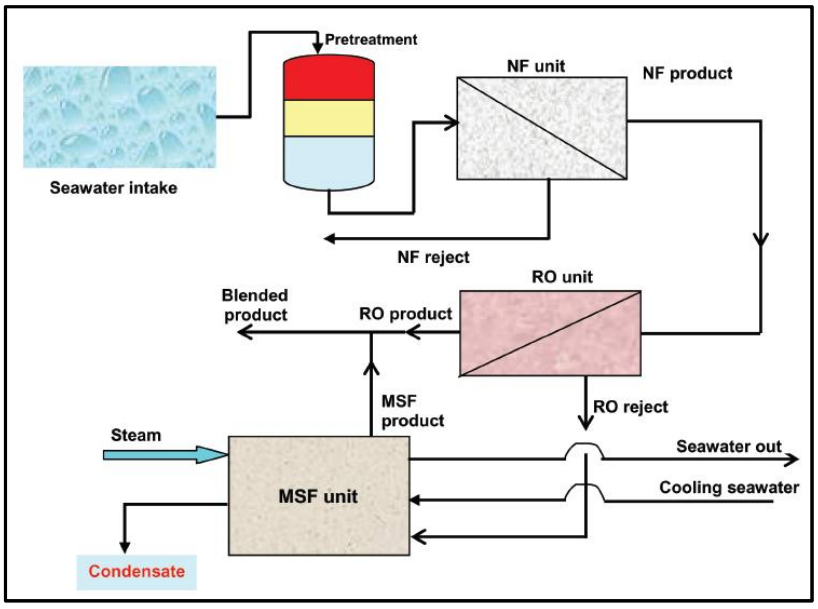

Figure 2-9: Schematic diagram of the trihybrid NF/RO/MSF desalination system [49].

Al-Rawajfeh [38], [73] studied the influence of NF pretreatment on scale formation in (MSF) desalination systems. The NF rejection and permeate flow rates were simulated by

the Hydranautics Nitto Denko Company (IMS software). The NF permeate was used as the feed to the MSF. Scaling potential decreased with increases in the percentage of NF-treated feed. The calcium carbonate and calcium sulfate deposition rates sharply decreased through successive stages. The Skillman index represents the ratio between the actual concentrations of calcium carbonate and calcium sulfate and their solubility at certain temperatures. Scale does not form when the solubility is greater than the actual concentration (i.e., the Skillman index is less than one). The effect of NF-treated feed percentage on the Skillman index is shown in Figure 2-10. The TBT can be increased up to 175°C at 100% NF pretreatment, as shown in Figure 2-11.

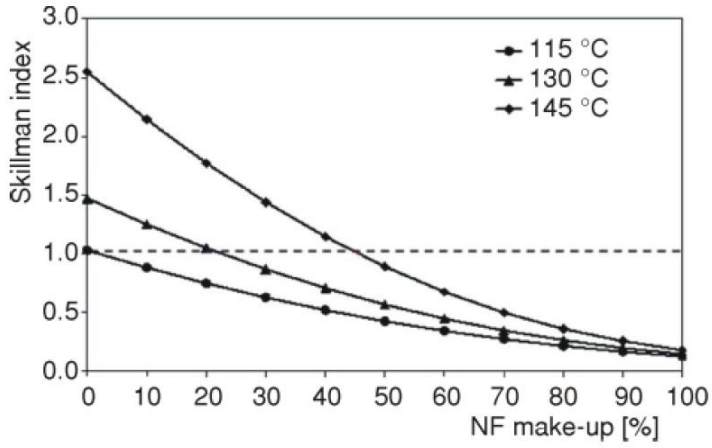

Figure 2-10: Effect of NF on sulfate scale potential in a BR-MSF plant [38].

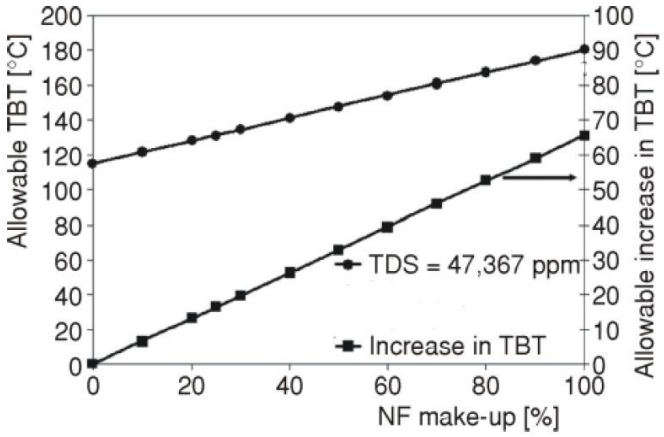

Figure 2-11: Shifting the maximum TBT by NF [38].

2.3.7 NF and salt production

Turek et al. [74] investigated three types of NF membranes (TFC-SR2 KOCH, NF270, and NF200) to evaluate their ability in an UF-NF-RO-MED-salt crystallization integrated system. They reported that salt crystallization resulted in decreased total costs and reduced waste products. This integrated system offered high water recovery (78.2%) and a water unit cost of \$0.5/m^3, which was less than those of RO and MED systems. Curcio et al. [75] investigated the performance of an integrated NF crystallization (NF-MC) system. An NF90 membrane was operated at 34.5 bar. The sulfate rejection was more than 99%, and the recovery factor was 50%. Drioli et al. [76] studied the performance of an MF-NF-RO-MD/crystallization system. The water recovery factor was 92.8%. The addition of MC to the membrane integrated system resulted in reduced fresh water costs and brine concentrations.

2.4 Other methods used as pretreatments

2.4.1 FO-MSF

Altaee et al. [5], [77], [78] developed a simple mathematical model to estimate the performance of a FO membrane when integrated with MSF or MED. The FO system used rejected brine from MSF or MED as a draw solution and seawater as the donor solution. The results showed that the concentrations of multivalent ions were reduced and the water flux across the FO membrane increased with increasing seawater salinity. The concentration of divalent ions decreased as the operating temperature in thermal plant decreased, which in turn increased the recovery rate of the FO system. Darwish et al. [79] studied the use of FO membranes as a pretreatment for an existing MSF. With an FO recovery of 40%, the MSF could operate at 135°C without significant calcium sulfate scaling. The osmotic pressure across the membrane decreased with increases in the FO recovery ratio.

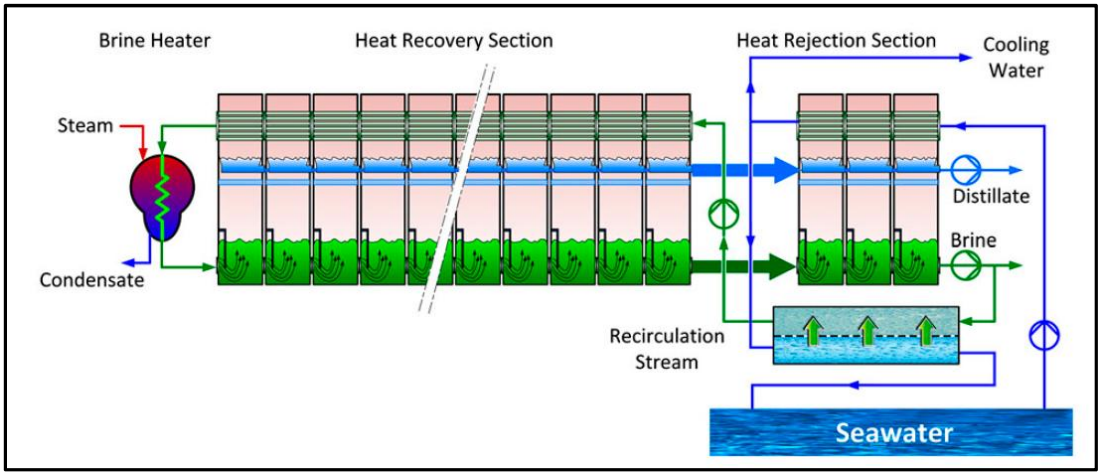

Figure 2-12: Schematic flow diagram of the FO-MSF hybrid system [79].

2.4.2 Salt precipitation and MSF

The use of salt precipitation as a pretreatment for seawater desalination was investigated [80]–[82]. Al-Rawajfeh [80] investigated the performance of salt precipitation as a pretreatment for MSF at different make-up percentages (0-100%). Calcium and magnesium ions were reduced by 98-99%, whereas sulfate ions were reduced by approximately 56%. The Skillman index was used to estimate the sulfate scale potential. The TBT reached 150°C at a 70% make-up in the MSF and reached 170°C at 100%. Ayoub et al. [81] showed that salt precipitation eliminated calcium ions and resulted in a high rejection of magnesium ions of approximately 99%.

Table 2-3: Comparison between different methods used as pretreatment for the thermal desalination process

Method	Maximum TBT	Advantages	Drawbacks	Reference
FO	135°C	Simple No pressure needed	Requires higher surface area	[5], [77]–[79]
Salt precipitation	170°C	Can eliminate 99% of scaling species	Large area Addition of alkalizing agents	[80]–[82]
NF	170°C	Can eliminate 99% of scaling species	High pressure	[38], [43]–[49]

2.5 Modeling of the NF membrane

NF modeling is critical for predicting flux, rejection, and separations. Modeling also reduces the number of experiments and thus saves time and money. Two main approaches

have been used to model the transport of ions and dissolved species. The first approach is based on the Spiegler–Kedem model [83]–[85], and the second approach is based on the Nernst–Planck equation [85], [86].

2.5.1 Spiegler–Kedem model

In the Spiegler–Kedem model, the NF membrane is considered a black box, and the porosity of the membrane is ignored. Therefore, complete details on the transport mechanisms cannot be determined [85]. This approach characterizes the membrane in terms of salt permeability and rejection coefficients. This model is applicable to binary salt systems. For multicomponent mixtures, this model cannot accurately quantify the effects of concentration polarization on membrane surfaces [83], [84].

$$J_s = P_s \frac{dC_s}{dX} + (1 - \sigma) C_s J_v \quad (2\text{-}1)$$

$$J_v = -P(\Delta P - \sigma \Delta \pi) \quad (2\text{-}2)$$

The governing equation of the Spiegler–Kedem model is given by Equation (2-1), where J_s represents the solute flux. The first term on the right-hand side of the equation represents the transport due to diffusion, whereas the second term represents the transport due to convection. P is the permeability of pure water, P_s is the permeability of the solute, x is the normal distance to the membrane, C is the concentration, and σ is the rejection coefficient. The volume flux is given by Equation (2), where J_v is the volume flux, ΔP is the pressure difference across the membrane and ΔΠ is the osmotic pressure difference.

The solute rejection is calculated by integrating Equation (2-1):

$$R = 1 - \frac{1-\sigma}{1-\sigma F} = 1 - \frac{C_m}{C_p} \quad (2\text{-}3)$$

$$F = \exp(1 - \frac{J_v(1-\sigma)}{P_s}) \quad (2\text{-}4)$$

where R is the rejection value, C_p is the permeate concentration and C_m is the feed concentration.

2.5.2 Extended Nernst–Planck equation

The extended Nernst–Planck equation [85], [86] describes ion transport in terms of the porosity ratio, membrane thickness, and membrane charge density. The rejection of mixed salts is accurately predicted by this model. However, concentration polarization effects are neglected. The model uses structural parameters, i.e., thickness, pore size, and tortuosity, to illustrate the mechanisms of transport of ions and dissolved species. The transport of solutes through pores in the membrane is based on hydrodynamic principles.

$$J_{i,pore} = -D_{i,pore}\frac{dC_{i,pore}}{dX} + K_{i,c}C_{i,pore}j_w \quad (2\text{-}5)$$

Equation (2-5) is the extended Nernst–Planck equation, where J_i is the flux. The first term on the right represents the transport due to diffusion, whereas the second term represents the transport due to convection. D is the solute diffusivity, and K is the mass transfer coefficient.

The Donnan–steric pore model (DSPM) [87], [88] is based on the extended Nernst–Planck equation. This model considers the effects of convection and diffusion on the transport of ions through membrane pores. This model characterizes the membrane in terms of the porosity ratio, pore radius, and membrane charge density.

The Donnan–steric pore and dielectric exclusion model (DSPM-DE) [89], [90] considers the dielectric exclusion phenomenon as an additional effect. The DSPM-DE model is based on the extended Nernst–Planck equation, as shown in Equation (2-6), and accounts for ionic diffusion, convection through membrane pores, and electro-migration effects inside the membrane. Ionic separation through the membrane is characterized by three separation mechanisms, i.e., steric hindrance, dielectric exclusion, and Donnan equilibrium.

$$J_{i,pore} = -D_{i,pore}\frac{dC_{i,pore}}{dX} - \frac{Z_i C_{i,pore} D_{i,pore}}{RT} F \frac{d\psi}{dX} + K_{i,c} C_{i,pore} j_v \qquad (2\text{-}6)$$

where J_i represents the flux. The first term on the right represents transport due to diffusion, the second term represents transport due to an electric field, and the third term represents transport due to convection. Z is the valence of the ionic species, R is the universal gas constant, T is temperature, F is the Faraday constant and ψ is the membrane potential.

Furthermore,

$$\frac{d\psi}{dx} = \frac{\sum_{i-1}^{n} \frac{z_i J_v}{d_{i,p}} (K_{i,c} C_i - C_{i,pore})}{\frac{F}{RT} \sum_{i-1}^{n} z_i C_i} \qquad (2\text{-}7)$$

$$\frac{dC_i}{dx} = \frac{J_v}{D_{i,pore}}\left(K_{i,c}C_i - C_{i,pore}\right) - \frac{z_i C_i}{RT}F\frac{d\psi}{dx} \quad (2\text{-}8)$$

$$\frac{C_i}{C_{i,pore}} = \psi \exp\left(-\frac{z_i F}{RT}\Delta\psi D\right) \quad (2\text{-}9)$$

2.5.3 NF transport mechanisms

The mechanisms responsible for solute transport through NF membranes are convection, diffusion, and electro-migration. The contributions of each mechanism have been investigated [91]–[93]. Convection is the dominant mechanism at high membrane thickness-to-porosity ratios, high permeate flux, and low membrane charge density. Diffusion is the dominant mechanism at low membrane thickness-to-porosity ratios, low permeate volume flux and high membrane charge density. Electro-migration dominates solute transport for moderate membrane charge densities [91].

2.5.3.1 Influence of the membrane charge density

The contributions of convection increase with decreasing membrane charge density because the concentration of co-ions inside the membrane is proportional to the convective flux of co-ions within the membrane. This flux increases as the membrane charge density decreases according to the Donnan exclusion model. Diffusion is the dominant mechanism involved in electrolyte transport. The contributions of diffusion increase with increases in the membrane charge density. However, both diffusion and convective flux decrease as the

membrane charge density increases. The decrease in convective co-ion flux is more significant than that in the diffusive co-ion flux [91]. Therefore, the contributions of diffusion increase and the contributions of convection decrease with membrane charge despite the decreased diffusive co-ion flux. As shown in Figure 2-13, the contributions of the three mechanisms level off at high membrane charge densities. The contributions of both convection and electro-migration tend to be equal due to the asymptotic behavior of the electrical potential gradient and co-ion concentrations in the membrane [91], [92].

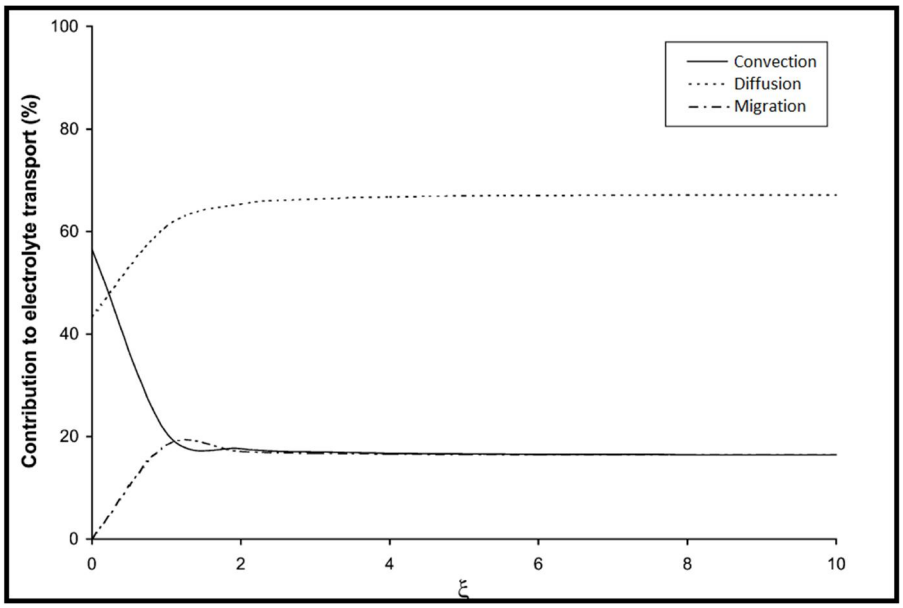

Figure 2-13: Effect of membrane charge density on the contributions of different transport mechanisms [91].

2.5.3.2 Influence of the effective pore radius

The diffusion contributions increase and the contributions of convection and migration decrease with decreases in the pore radius (Figure 2-14). Although the mean co-ion convective and migration flux decreases with decreasing pore size, the decrease is less significant than that of the mean co-ion diffusion flux. At a low permeate flux, the dominant

mechanism in electrolyte transport is diffusion because transport by diffusion is enhanced at low permeate flux [91], [92].

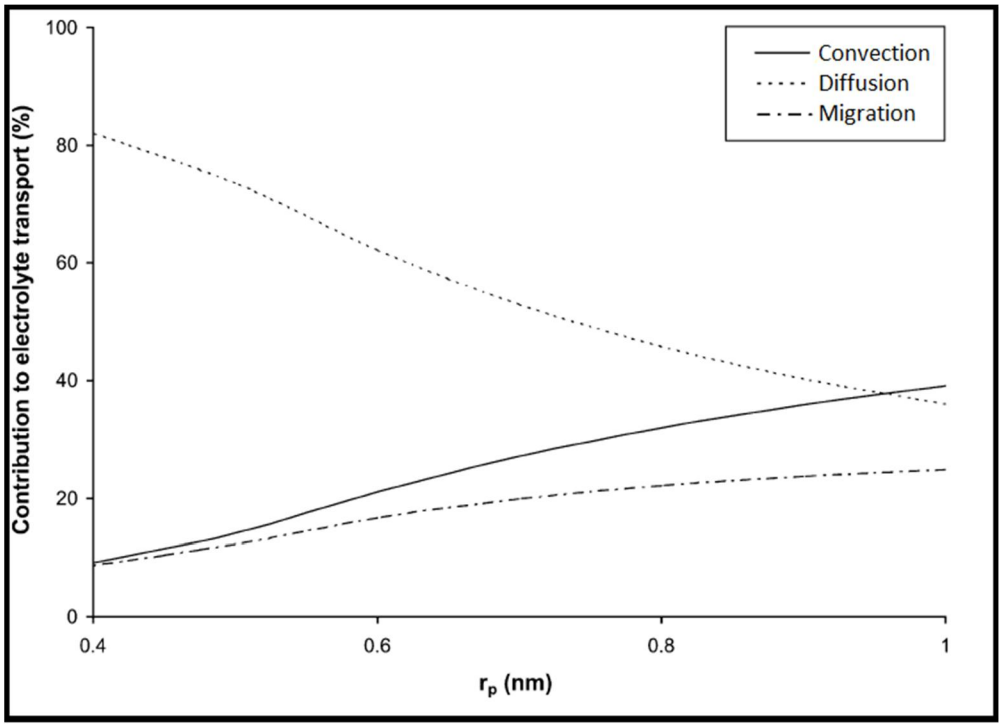

Figure 2-14: Effect of membrane pore size on the contributions of different transport mechanisms [91].

2.5.3.3 Influence of the permeate flux

As the permeate volume flux decreases, the contributions of convection and migration decrease, as shown in Figure 2-15. Convection becomes the dominant mechanism at high permeate volume flux, whereas diffusion is the dominant mechanism at low permeate volume flux. The contribution of diffusion to solute transport increases with decreasing permeate volume flux because diffusion flux reaches a critical value at high permeate flux, whereas convection flux and electro-migration increase. The contributions of electro-migration and convection tend to be equal at any permeate flux at high membrane charge densities [91], [93].

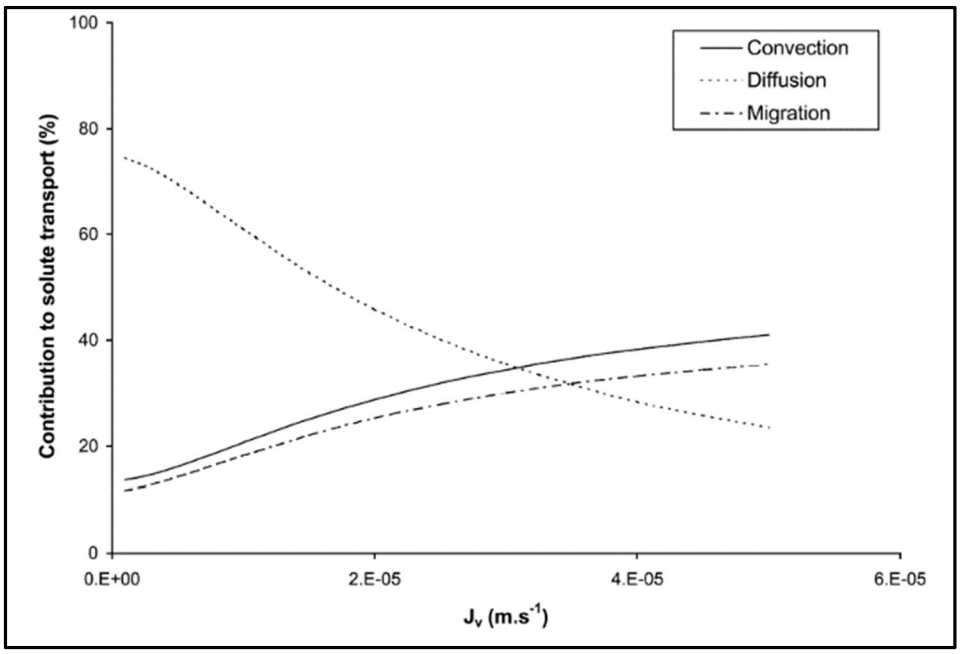

Figure 2-15: Effect of flux on the contributions of different transport mechanisms [91].

2.5.3.4 Influence of the diffusion coefficient

The diffusion coefficient is the ratio between the molar flux due to molecular diffusion and the species concentration gradient. For unequal diffusion coefficients between the co-ions and counter ions, the contributions of electro-migration and convection tend to reach a constant value, and the electro-migration contribution has a value at a membrane charge density of zero due to the diffusive potential formed by the presence of more transportable ions. The contribution of convection decreases and the contribution of diffusion increases with increases in the membrane charge density. Electro-migration is the dominant mechanism for modest values of membrane charge density. This phenomenon occurs only when the co-ion diffusion coefficients surpass those of the counter-ions. Electro-migration remains the dominant mechanism, even at high membrane charge density values, if the permeate flux is increased [91].

2.5.3.5 Influence of the thickness-to-porosity ratio

Figure 2-16 shows that as the thickness-to-porosity ratio decreases, the contribution of diffusion to solute transport increases, whereas the contributions of convection and electro-migration decrease due to the decrease in the Peclet number in the membrane. As the thickness-to-porosity ratio increases, these contributions vary even though the retention remains constant. The variations in convection, diffusion and electro-migration balance each other such that the amount of solute transport through the membrane to the permeate remains constant [91].

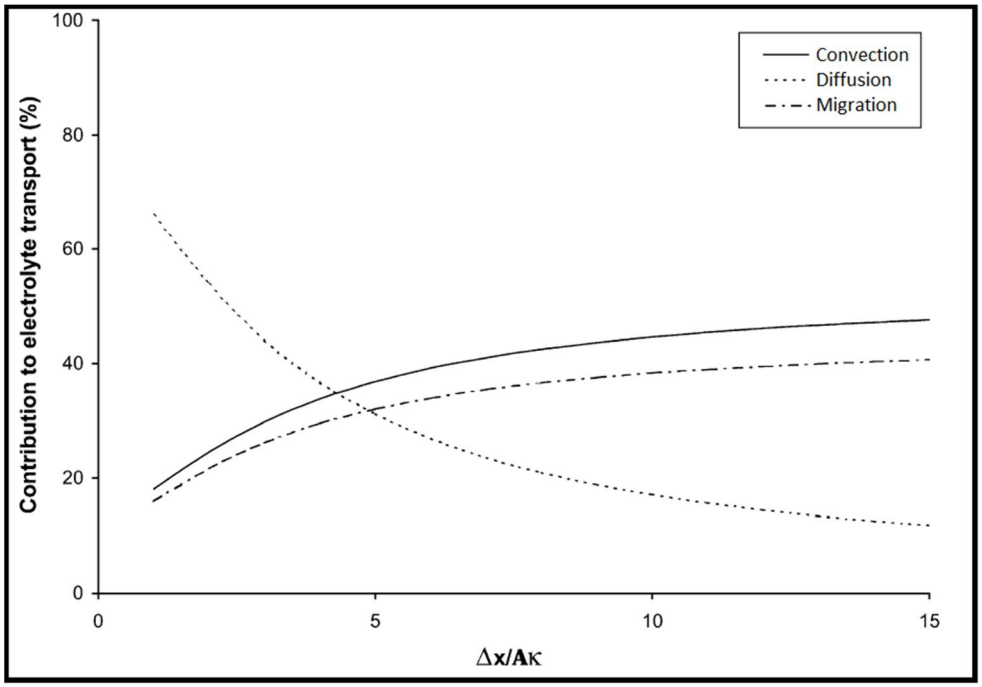

Figure 2-16: Effect of the membrane thickness-to-porosity ratio on the contributions of different transport mechanisms [91].

Ahmad et al. [83] developed a model for multiple solute filtration by extending the Spiegler–Kedem model. The model parameters included the permeability of pure water, a solute permeability constant, a rejection coefficient and a mass transfer coefficient. The parameters were estimated using the Levenberg-Marquardt method and the Gauss-Newton algorithm. The simulation results showed that the flux and permeate concentrations were in good agreement with experimental data. Radcliffe et al. [86] discussed the use of the extended Nernst–Planck equation for NF and reverse osmosis modeling. The role of dielectric exclusion from the NF membrane was discussed. However, the inability to explain the physical properties and physicochemical phenomena inside nano-pores was a major issue when applying this theory to seawater desalination.

Aleman et al. [87] developed a mathematical model to predict the performance of NF membranes based on the Nernst–Planck equation, Donnan equilibrium model, and Gouy-Chapman theory. The model parameters were the permeability of pure water, pore size, and surface electrical potential and were independent of the concentration and operating pressure. Roy et al. [89] modeled different NF configurations using the Donnan–steric pore and dielectric exclusion model. Flat sheet and spiral wound membrane configurations were compared. The results revealed that the feed pressure and flow rate affected the solute rejection and solute recovery ratios. Both the flat sheet and spiral wound membrane configurations yielded the same results.

2.6 Membrane fouling

Fouling is one of the main problems in NF and results in a shortened membrane lifetime. Fouling also requires membrane chemical cleaning, particularly if high concentrations of

organic and inorganic components are filtered from the feed [94]–[97]. Fouling is caused by the adherence of inorganic and organic materials to membrane surfaces and pores. Inorganic fouling is due to the buildup of salt scalants on the membrane surface, whereas organic fouling is caused by natural organic matter, such as derivatives of humic acid [98]–[100]. Al-Amoudi et al. [101], [102] discussed organic and inorganic fouling, strategies to minimize fouling, membrane cleaning methods and the effects of pressure, temperature, surface roughness, permeate flux and pH. Organic fouling involves interrelationships between chemical and physical interaction. Inorganic fouling is a result of scale formation. To avoid scaling, NF systems should be operated at conditions lower than critical solubility limits. Fouling can be reduced by membrane treatment, membrane modification, feed pretreatment and chemical cleaning.

Matin et al. [103] discussed the causes of biofouling, biofilm formation, the role of the EPS and the events that lead to biofouling. They found that membrane surface modification was more promising than biocide and feed pretreatment because biocide and feed pretreatment aim to limit microbial concentrations in the feed stream, whereas membrane surface modification reduces the adhesion of bacteria or inactivates bacteria if adsorbed. A mathematical model for a cross-flow NF system examined membrane resistance to estimate the scaling potential of RO systems using NF membranes [104], [105]. The concentrations of the feed water were estimated, and the concentrations of the sulfate and carbonate ions were calculated. The results showed that surface foulant contents were primarily due to calcium carbonate and calcium sulfate.

2.6.1 Effect of pressure

Lin et al. [106] examined the effects of a constant flow velocity of 2,000 ppm for $CaSO_4$ deionized water solution at membrane feeds of 345-966 kPa. The feed water recovery increased with increases in the operating pressure. Because of this relationship, the osmotic pressure and concentration polarization at the surface increased; thus, the flux reduction was sharp. The nucleation stage was considerably shorter at high operating temperatures due to the high supersaturation. Lee et al. [107], [108] found that concentration polarization and surface crystallization increased as the operating pressure increased. Heterogeneous crystallization was favored at high pressures and low velocities.

2.6.2 Effect of feed flow rate

The feed flow rate has a significant impact on crystal growth and scale precipitation, particularly in homogenous crystallization. Vrijenhoek et al. [109] reported that fouling significantly decreased with increases in the cross-flow velocity. Lee et al. [107], [108] showed that at high feed flow rates, the dominant mechanism of membrane fouling was bulk crystallization rather than surface crystallization. At lower feed flow rates, the dominant mechanism was surface crystallization. The relationship between deposited mass and flux decline was linear, which indicated that the flux drop was due to NF fouling. Therefore, the feed concentration at the membrane wall will be higher than the bulk concentration because of concentration polarization at lower flow rates.

2.6.3 Effect of temperature

Temperature has an influence on scale formation on NF membrane surfaces. For specific precipitates, the thermodynamic solubility product is a function of temperature [110]. Her et al. [111] concluded that calcium carbonate particles were detected on the NF membrane

surface at 20°C. Increasing temperatures will decrease the solubility product constants of $CaCO_3$ and $CaSO_4$, producing a homogenous crystallization. In the bulk concentration, calcium carbonate precipitation occurs on the membrane surface due to high supersaturation and high temperatures [107], [108]. Andirstsos et al. [112] reported on the temperature effect due to the crystal structure of $CaCO_3$. They reported that the deposits were calcite at 25°C and aragonite at 45°C.

2.6.4 Effect of surface roughness

Hobbs et al. [113] investigated the effect of surface roughness on fouling. A membrane was characterized using streaming potential analysis (SPA) to measure the surface charge, AFM to measure the surface roughness, and contact angle measurements to determine the hydrophobicity. The results showed that membrane fouling increased with increasing surface roughness. Vrijenhoek et al. [109] used AFM to show that more particles were deposited as the surface roughness increased; this phenomenon resulted in a greater flux decline.

2.7 Graphene Oxide

GO is used directly as an effective selective layer for this type of GO-based membrane, GO layers were deposited on a membrane substrate surface to improve membrane performance. Aghigh et al. [20] discussed the recent progress in Graphene research for water desalination using novel methods such as Nano-porous Graphene (NG) sheets as well as Capacitive Deionization (CDI) method. Among which most promising uniform NG sheets can be used for water filtration and desalination. Ali et al. [114] studied thin film composite membranes prepared from m-phenylenediamine and 1,3,5- benzene tricarbonyl

chloride by interfacial polymerization on the surface of a polysulfone substrate, and graphene oxide was embedded into the membrane during membrane formation to improve the membrane performance. A portion of the data available for GO membranes is presented shown in Table 2-4. The rejection percentages of the GO membranes were highly dependent on the operating conditions, ion compositions and membrane characteristics.

Table 2-4: Performance of graphene oxide membranes

Membrane	GO concentration ppm	Pressure (bar)	NaCl conc. (ppm)	Water flux (L/m2·h)	Salt rejection (%)	Water contact angle (°)	Reference
MPD/TMC	76	15	2000	16.6	99	47	[115]
MPD/TMC	100	15	2000	29.6	98	56	[116]
MPD/TMC	1000	55	32000	28	98	55.5	[117]
MPD/TMC	2000	15	2000	22	88	65	[118]
MPD/TMC	20000	15.5	2000	14	96	26	[119]
MPD/TMC	50	15	2000	43.3	98.87	56.5	[120]

2.8 Concluding remarks

NF can be used to reject calcium sulfate and calcium carbonate. The process has the potential to eliminate scaling species in seawater desalination plants. This elimination allows for increased TBT in thermal desalination processes, which in turn enables higher numbers of stages in the MSF or MED processes and thus increases the GOR. The performances of NF membranes integrated with various types of desalination technologies, including multistage flash, reverse osmosis, forward osmosis, membrane distillation and ion-exchange processes, have been reported. The operating pressures varied from 2 to 20 bar, which is lower than those used in many typical RO processes. The major problem

encountered by these systems was fouling, which results in high energy demand, high operation costs and reduced membrane lifetimes.

Increasing the operating pressure will increase salt rejection and permeate flux because of the contribution of convection at high pressures due to high water flux. However, at extremely high pressures (e.g., 34 bar), the nucleation stage is considerably shorter due to the greater degree of supersaturation. For some salts, the rejection decreases with increasing pressure due to increased membrane polarization. Thus, salt rejection decreases at high pressures.

Temperature has a small effect on ion rejection. Increasing the temperature increases the permeate flux and ion rejection (however, the Na and Cl ion rejection slightly decrease). Temperature has an influence on scale formation on membrane surfaces. For a specific precipitate, the thermodynamic solubility product is a function of temperature. Increasing the temperature will decrease the solubility product constants of $CaCO_3$ and $CaSO_4$, resulting in homogenous crystallization. In the bulk concentration, calcium carbonate precipitation on membrane surfaces occurs due to high supersaturation at high temperatures.

Salt rejection and permeate flux decrease with time before chemical cleaning and decrease more sharply after chemical cleaning. At high operating pressures, the duration of the nucleation stage is considerably shorter due to the greater degree of supersaturation, which increases membrane fouling. At lower feed flow rates, the dominant mechanism is surface crystallization. At higher feed flow rates, the dominant mechanism of membrane fouling is bulk crystallization. The relationship between deposited mass and flux decline is

linear, which indicates that flux decreases are due to membrane fouling. The surface foulant contents are primarily attributed to calcium sulfate and calcium carbonate. Increasing the surface roughness will increase membrane fouling.

CHAPTER 3

METHODOLOGY AND EXPERIMENTAL SETUP

3.1 Objective and Methodology

The objective of this work is to develop a membrane composed of Polyether sulfone (PES) as a support coated with Graphene oxide. The next step is to investigate experimentally the performance of developed membrane and compare it with the commercial NF membrane. This is considered as a pretreatment step for seawater desalination, the following procedure is applied:

- Coating Ultrafiltration PES membrane with graphene oxide with different number of deposition, using different concentrations.
- Reduce the graphene oxide by subjecting the membrane to the HI vapor and study the effect of subjected time on the interlayer spacing.
- Test the coated membrane in a diffusion cell using MgSO4 Solution to study the effect of the time through which membrane is subjected to HI vapor, number of deposition and concentrations.
- Test the coated membrane using cross flow arrangement and compare it with NF using $MgSO_4$ Solution, $CaSO_4$ solution and seawater.
- Characterize the developed membranes using SEM, optical microscope and water contact angle measurements.

3.2 Synthesize of the membrane

3.2.1 Material

PES membrane with 30 nm pore, 47mm diameter were purchased from Sterlitech Kent, Washington, USA [121]. NF270 was purchased from Dow water & process solutions, Midland, Michigan, USA [122]. A highly concentrated graphene oxide dispersion in water (60 ml) with concentration of 5.5mg/ml was purchased from Graphene Supermarket Calverton, New York, USA. Polyacrylamide (PAM) and Polyethyleneimine (PEI) were purchased from Polyscience, Warrington, Pennsylvania, USA [123]. Magnesium sulfate heptahydrate extra pure, Calcium sulfate, Hydriodic acid 55% AR with stabilizer, and Hydrogen Iodide (HI) solution were purchased from Loba Chemie, Wodehouse road, Mumbai, India [124].

3.2.2 Methods of preparation

3.2.2.1 Solutions Preparation

Two solutions were prepared from the highly concentrated GO (5.5mg/ml) and Deionized (DI) water to obtain a 0.15 mg/ml, 0.5 mg/ml concentration solutions. The DI water was prepared using Milli-Q integral water purification system shown in Figure 3-2 [125]. The solutions were stirred for 20min to obtain a homogeneous dispersion of GO flakes in DI water. The PAM solution was prepared by adding 0.2g of PAM over 150ml DI water and was stirred for 30min. The PEI solution was prepared by adding 1ml of PEI over 100ml DI water and was stirred for 30min.

Figure 3-1: Milli-Q integral water purification system for ultrapure water.

Magnesium sulfate solution was prepared by adding15g of $MgSO_4$ to 5L of DI water and was stirred for 30min to make a 3000ppm $MgSO_4$ solution. Calcium sulfate solution was prepared by adding12.5g of $CaSO_4$ to 5L of DI water and was stirred for 30min to make a 2500ppm $CaSO_4$ solution. Table 3-1 presents the solution concentration used.

Table 3-1: Solutions prepared

PAM	1.34mg/ml DI water
GO	0.15 mg/ml, 0.5 mg/ml in DI water
$MgSO_4$	3000ppm
$CaSO_4$	2500ppm

3.2.2.2 GO/PAM-PES and rGO/PAM-PES

The spin coater used is SCS G3 Spin Coater series shown in Figure 3-2 [126]. The PES membrane with a diameter of 47mm was washed by DI water then placed in spin coater. After that, 1 ml of PAM solution was added and left to spin at 200rpm for 2 mins then 3000rpm for 6 mins. It was then washed by 2ml of DI water and placed on the spinner at 3000rpm for 6 mins. Then 1ml of GO solution was deposited over the membrane at 200rpm for 2 mins then 3000rpm for 6 mins. The last step was repeated depending on the number of depositions. Table 3-2 and Figure 3-3 presents the procedure of coating the ultrafiltration membrane.

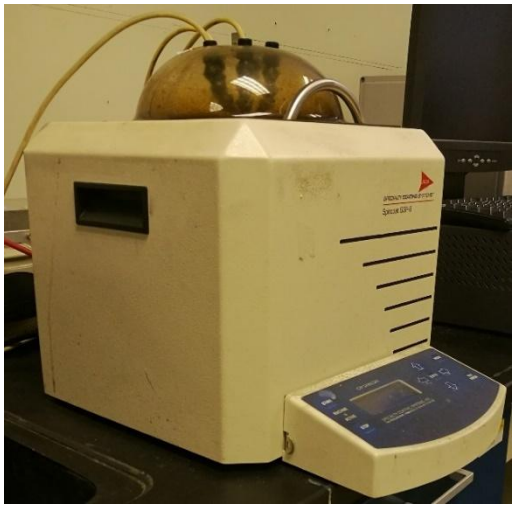

Figure 3-2: SCS G3 Spin Coater series

Table 3-2: Procedure of developing GO/PAM-PES and rGO/PAM-PES

Soltions	PAM	0.2 gram PAM - 150 ml of DI water
	GO	0.15 mg/ml or 0.5 mg/ml
GO/PAM-PES membrane	Spin Coating	200 rpm for 120 sec - 3000 rpm for 360 sec
	Deposition	1ml PAM -> washing -> 1 ml GO
rGO/PAM-PES membrane	GO/PAM-PES membrane subjected to HI vapor	

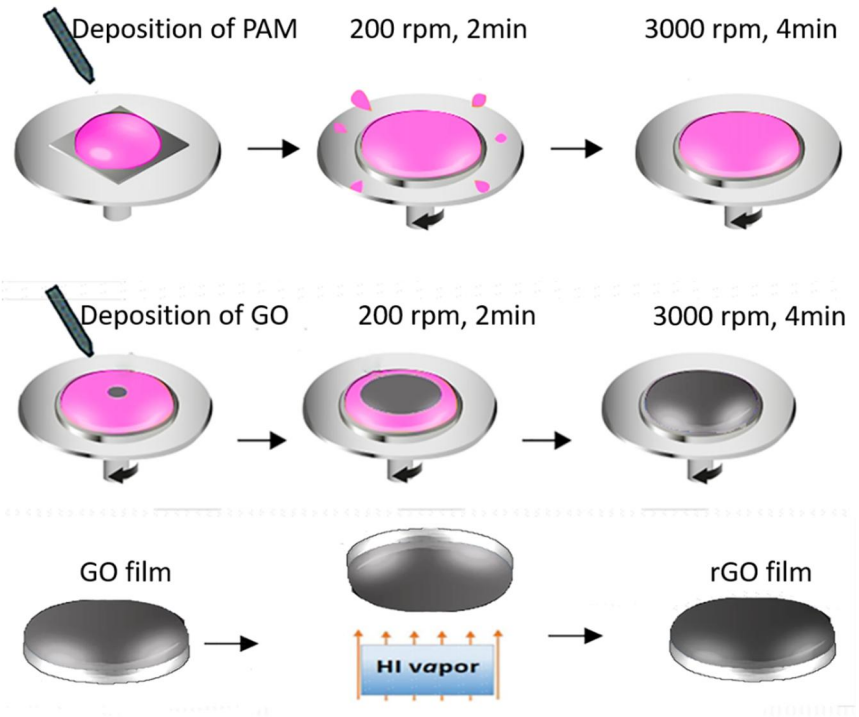

Figure 3-3: Procedure of developing GO/PAM-PES and rGO/PAM-PES

The interlayer spacing is controlled in reduced graphene oxide (rGO) membranes by subjecting the GO membrane to HI vapor. The developed GO/PAM-PES membrane was subjected to HI vapor for different amount of time and at different temperatures to study the effect of time and temperature over the interlayer spacing.

3.2.3 Characterization

Water contact angle measurements (CA) were carried out using an automatic dispenser (Model 500, Ramé-Hart) to find out the effect of the time duration in which membrane is subjected to HI vapor on the contact angle. The surface of the coated GO layers was analyzed by optical microscope. Whereas the structure and topography of the coated GO layers were further analyzed by using a field emission scanning electron microscope (FESEM TSCAN-MIRA 3 LM).

3.3 Membrane performance

The performance of the developed membranes was evaluated by a diffusion test using $MgSo_4$ solution and a cross flow test using $MgSo_4$ solution, $CaSo_4$ solution and real seawater.

A conductivity probe supplied by eDAQ, Denistone East, New South Wales, Australia [127] was used. The conductivity meter was calibrated for $MgSo_4$ solution, $CaSo_4$ solution. The calibration graphs produced from a series of standard solutions were made up using $MgSO_4$ and measuring the corresponding conductivity values in millisiemens (mS). This curve was used to convert the conductivity readings into ppm.

3.3.1 Diffusion test

The diffusion cell used was divided into two glass cells (7ml each) with 3 mm diameter outlet, purchased from Permegear, Hellertown, Pennsylvania, USA [128]. The two cells were washed by DI water then the developed membranes were placed between the two cells as shown in Figure 3-4. Washing was done by filling the cell with the DI water and stirred for 3 min. Then the DI water was removed by a syringe, then this steps were repeated

for the other cell using $MgSo_4$ solution, the washing steps were done for three times. After that, one cell was filled with $MgSo_4$ solution and the other one was filled with DI water. Both were stirred at 700 rpm. The conductivity of the DI water side was measured every 1 min for 10 min using the conductivity meter. Three samples of each membrane were tested for precision.

The diffusion flux of $MgSo_4$ ions (Mol/L.s) passing through the membrane was calculated after plotting the normalized concentration reading versus the time. The diffusion flux for the PES was considered as a reference for other prepared samples and the percentage of rejection was calculated per the following equation:

$$Rejection = \frac{D_s - D_b}{D_b} \times 100\ \%$$

D_b is the diffusion flux for the PES and Ds is the diffusion flux for the prepared sample.

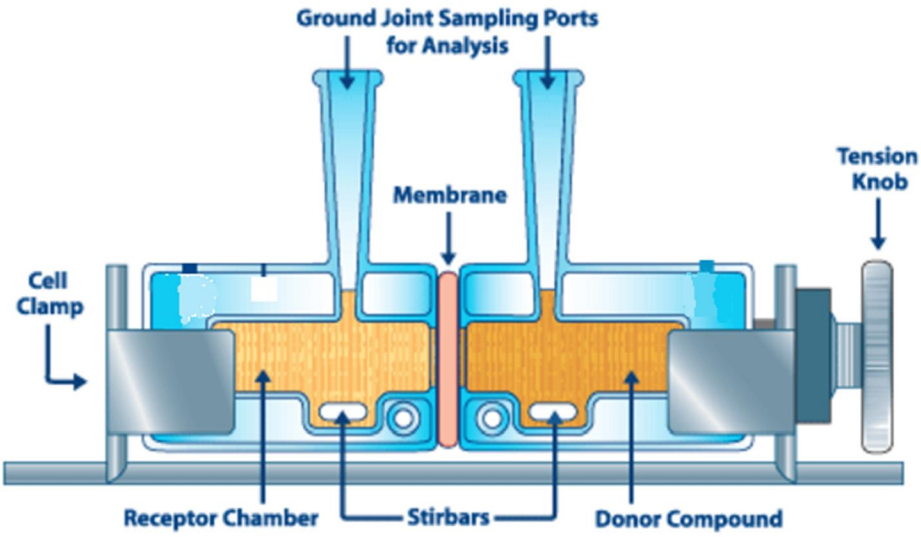

Figure 3-4: Diffusion cell [128].

3.3.2 Cross flow test

The cross-flow system consists of a test cell, variable speed pump, pressure gauge and a relief valve. The variable speed pump was purchased from Eldex, California, USA with speed variation that ranges between 0.01-10 ml/min and can handle a pressure up to 40 bar [129]. The membrane effective area of the cell used is 4.906 cm^2, the pressure was controlled by the relief valve as shown in Figure 3-5. There is a safety relief valve calibrated at 40 bar. The solution was pumped through the system for one and half hour to reach steady state. The effect of pressure and the inlet flow rate on the rejection and the permeate flux were studied for $MgSo_4$ solution, $CaSo_4$ solution and real seawater. The rejection and flux were measured at five values of pressure starting with 5 bar with step 2.5 and four value of inlet flow rate starting with 2.5ml/min with step 2.5. The rejection for the $MgSo_4$ and $CaSo_4$ solutions were measured by the conductivity meter while for the seawater the cations were measured by ICP-MS and the anions with IC. On the other hand, the permeate flux was calculated by dividing the measured output volume over time and

membrane area. The developed membranes were compared with a commercial NF membrane. Three samples of each membrane were tested for precision.

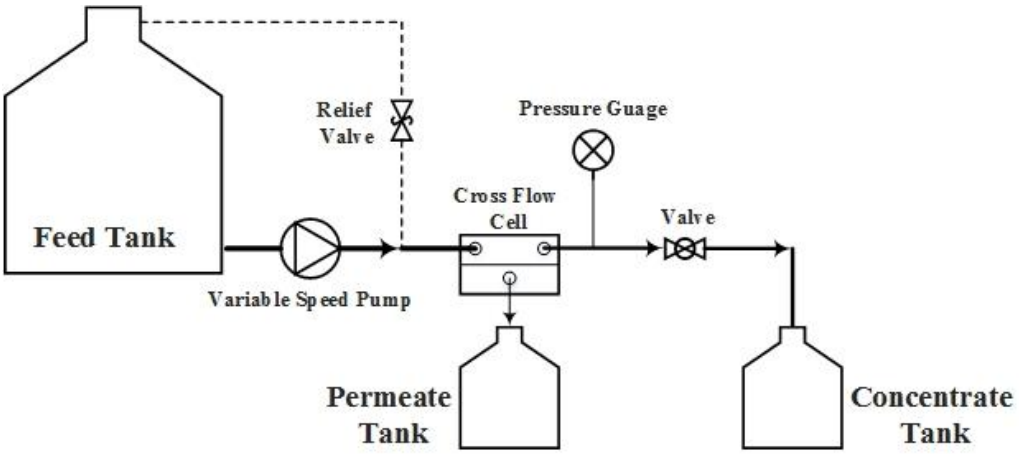

Figure 3-5: Schymatic diagram of the cross flow test

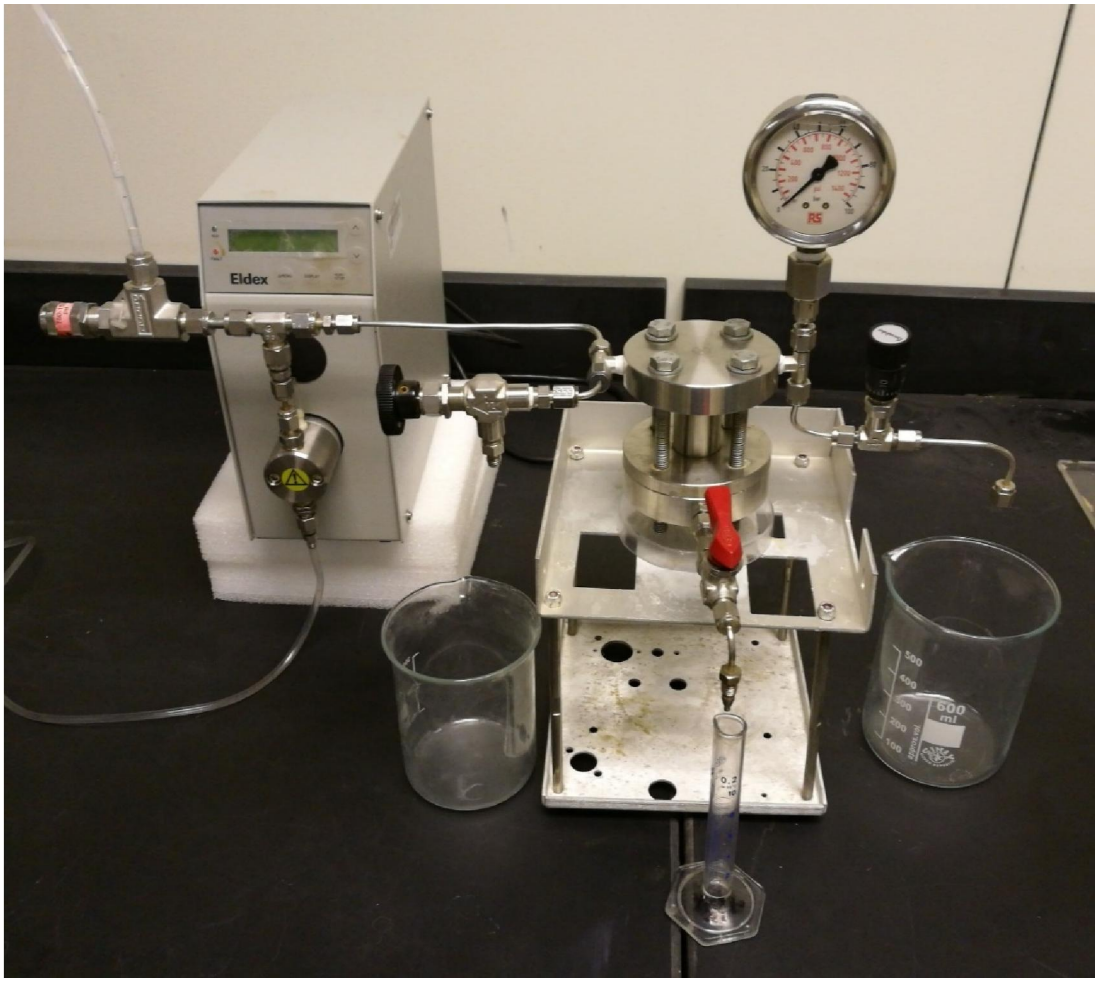

Figure 3-6: Cross flow permeation test system.

CHAPTER 4

RESULTS & DISCUSSION

4.1 Optimization

The aim of this chapter is to optimize different parameters for membrane coating. The effect of deposition method, GO concentration, polyelectrolyte, coating method, number of layers and reduction time are investigated.

4.1.1 Effect of polyelectrolyte

Polyelectrolyte must be used as a cross linking agent between the PES and GO layers since GO detaches from the PES as shown in Figure 4-1. PAM and PEI were used as adhesion layer between the GO and PES. The rGO/PAM-PES and rGO/PEI-PES membrane was subjected to HI vapor for 30 min. In the beginning, the two membranes were tested in a diffusion test cell using the $MgSO_4$ solution. After that, the membranes were tested at 10 bar with 10 ml/min inlet flow rate using $MgSO_4$ solution. The results showed that after the cross-flow test, there were some detachments for rGO/PEI-PES while there was full coverage for rGO/PAM-PES membrane as shown in Figure 4-2.

The interaction between PAM and PES takes place because of the dipole-dipole forces between CH_2 and C=O groups of the PAM and S=O groups of the PES. The chemical structure of GO/PAM-PES and GO/PEI-PES is shown in Figure 4-3. The interaction between the negatively charged GO and positively charged PAM is an electrostatic inter

action between COO^- groups of the GO layers and NH_2^+ groups of the PAM as well as the hydrogen bond between OH^- groups of the GO and NH_2^+ groups of the PAM. [130].

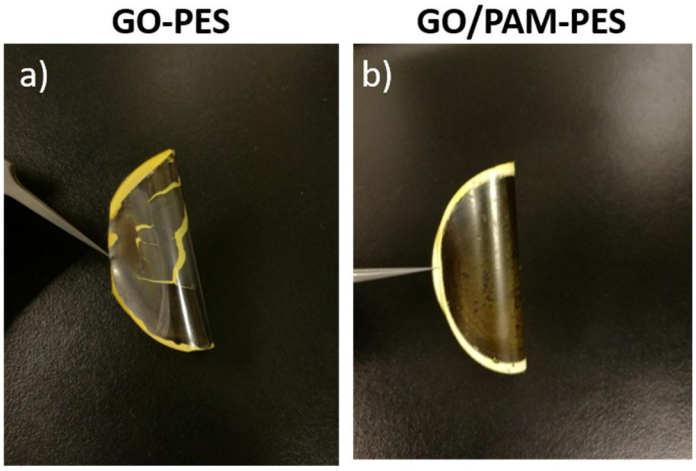

Figure 4-1: Detachments of GO layer from PES a) GO-PES, b)GO/PAM-PES

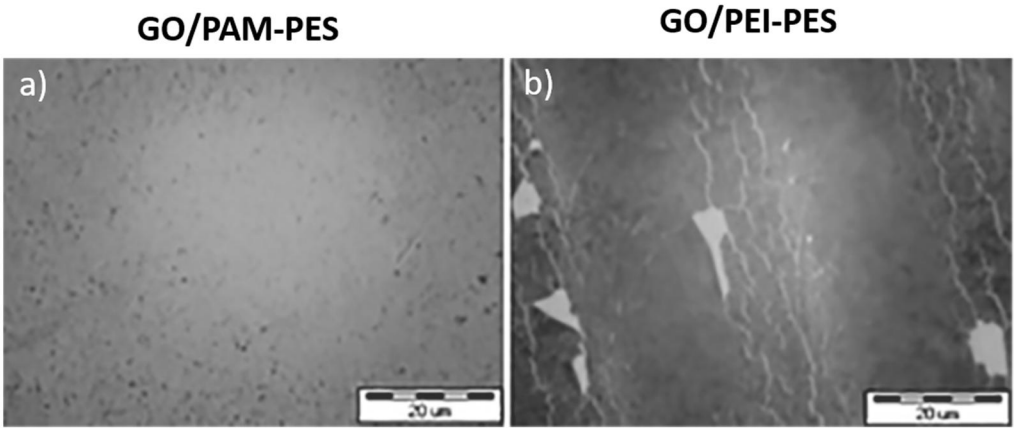

Figure 4-2: optical micrsocpe image for a) rGO/PAM-PES, b) rGO/PEI-PES.

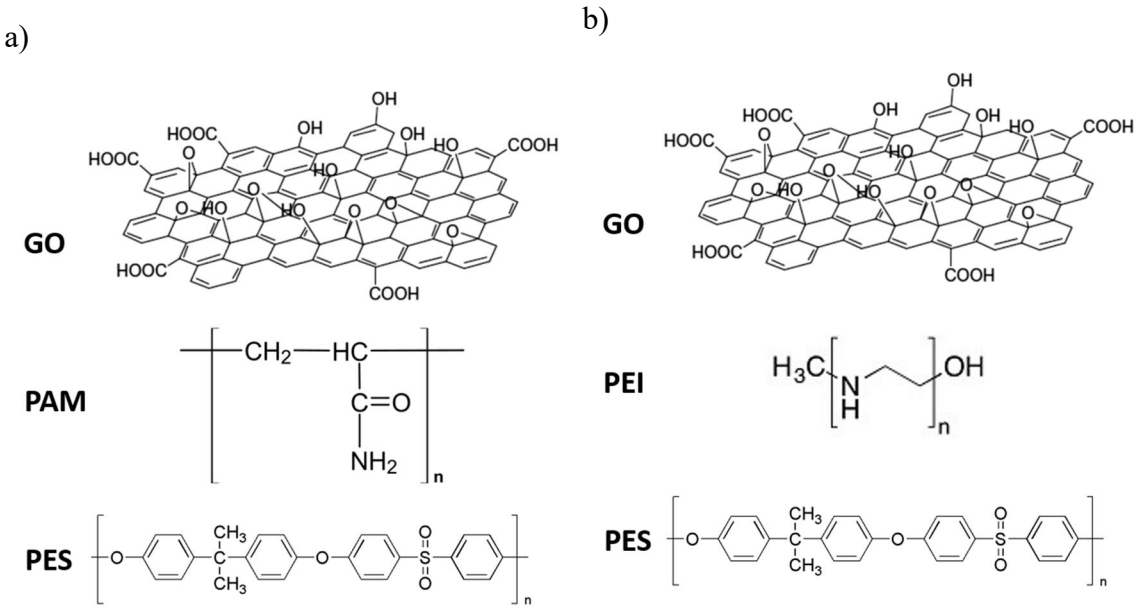

Figure 4-3: chemical structure a) GO/PAM-PES, b) GO/PEI-PES

4.1.2 GO

The effect of the number of depositions of GO on the PES substrate surface is studied using a cross flow test loop and SEM images. Three samples were made, using spin coating as discussed before for a low concentration solution of the GO (0.15 mg/ml). In the beginning, the three membranes were tested by diffusion test using the $MgSO_4$ solution. Mg^{2+} and SO_4^{2-} diffusion rate for the PES-bare substrate was used as a reference value. Thus, the ions rejection percentage for the PES-bare PES membrane was considered as the zero percent. The y-axis is the ion concentration of the DI water side measured every 1 min for 10 min using the conductivity meter as shown in Figure 4-4. It was observed that increasing number of layers increased the rejection.

After that, using cross flow test, the three membranes were tested at a pressure of 10 bar with an inlet flow rate of 30 ml/min for $MgSO_4$ solution. The permeate flux decreased significantly as the number of depositions increase, however the salt rejection increase did not exceed 3% (Table 4-1).

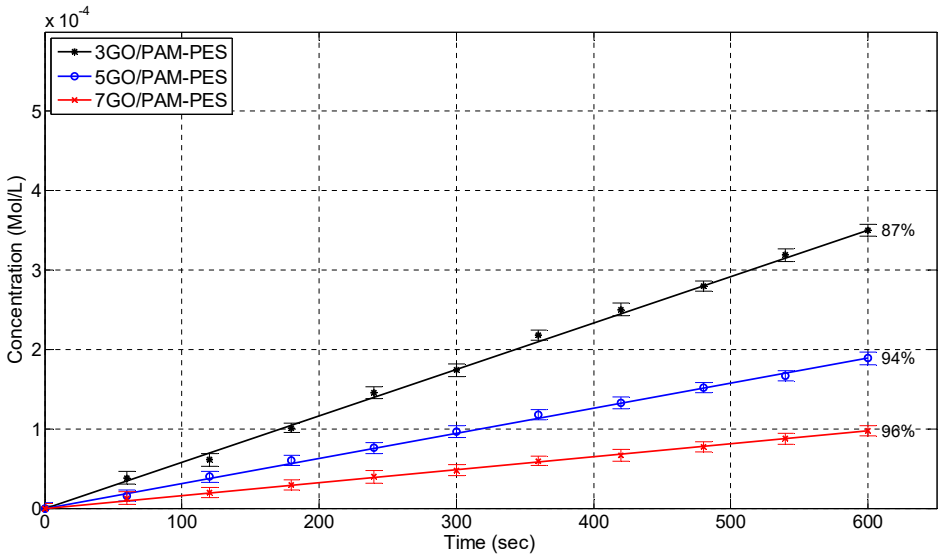

Figure 4-4: Diffusion test results for GO membranes.

Table 4-1: Cross flow test results for GO membranes.

Membrane	Rejection (%)	Permeate Flux (l/m2 hr.)
3GO/PAM-PES	10.0%	607.4
5GO/PAM-PES	11.5%	88.2
7GO/PAM-PES	13.8%	25.3

To understand the previous results, we used SEM to characterize the surface structure of the GO/PAM-PES samples after completing the diffusion study experiment as shown in Figure 4-5. Higher magnification images reveal clearly the presence of cracks. It is believed

that presence of these cracks within GO flakes affected ions rejection percentage, since all three membranes resulted in low rejection.

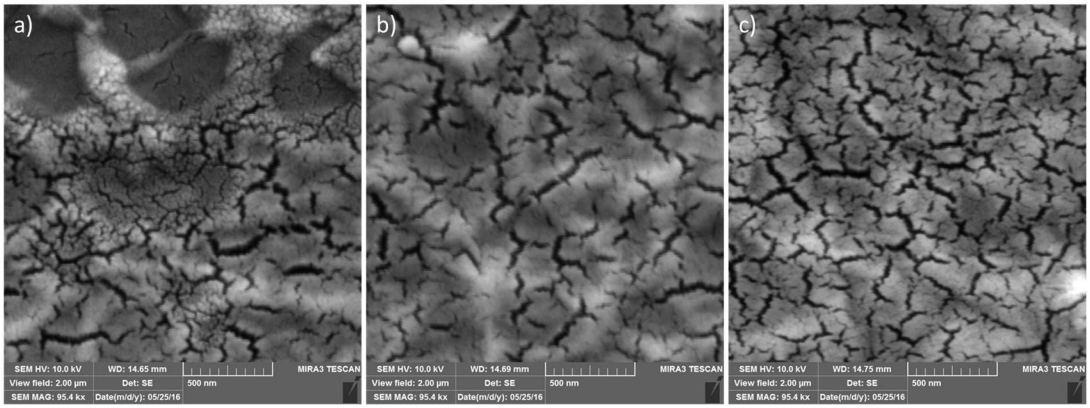

Figure 4-5: SEM results for GO/PAM membranes a) 3GO/PAM-PES, b) 5GO/PAM-PES, c) 7GO/PAM-PES.

4.1.3 Graphene oxide and reduced graphene oxide

2GO/PAM-PES and 2rGO/PAM-PES membranes were compared using diffusion and cross flow test. Subjecting GO membrane to HI vapor will remove some of the hydroxyl, carbonyl and carboxyl groups, which decrease the interlayer spacing as shown in Figure 4-6: Graphene oxide and reduced graphene oxideFigure 4-6. The membranes were prepared using spin coating as discussed before for the high concentration solution of the GO (0.5 mg/ml). The 2rGO/PAM-PES membrane was subjected to HI vapor for 30 min at 80C. In the beginning, the two membranes were tested by diffusion test using the $MgSo_4$ solution. It was observed that the 2rGO/PAM-PES membrane has higher rejection than the 2GO/PAM-PES membrane as shown in Figure 4-7. After that, the membranes were test in the cross-flow test at a pressure of 10 bar and with an inlet flow rate of 10 ml/min using $MgSO_4$ solution. The permeate flux decreases using the 2rGO/PAM-PES membrane.

However, the salt rejection for the 2rGO/PAM-PES membrane was almost double 2GO/PAM-PES membrane (Table 4-2). This is due to the decrease in interlayer spacing and solving the Nano cracks problem. SEM images for the surface of the membrane are shown in Figure 4-8.

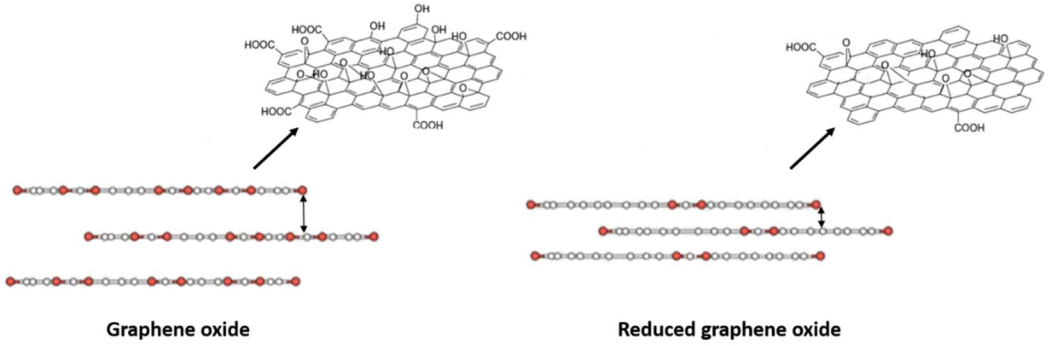

Figure 4-6: Graphene oxide and reduced graphene oxide

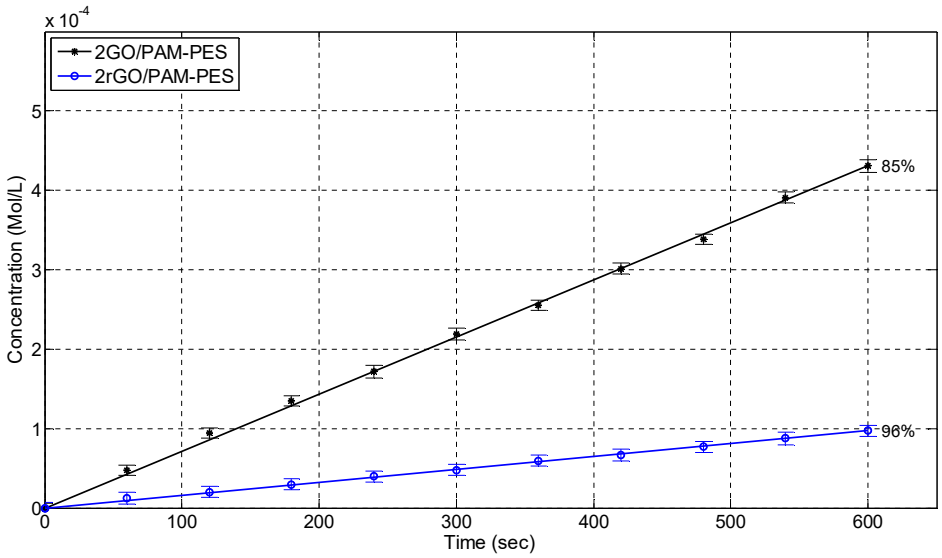

Figure 4-7: Comparsion between 2GO/PAM-PES and 2rGO/PAM-PES membrane using diffusion test.

Table 4-2 : Comparsion between 2GO/PAM-PES and 2rGO/PAM-PES membrane using cross flow test.

Membrane	Rejection (%)	Permeate Flux (l/m2 hr.)
2rGO/PAM-PES	25.48%	128.9
2GO/PAM-PES	13.82%	160.5

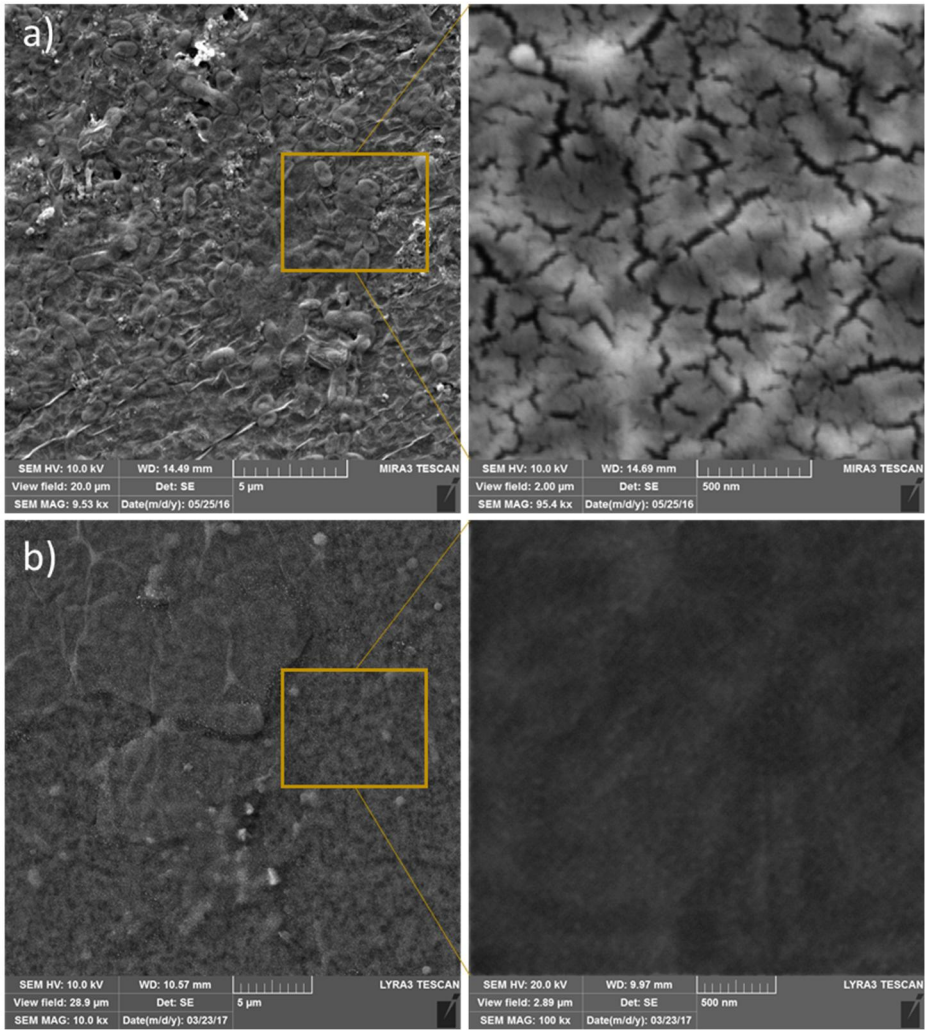

Figure 4-8 : SEM images for a) 2GO/PAM-PES b) 2rGO/PAM-PES

4.1.4 Effect of coating method

To compare between different coating methods, two samples were made using spin coating (2rGO/PAM-PES, 4rGO/PAM-PES) where 2 and 4 represents the number of GO depositions, one for each dead end and dip coating and tested using cross flow test. The spin coating was discussed before, whereas the dead-end samples were coated with PAM using spin coating. Then the membrane was placed in a dead-end cell where a solution of 1 mg of GO and 20 ml of DI water was placed under air pressure of 20 bar until all water

passes leaving the GO flakes on the membrane surface (about 20 min) and it was then left to dry for 24 hours. For the dip coating membrane, the PES membrane was coated with PAM using spin coating after that 2 ml of the high concentration GO solution (0.5 mg/ml) were prepared and placed over the membrane until it dries out. All the four membranes were subjected to HI vapor for 1 hour. Using the $MgSO_4$ solution over the cross-flow test at 10 bar and 10 ml/min as inlet flow rate, it was observed that the spin coating yields better results for both rejection and permeate flux as shown in Table 4-3. The flux for the dead end and 4rGO/PAM-PES decreased significantly since their thicknesses were much higher than 2rGO/PAM-PES.

Table 4-3: Comparison between spin coating, dead end and dip coating using cross flow test

Membrane	Method	GO Concentration	Rejection (%)	Permeate Flux (l/m2 hr)
2rGO/PAM-PES	Spin coating	0.5 mg/ml	25.48	128.9
4rGO/PAM-PES	Spin coating	0.5 mg/ml	26.62	9.4
rGO/PAM-PES	Dead End	1 mg	24.89	13.03
rGO/PAM-PES	Dip coating	1 mg	19.30	70.5

4.1.5 Deposition method

Two methods of deposition were used for comparison. The first one is the layer by layer (LBL) method; one deposition of PAM is followed by one deposition of GO for two times (PAM-GO-PAM-GO), this membrane is referred as 2rGO/2PAM-PES where 2 represents number of depositions. The second was one deposition of PAM then two depositions of GO (PAM-GO-GO), this membrane is referred as 2rGO/PAM-PES where 2 represents

number of depositions of GO as shown in Figure 4-9. The GO solution concentration used was 0.5mg/ml, and both membranes were subjected to HI vapor for 30 min at 80ºC. In the beginning, the two coated membranes were tested in a diffusion test cell using the $MgSO_4$ solution. The membranes were tested at 10 bar with 10 ml/min inlet flow rate using $MgSO_4$ solution. The results showed that LBL method yields lower ion rejection using the diffusion test cell as shown in Figure 4-10. Moreover, the cross-flow test results show that 2rGO/PAM-PES has higher rejection whereas, the permeate flux is lower than 2rGO/2PAM-PES as shown in Table 4-4.

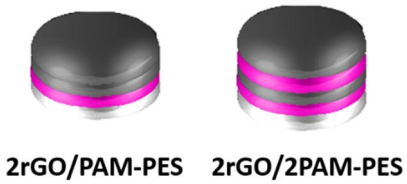

Figure 4-9: 2rGO/PAM-PES and 2rGO/2PAM-PES

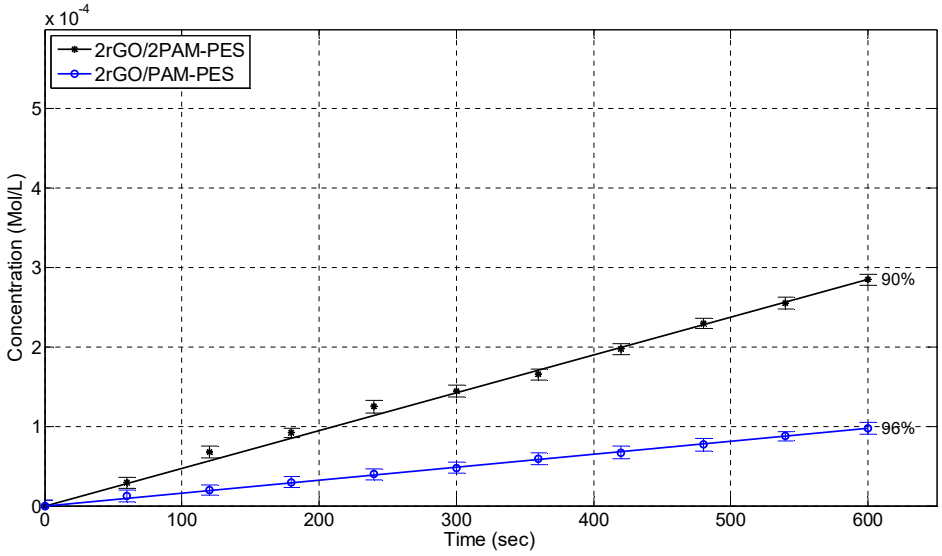

Figure 4-10: Comparsion between LBL and one layer PAM using diffusion test

Table 4-4: Comparsion between LBL and one layer PAM using cross flow test

Membrane	Rejection (%)	Permeate Flux (l/m2 hr)
2rGO/PAM-PES	25.48	128.9
2rGO/2PAM-PES	3.06	386.2

4.1.6 Effect of number of layers

The effect of number of layers was investigated by cross flow test. Three membranes were coated with 1, 2 and 4 depositions using the high concentration GO solution (0.5mg/ml) and subjected to HI vapor for 30min at 80ºC. In the beginning, the three membranes were tested by diffusion test using the $MgSO_4$ solution. It was observed that increasing number of layers increased the rejection as shown in Figure 4-11. After that, using cross flow test, it was showed that increasing the number of layers decreased the permeate flux significantly, whereas the rejection increased with increasing number of depositions from 1 to 2. However, 2 and 4 depositions yielded almost the same results as shown in Table 4-5. Thus, there is no need to do more than 2 depositions since it decreased the flux and had a small effect on the rejection.

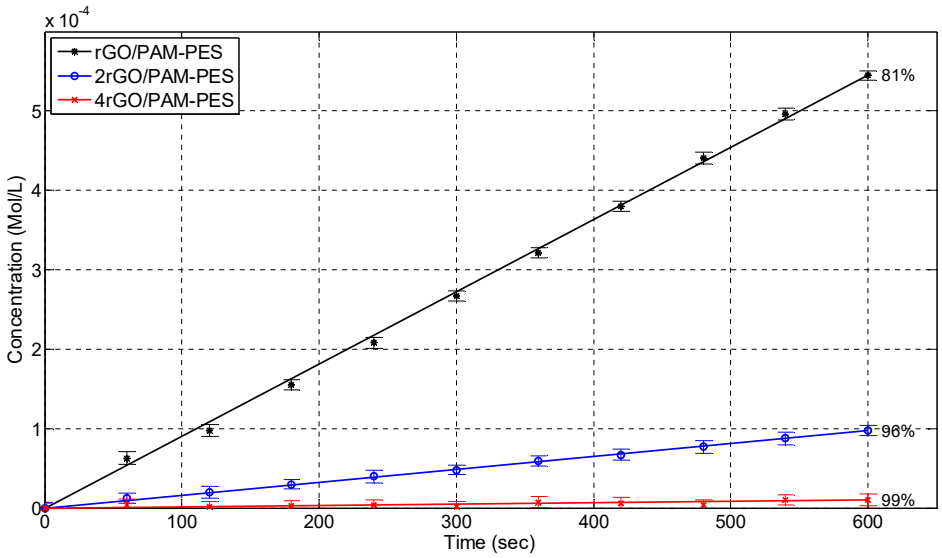

Figure 4-11: Effect of number of layers on rejection using diffuion test.

Table 4-5: Effect of number of layers on rejection and flux using cross flow test.

Membrane	Rejection (%)	Permeate Flux (ml/m2 sec)
rGO/PAM-PES	2.70	946.8
2rGO/PAM-PES	25.48	128.9
4rGO/PAM-PES	26.62	9.4

4.1.7 Effect of reduction time and the HI solution temperature

Interlayer spacing can be controlled through the reduction process. Subjecting the GO membrane to HI vapor removes some of the hydroxyl, carbonyl and carboxyl groups, which decreases the interlayer spacing, thus the 2rGO/PAM-PES membrane was subjected to HI vapor for different period to study the effect of reduction time over the interlayer spacing.

In this experiment, the membrane was subjected to HI vapor at two different temperatures (25ºC, 80ºC). The prepared 2rGO/PAM-PES membranes were tested using a diffusion cell for ten minutes using $MgSO_4$ solution and compared with 2GO/PAM-PES. Mg^{2+} and SO_4^{2-} diffusion rate for the PES-bare substrate was used as a reference value. Thus, the ions rejection percentage for the PES-bare PES membrane was considered as the zero percent. The y-axis is the ion concentration of the DI water side measured every 1 min for 10 min using the conductivity meter.

The results showed that the rejection increased with increasing the reduction time. This is due to decreasing the interlayer spacing. The rejection increased by 7% with increasing reduction time for the low concentration (0.15mg/ml) solution at ambient temperature, whereas the rejection increased by 14% with increasing reduction time at 80ºC as shown in Figure 4-12.

However, for the higher concentration (0.5mg/ml), the 24 hr. at 25ºC and 45min and 1 hr. at 80ºC 2rGO/PAM-PES membranes blocked $MgSO_4$ as shown in Figure 4-13. Therefore, HI temperature have an impact on ion rejection whereas, the GO concentration is the significant parameter that affect the ion rejection. The effect of water contact angle on reduction time was studied for the high concentration 2rGO/PAM-PES membrane reduced at HI temperature of 80ºC. It was found that increasing reduction time increased the contact angle as shown in Figure 4-14.

a)

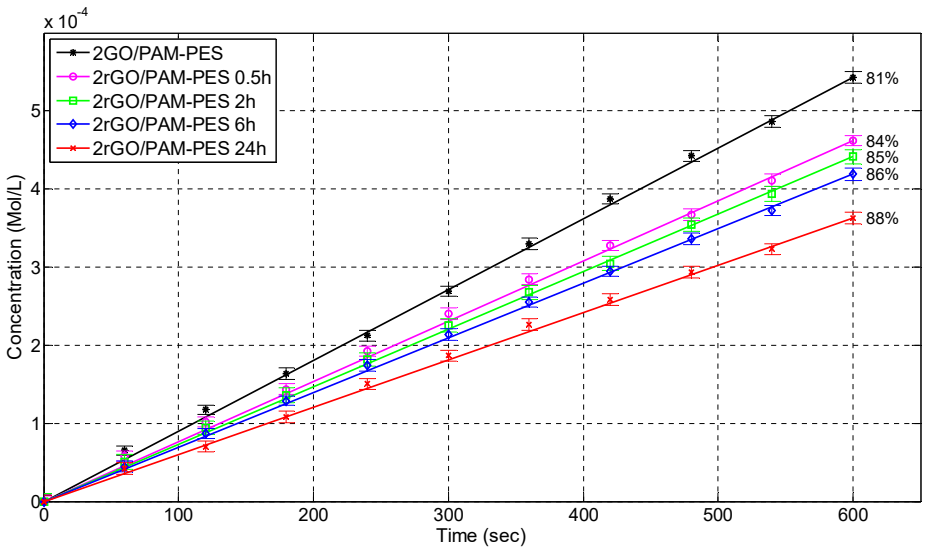

b)

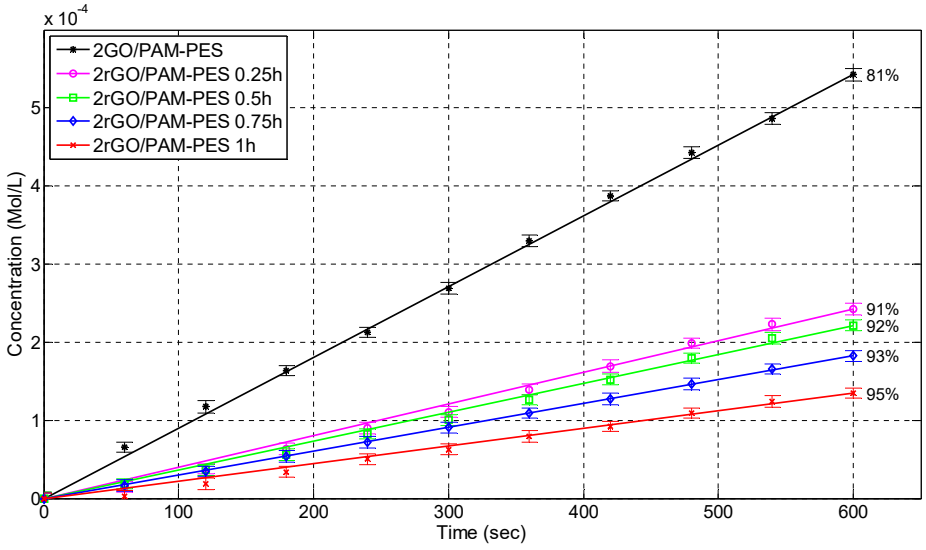

Figure 4-12: Effect of reduction time and HI temperature at low concentration using Diffusion test a) 25C, b) 80C.

a)

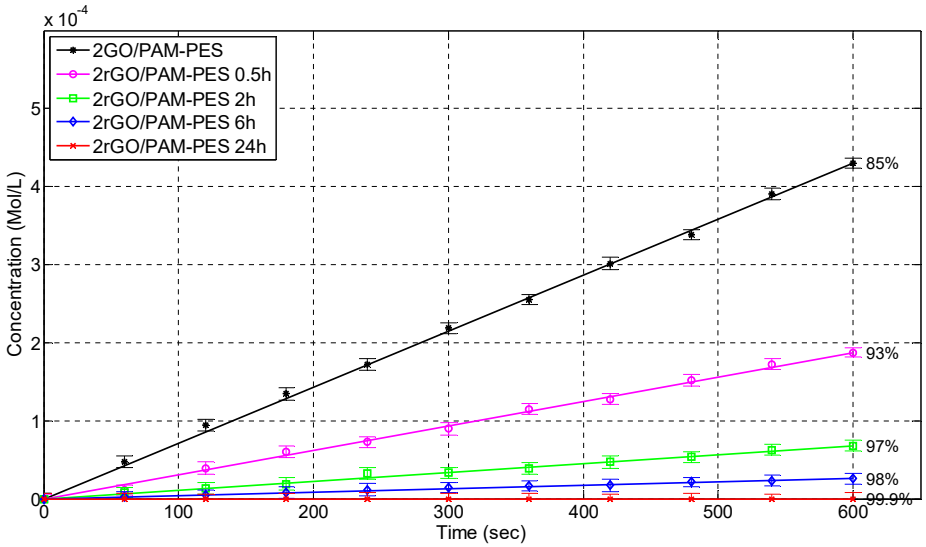

b)

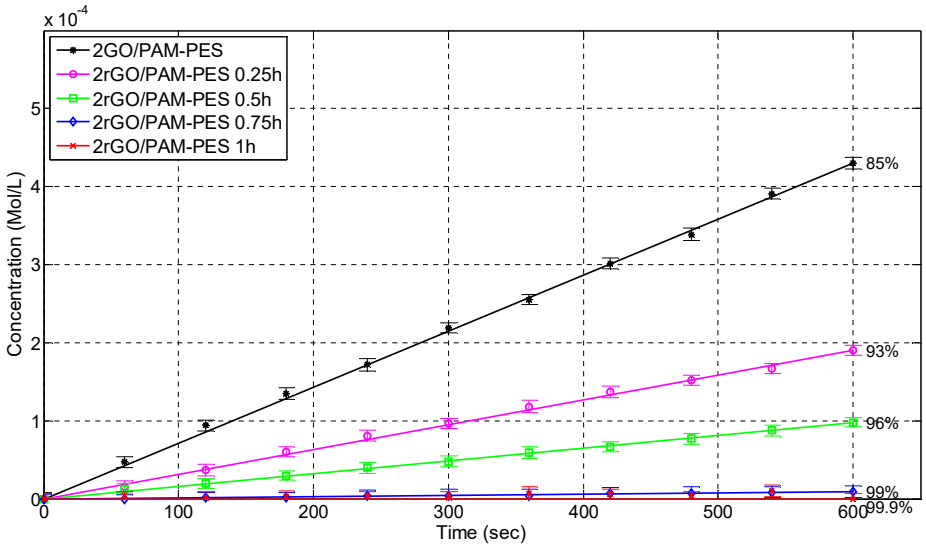

Figure 4-13: Effect of reduction time and HI temperature at High concentration using Diffusion test a) 25C, b) 80C.

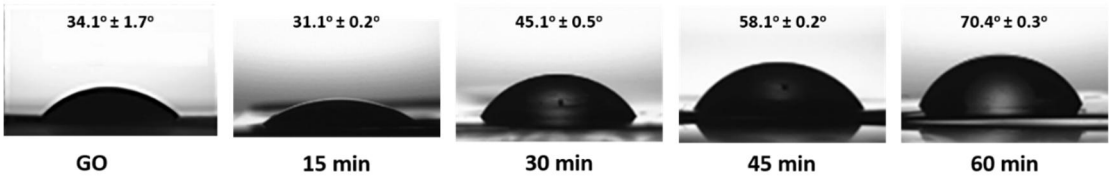

Figure 4-14: Effect of reduction time on water contact angle for 2rGO/PAM-PES membrane reduced at HI temperature 80ºC.

4.2 Summary

The effect of deposition method, GO concentration, polyelectrolyte, coating method, number of layers and reduction time were investigated. PAM must be used as a cross linker between the PES and the GO. It was shown that the GO thickness is the most significant parameter that affects the ion rejection. To estimate the interlayer spacing, diffusion test was performed using $MgSO_4$ solution and compared with KCL solution. The hydrated diameter for K^+ and CL^- is 0.66 nm, whereas the Mg^{2+} is 0.86 nm and SO_4^{2-} is 0.758 nm as shown in

Table 1-2. The 24 hr. at 25C and 45min and 1 hr. at 80C 2rGO/PAM-PES membranes blocked $MgSO_4$ as shown in Figure 4-15. However, for the KCL solution, the rejection was 55.8% and 63.9% respectively[131]. Thus, the interlayer spacing is between 0.758 nm and 0.66 nm which make these membranes has the potential for eliminating the divalent ions.

a)

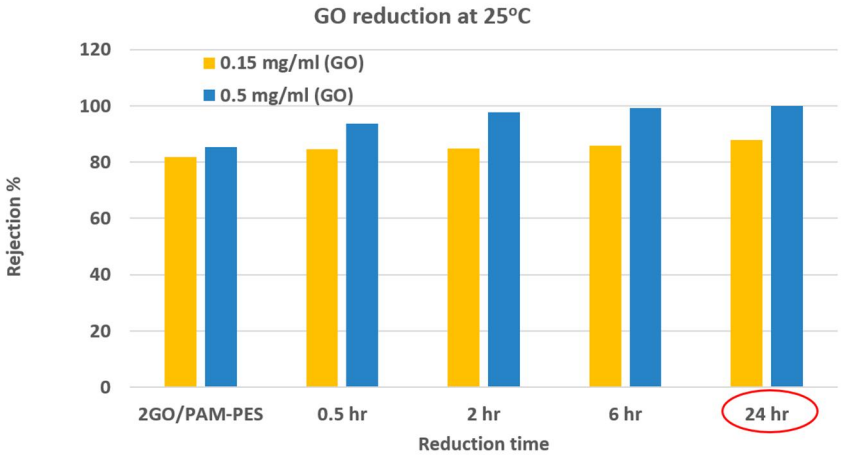

b)

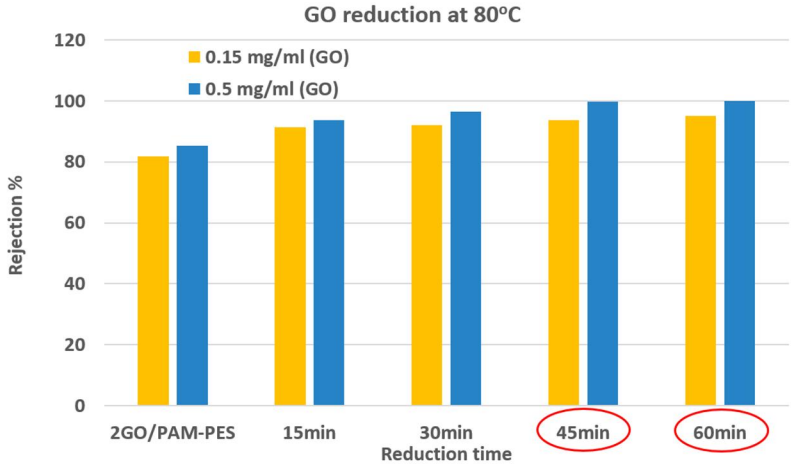

Figure 4-15: Effect of GO concentration, reduction time and the HI solution temperature a) 25^{O}C, b) 80^{O}C on ion rejection.

CHAPTER 5

CROSS FLOW TEST

5.1 Introduction

Brine temperature limitations in thermal seawater desalination techniques (e.g., MSF and MED) are dependent on the presence and concentrations of divalent ions. Temperature, pH, TDS, and ion concentrations influence the rate of scale formation. The TBT is generally less than approximately 112°C in MSF and 66°C in MED. There are two types of scalants in MSF and MED technologies: alkaline scales caused by calcium carbonate and magnesium hydroxide and non-alkaline scales caused by calcium sulfate [4]. Therefore, eliminating Mg, Ca and SO_4 will increase the top brine temperature (TBT) in thermal seawater desalination plants. The aim of this chapter is to test the 45min at 80C 2rGO/PAM-PES membrane using cross flow arrangement and compare it with commercial NF using $MgSO_4$ Solution, $CaSO_4$ solution and real seawater.

5.2 Tested Membranes

2rGO/PAM-PES membrane, commercial Nanofiltration (NF270), and NF-GO membrane were tested. The NF270 membrane with an area 4*4cm was washed by DI water then placed in spin coater. After that, 1 ml of PAM solution was added and left to spin at 200rpm for 2 mins then 3000rpm for 6 mins. It was then washed by 2ml of DI water and placed on the spinner at 3000rpm for 6 mins. After that, 1ml of GO solution (0.5mg/ml)

was deposited over the membrane at 200rpm for 2 mins then 3000rpm for 6 mins. The difference between NF-GO and 2rGO/PAM-PES membrane is that GO on the NF 270 is to enhance the antifouling and antibacterial properties while the NF270 is the selective layer. However, for 2rGO/PAM-PES membrane, the rGO is the active selective layer beside it's high antifouling and antibacterial properties.

The effect of pressure and the inlet flow rate on the rejection and the permeate flux were studied. The rejection and flux were measured at five values of pressure starting with 5 bar with step 2.5 and four value of inlet flow rate starting with 2.5ml/min with step 2.5. The rejection was measured by the conductivity meter. whereas, the permeate flux was calculated by dividing the measured output volume over time and membrane effective area.

5.3 Cross flow test for $MgSO_4$ and $CaSO_4$

Magnesium sulfate solution was prepared by adding15g of $MgSO_4$ to 5L of DI water and was stirred for 30min to make a 3000ppm $MgSO_4$ solution. Whereas, calcium sulfate solution was prepared by adding12.5g of $CaSO_4$ to 5L of DI water and was stirred for 30min to make a 2500ppm $CaSO_4$ solution.

5.3.1 Effect of pressure

2rGO/PAM-PES membrane was tested and compared with commercial Nanofiltration (NF270), and NF-GO membrane at 10ml/min as inlet flow rate. Increasing pressure increased both the rejection and the permeate flux. NF270 gives the highest permeate flux and rejection for Mg^{2+} and SO_4^{2-} ions. Whereas, NF-GO had more ion rejection than 2rGO/PAM-PES except at 15bar. 2rGO/PAM-PES ion rejection increases significantly with pressure as shown in Figure 5-1. After that, $CaSO_4$ solution was tested for the three

membranes at 10ml/min as inlet flow rate. Increasing pressure will increase both the rejection and the permeate flux. NF270 gives the lowest rejection for Ca^{2+} and SO_4^{2-} ions. Whereas, NF-GO had more ion rejection than 2rGO/PAM-PES at low pressure while, 2rGO/PAM-PES had the highest rejection at high pressure (more than 10 bar). 2rGO/PAM-PES had almost the same rejection for both $MgSO_4$ and $CaSO_4$ solutions. Furthermore, NF-GO gives the highest permeate flux as shown in Figure 5-2. The low rejection for $CaSO_4$ solution using NF270 is due to the concentration polarization, where high Ca^{2+} concentration in the layer near the membrane surface, thus more Ca^{2+} ions tend to diffuse through the membrane. 2rGO/PAM-PES had almost the same rejection for $MgSO_4$ and $CaSO_4$ solution this due that Mg^{2+} and Ca^{2+} ions had almost the same hydrated diameter [10].

a)

b)

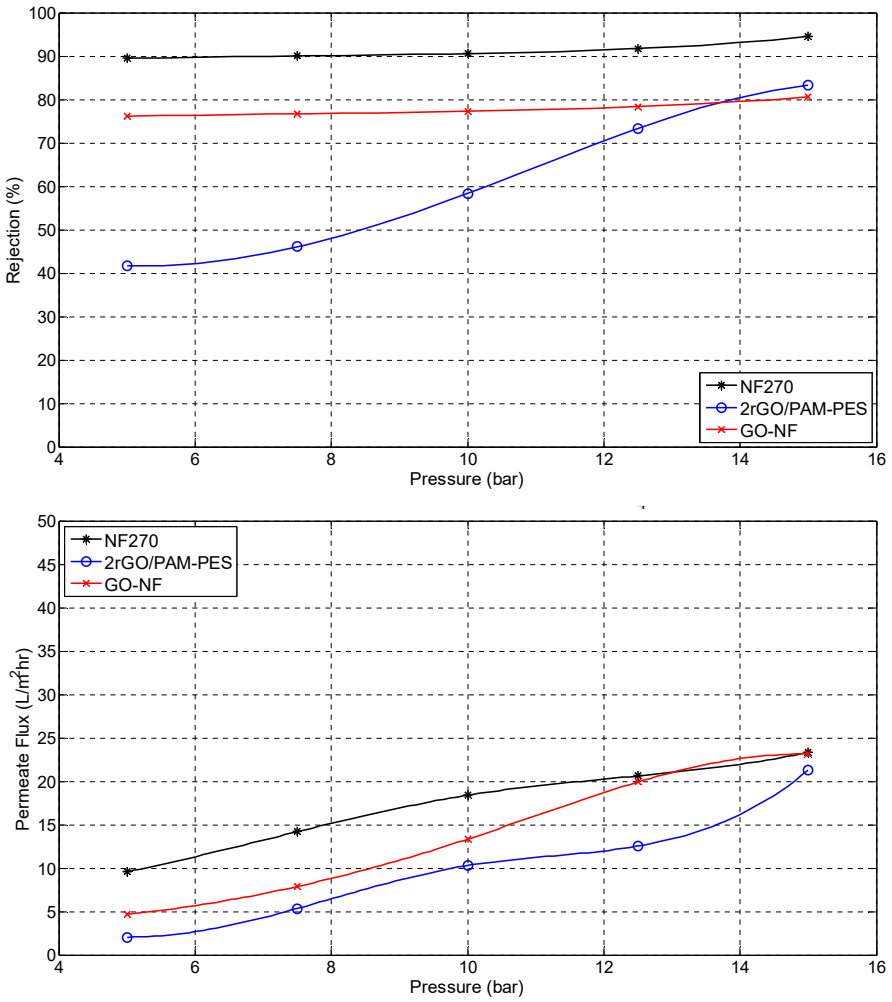

Figure 5-1: Effect of pressure using $MgSo_4$ solution on the a) rejection, b) permeate flux.

a)

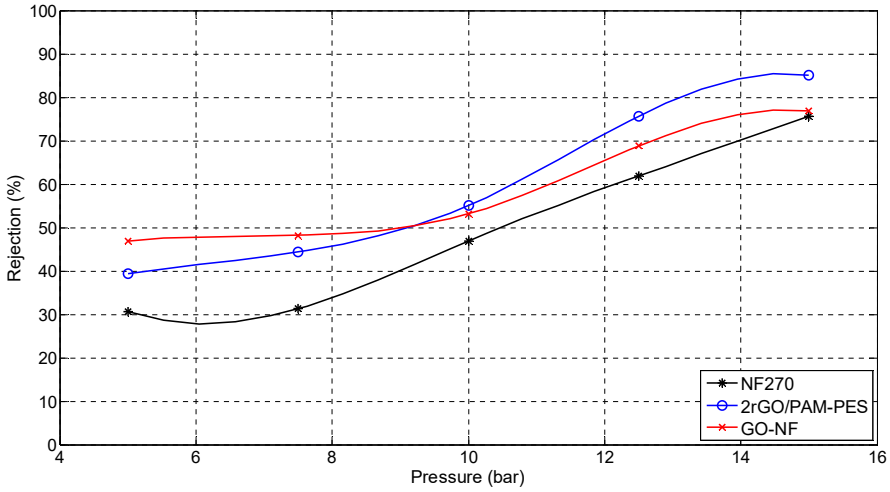

b)

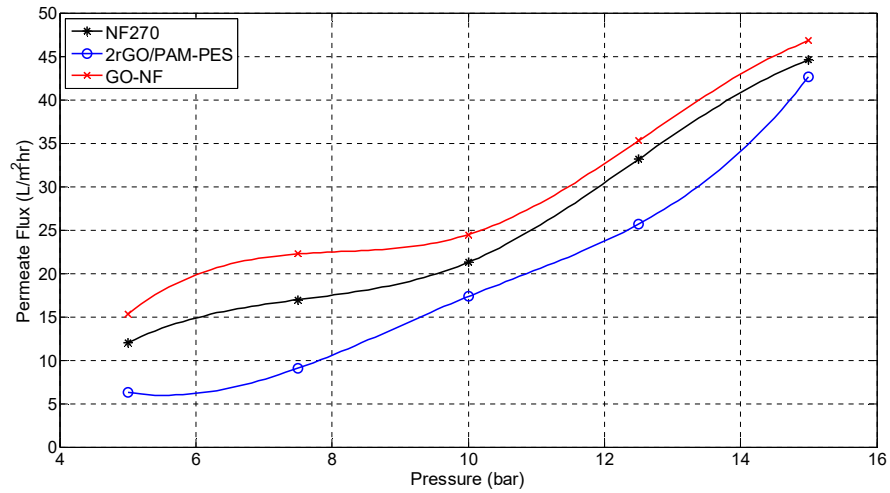

Figure 5-2: Effect of pressure using $CaSo_4$ solution on the a) rejection, b) permeate flux.

5.3.2 Effect of inlet flow rate

The effect of inlet flow rate on the rejection and permeate flux is studied for 2rGO/PAM-PES, and compared with NF270, and NF-GO membrane at 10 bar. Increasing inlet flow rate, slightly increases the rejection. NF270 results in the highest permeate flux and rejection for Mg^{2+} and SO_4^{2-} ions. The rate of increase in the permeate flux decreases as the inlet flow rate increased as shown in Figure 5-3. After that, $CaSO_4$ solution was tested

for the three membranes at 10 bar. Increasing inlet flow rate, slightly increases the rejection. 2rGO/PAM-PES yields the highest rejection for Ca^{2+} and SO_4^{2-} ions. NF-GO yielded high rejection close to 2rGO/PAM-PES. The permeate flux rate increases with the increase in the inlet flow rate as shown in Figure 5-4.

a)

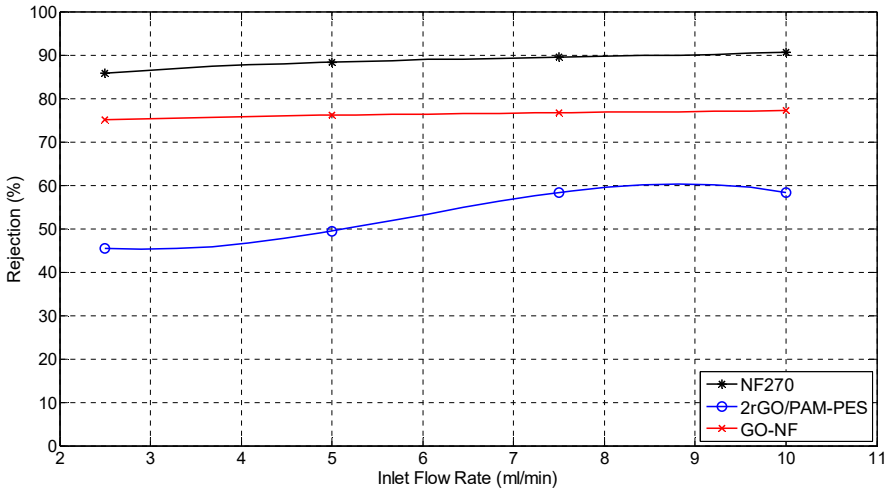

b)

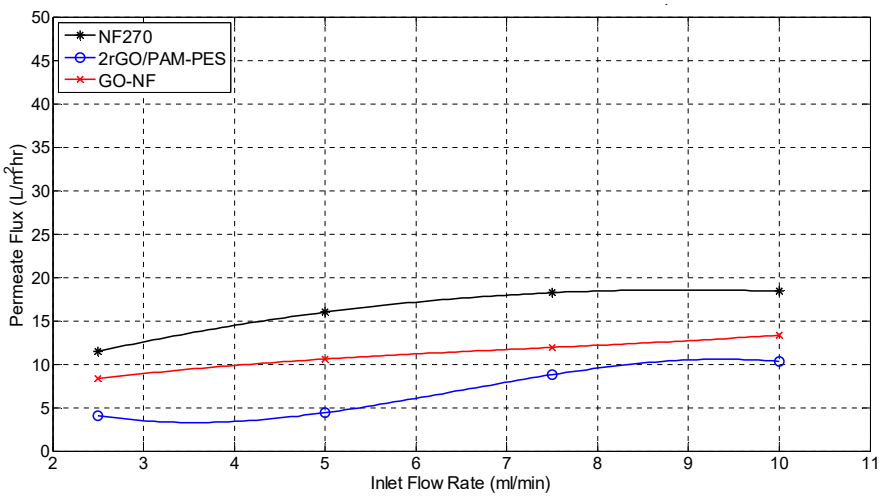

Figure 5-3: Effect of inlet flow rate using $MgSo_4$ solution on the a) rejection, b) permeate flux.

a)

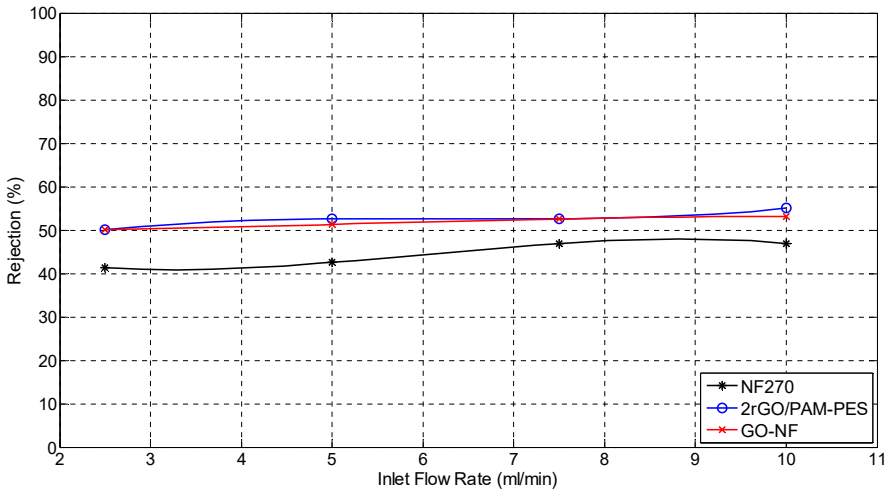

b)

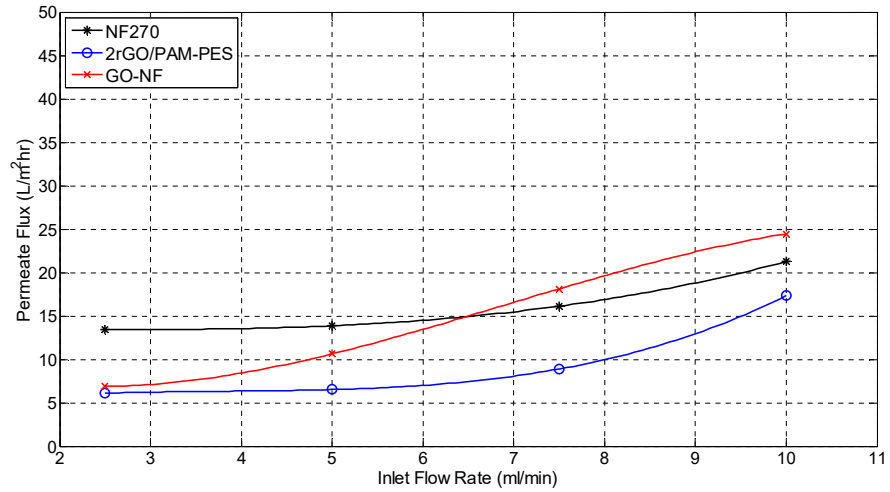

Figure 5-4: Effect of inlet flow rate using $CaSO_4$ solution on the a) rejection, b) permeate flux

5.4 Cross flow test for seawater

The effect of pressure and the inlet flow rate on the rejection and the permeate flux were studied using real seawater. The rejection of the cations was measured by Inductively coupled plasma mass spectrometry (ICP-MS), whereas, the anions was measured by Ionic

chromatography (IC). The permeate flux was calculated by dividing the measured output volume over time and membrane effective area. The seawater composition is represented in Table 5-1.

Table 5-1: Composition of Used seawater

Ions	Ppm
Na^{+}	13905
Mg^{2+}	1564
K^{+}	400
Ca^{2+}	520
Cl^{-}	27917
SO_4^{2-}	3312

5.4.1 Effect of pressure

2rGO/PAM-PES membrane was tested and compared with commercial Nanofiltration (NF270), and NF-GO membrane at 10ml/min as inlet flow rate. 2rGO/PAM-PES yields the highest rejection for Mg^{2+} and Ca^{2+} ions while NF270 yielded the highest rejection for SO_4^{2-} ions. Whereas, NF-GO had more Ca rejection than NF270 while for Mg^{2+} both almost had the same rejection. 2rGO/PAM-PES ion rejection increases significantly with pressure as shown in Figure 5-5.

The mechanisms responsible for solute transport through NF membranes are convection, diffusion, and electro-migration [91]–[93]. The low rejection for Ca^{2+} ions using NF270 is due to the concentration polarization, where high Ca^{2+} concentration in the layer near the membrane surface, thus more Ca^{2+} ions tend to diffuse through the membrane.

On the other hand, rGO membrane water passes between interlayer spacing. Therefore ion rejection depends on the interlayer spacing and electrostatic interactions [20]. 2rGO/PAM-PES had almost the same rejection for Mg^{2+} and Ca^{2+} ions, while SO_4^{2-} ions had higher rejection this due electrostatic interaction as the GO and SO_4^{2-} ions are negatively charged. However, at high pressure the Mg^{2+}, Ca^{2+} and SO_4^{2-} ions had almost the rejection as shown in Figure 5-5.

a)

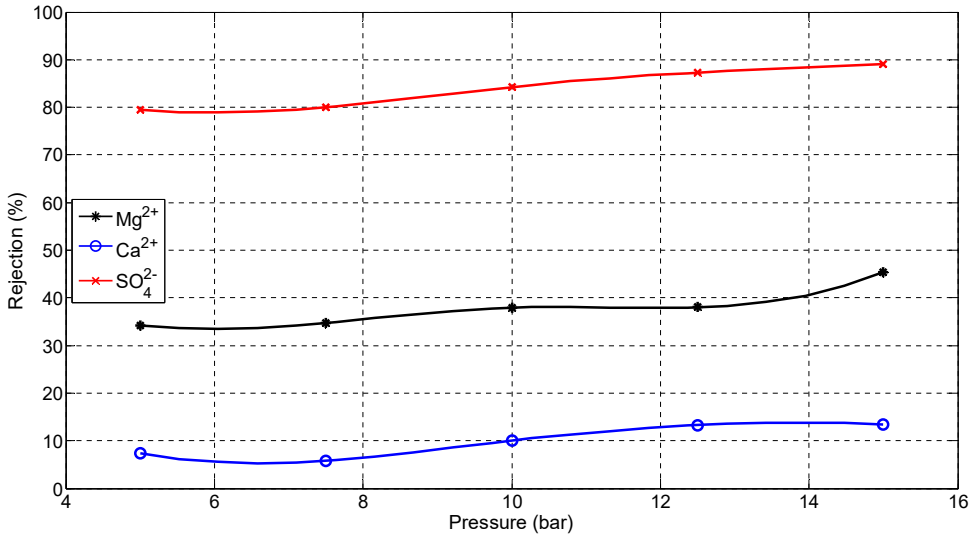

b)

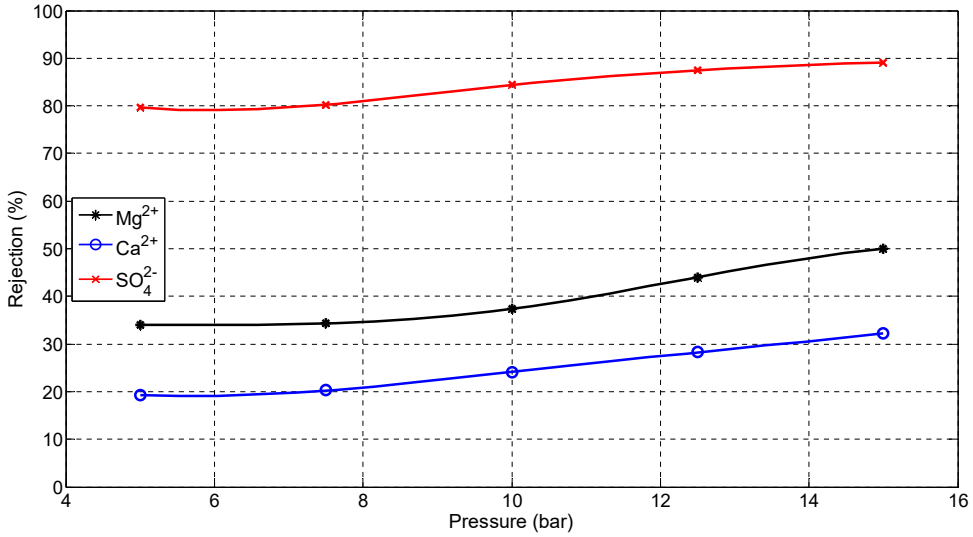

c)

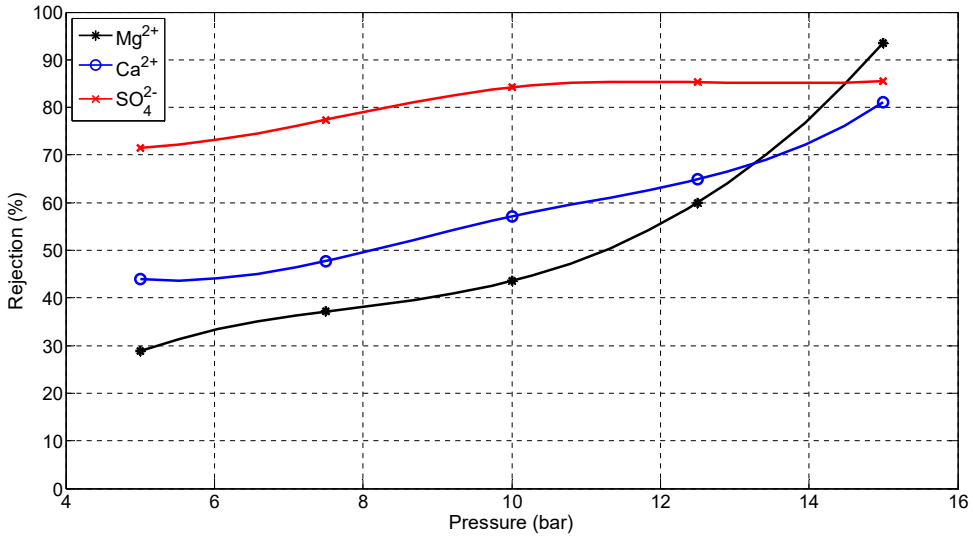

Figure 5-5: Effect of pressure using seawater on the rejection a) NF270, b) NF-GO, c) 2rGO/PAM-PES.

5.4.2 Effect of inlet flow rate

The effect of inlet flow rate on the rejection and permeate flux was studied for 2rGO/PAM-PES, and compared with NF270, and NF-GO membrane at 10 bar. Increasing inlet flow rate, slightly increased the rejection. 2rGO/PAM-PES yielded the highest rejection for Ca^{2+} ions while for Mg^{2+} the rejection increased significantly with inlet flow

rate. NF-GO yielded high Mg^{2+} rejection close to NF270. NF270 had the lowest Ca^{2+} rejection as shown in Figure 5-6.

a)

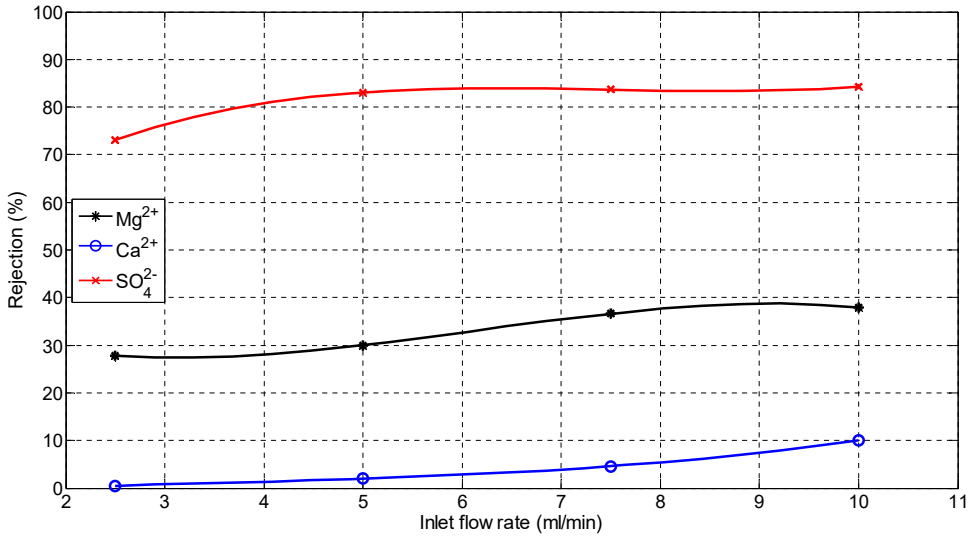

b)

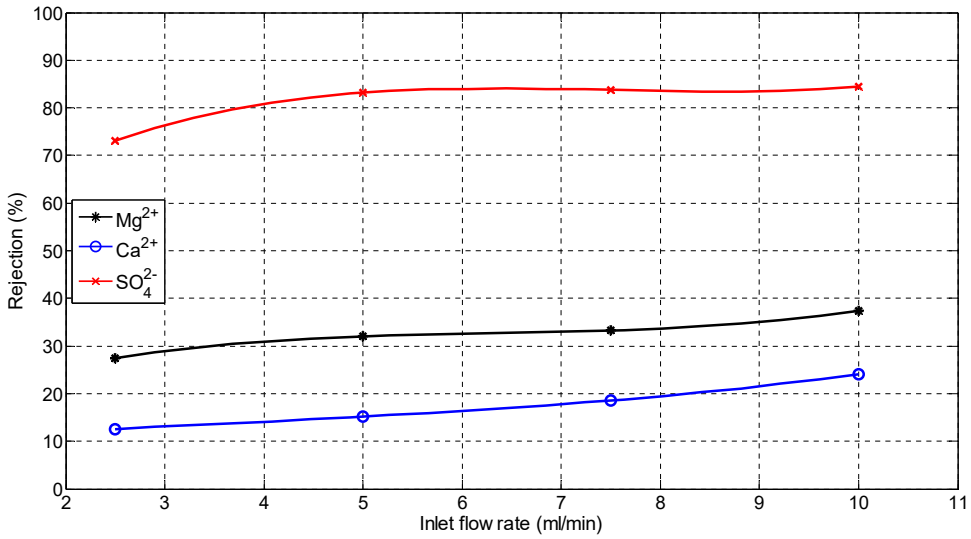

c)

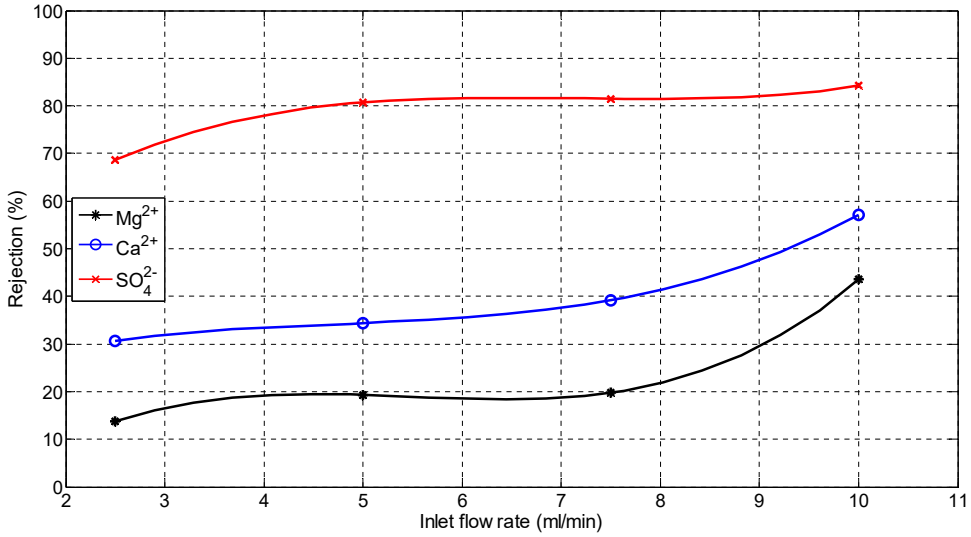

Figure 5-6: Effect of inlet flow rate using seawater on the rejection a) NF270, b) NF-GO, c) 2rGO/PAM-PES.

5.5 Characterization of the 2rGO/PAM-PES membrane surface

Figure 5-7 shows the SEM images and EDX results for the membrane surface before and after the cross-flow test using seawater. Lower magnification SEM images showed that deposition cycles provide full coverage of GO on the PES substrate surfaces. The SEM images shows that there is no change in the surface after test, whereas, the EDX results shows some ions that are attached to the surface; chloride, potassium and magnesium however there were no calcium and sodium attached on the surface.

a)

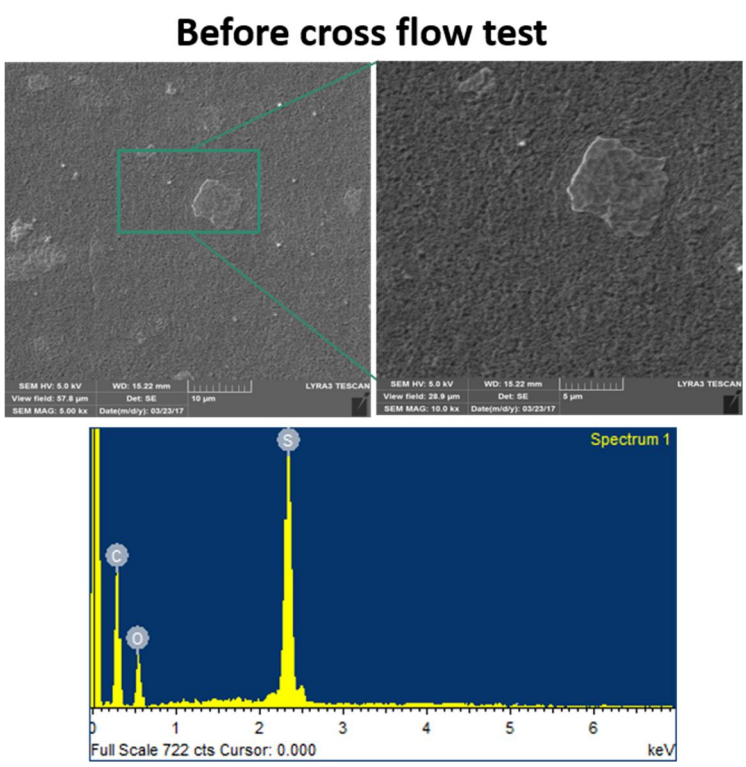
Before cross flow test
SEM HV: 5.0 kV
WD: 15.22 mm
LYRA3 TESCAN
View field: 57.6 µm
Det: SE
10 µm
SEM MAG: 5.00 kx
Date(m/d/y): 03/23/17
SEM HV: 5.0 kV
WD: 15.22 mm
LYRA3 TESCAN
View field: 28.9 µm
Det: SE
5 µm
SEM MAG: 10.0 kx
Date(m/d/y): 03/23/17
Spectrum 1
S
C
O
0
1
2
3
4
5
6
Full Scale 722 cts Cursor: 0.000
keV

b)

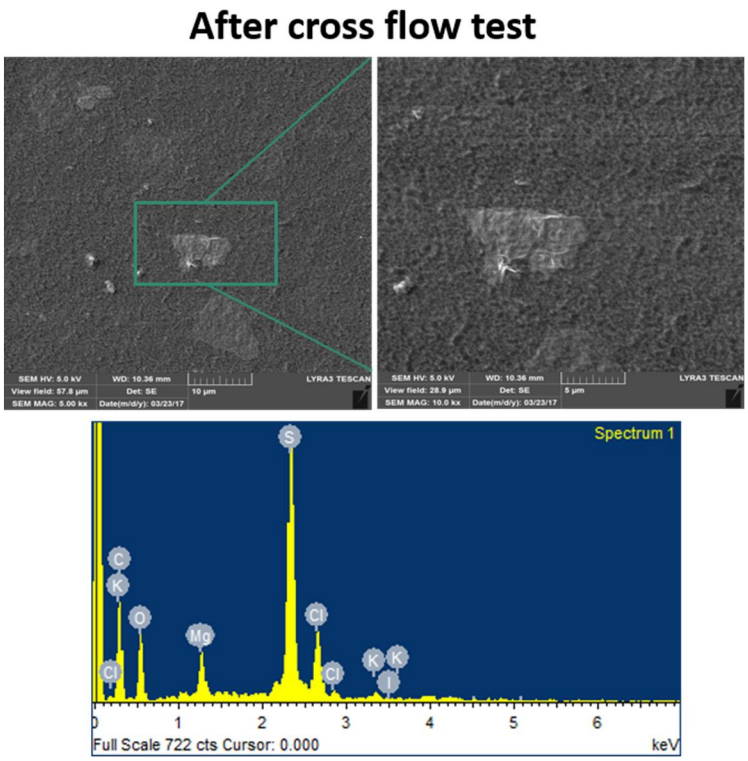

Figure 5-7: SEM results for 2rGO/PAM-PES membranes a) before cross flow test, b) after cross flow test.

5.6 Top Brine Temperature (TBT)

5.6.1 PhreeQC

PHREEQC stands for PH REdox EQuilibrium in C language, and is a widely used geochemical modeling software available from the USGS. Details can be found in (PARKHURST,1995). It is available for download in versions for Windows and UNIX.

It was designed to perform a wide variety of low-temperature aqueous geochemical calculations based on an ion-association aqueous model, and has capabilities to:

1. Speciation and Saturation Index calculations;

2. Batch reaction and one-dimensional (1D) transport calculations involving reversible reactions (including aqueous, minerals, gas, solid-solution, surface-complexation, and ion exchange equilibrium) and irreversible reactions (including specified mole transfer of reactants, kinetically controlled reactions, mixing of solutions and temperature changes);
3. Inverse modeling, which finds sets of mineral and gas mole transfers that considers differences in composition between waters.

5.6.2 Saturation index

Saturation index (SI) indicates the state of dis-equilibrium with respect to a given mineral. SI is expressed as

$$SI = \log(\frac{IAP}{K})$$

When a mineral is in equilibrium within a solution, the SI is zero: a negative SI indicates

under saturation, and a positive SI, supersaturation. The Ion Activity Product (IAP) is calculated per

$$IAP = \frac{C^c D^d}{A^a B^b}$$

where A, B, C and D are activities of the ions and a, b, c and d denote the respective stoichiometric values. The interpretation of IAP is the following:

1. IAP > K: The reaction is progressing from left to right, producing more products. This state is also described to as supersaturated.

2. IAP = K: The reaction is in equilibrium, and there is equal flow of reaction to the right and to the left
3. IAP < K: The reaction is progressing from right to left, producing more reactants. This state is also described as under saturated.

With the SI approach, it is possible to predict the reactive mineralogy from the water composition. If the SI for a mineral is less than zero, the aqueous solution is under saturated with respect to that mineral - which corresponds to the state where the mineral may dissolve to reach equilibrium concentrations. If the SI is greater than zero, then more mineral may precipitate from the aqueous solution (oversaturated). To conclude, when the SI is close to zero (it is ok to consider a small range of values to be in equilibrium), the water is in near-saturation with respect to that mineral (ALLEY, 1993).

5.6.3 TBT for the testes membrane

Using Phreeqc we were able to calculate the saturation index for the NF, NF-GO and 2rGO/PAM-PES permeates at different pressure as shown in Figure 5-8. When the saturation index is zero, the solution is in equilibrium the corresponding temperature will be the top brine temperature. The top brine temperature before treatment was 102ºC without antiscalant after the treatment TBT reaches 148ºC using NF, 160ºC using NF-GO and 166ºC using rGO membrane as shown in Figure 5-9.

a)

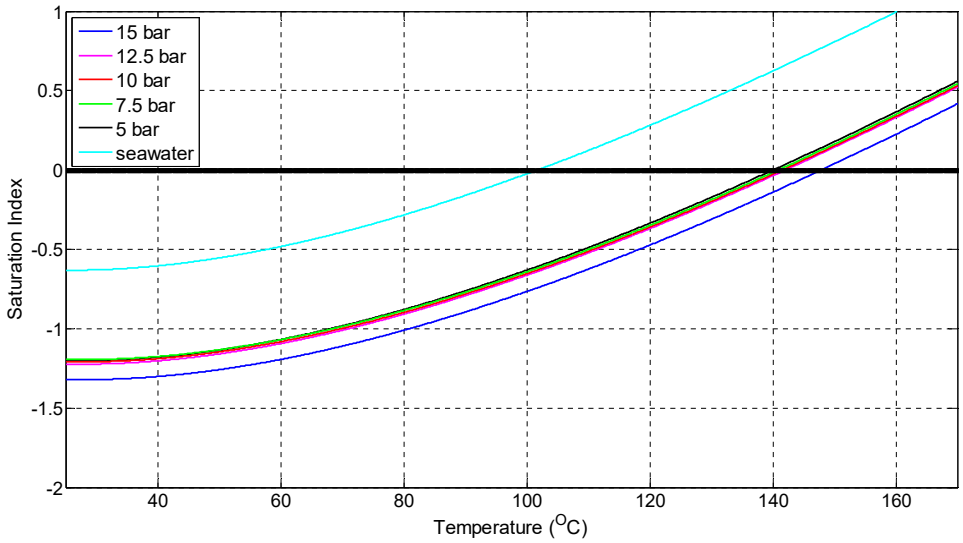
15 bar
12.5 bar
10 bar
7.5 bar
5 bar
seawater
Saturation Index
Temperature (OC)
1
0.5
0
-0.5
-1
-1.5
-2
40
60
80
100
120
140
160

b)

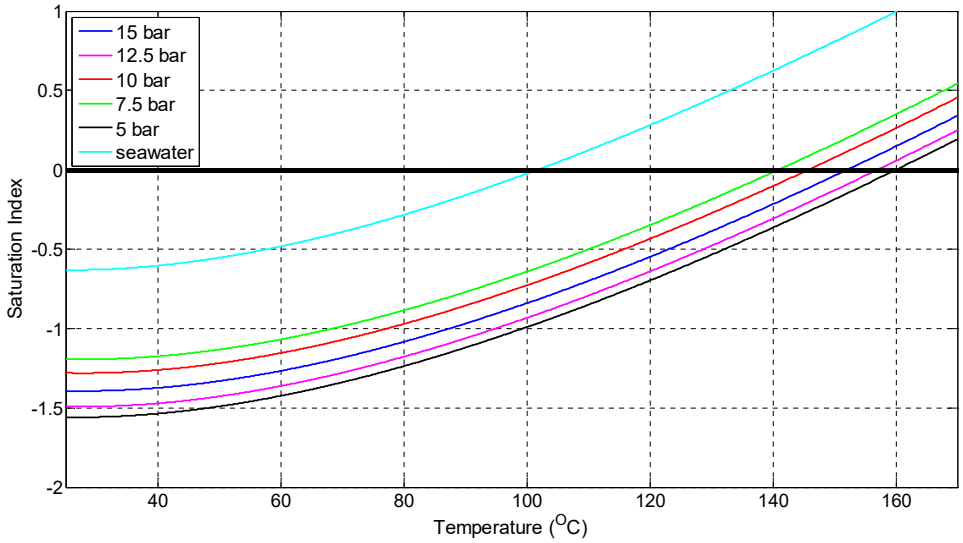
15 bar
12.5 bar
10 bar
7.5 bar
5 bar
seawater
Saturation Index
Temperature (OC)
1
0.5
0
-0.5
-1
-1.5
-2
40
60
80
100
120
140
160

c)

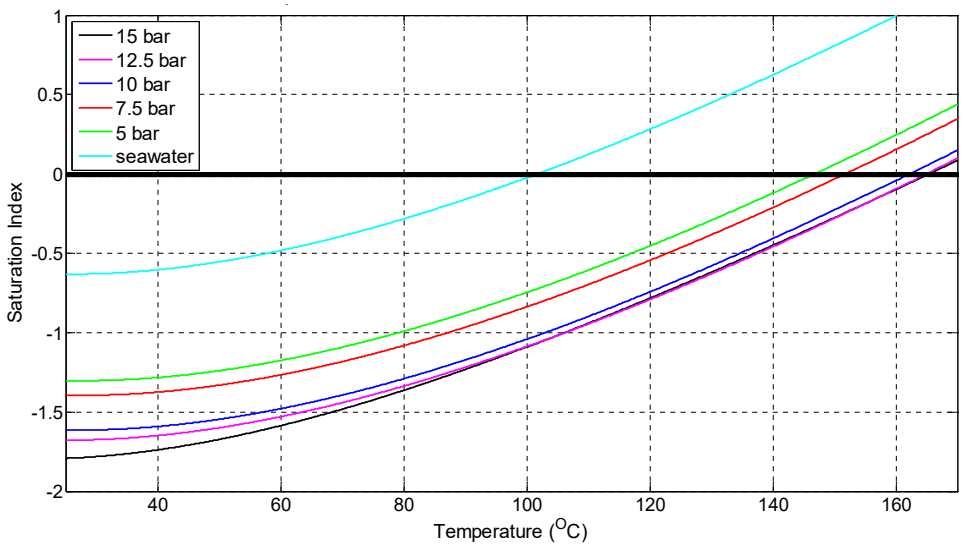

Figure 5-8: Effect of pressure on the saturation index a) NF270, b) NF-GO, c) 2rGO/PAM-PES.

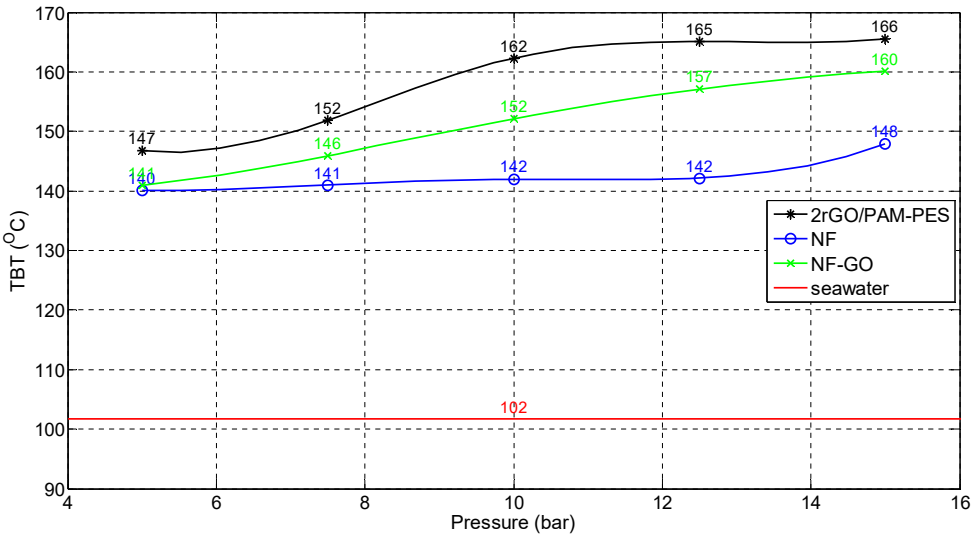

Figure 5-9: Effect of pressure on top brine temperature

CHAPTER 6

CONCLUSIONS AND FUTURE WORK

This thesis comprehensively examines the synthesis of graphene oxide (GO)/ polyacrylamide (PAM) over polyether sulfone (PES) membranes as a substrate to be used as a pretreatment step for thermal seawater desalination application. GO/PAM-PES membranes were prepared via spin coating technique then reduced to 2rGO/PAM-PES by subjecting the membrane to hydrogen iodide (HI).

The use of positively charged polyacrylamide (PAM) as an adhesive layer on PES membrane surface has further improved GO and rGO stability on PES membrane surface compared to polyethylenimine (PEI). The results showed that the spin coating yields better results for both rejection and permeate flux. It was shown that using reduced graphene oxide (rGO) instead of GO increased ion rejection. There is no need to do more than 2 depositions of GO since increasing number of depositions decreases the flux and has a small effect on the rejection. The effects of HI temperature and reduction time on the ion rejection and permeate flux were investigated diffusion test and the results showed that the rejection increased with increasing the reduction time, this is due to decreasing the interlayer spacing. Increasing the HI temperature will increase the rate of reduction.

2rGO/PAM-PES membrane subjected to HI vapor for 45min at 80ºC, commercial Nanofiltration (NF270), and NF-GO membrane were tested in a cross flow arrangement with $MgSO_4$, $CaSO_4$ and seawater. The difference between NF-GO and 2rGO/PAM-PES membrane is that GO on the NF 270 is to enhance the antifouling and antibacterial

properties while the NF270 is the selective layer. However, for 2rGO/PAM-PES membrane, the rGO is the active selective layer beside its high antifouling and antibacterial properties.

Increasing pressure will increase both the rejection and the permeate flux. Using seawater, 2rGO/PAM-PES yields the highest rejection for Mg and Ca ions compared with commercial Nanofiltration membrane (NF270). 2rGO/PAM-PES had almost the same rejection for Mg^{2+} and Ca^{2+} ions, while SO_4^{2-} ions had higher rejection this due electrostatic interaction as the GO and SO_4^{2-} ions are negatively charged. However, at high pressure the Mg^{2+}, Ca^{2+} and SO_4^{2-} ions had almost the rejection. The low rejection for Ca^{2+} ions using NF270 is due to the concentration polarization, where high Ca^{2+} concentration in the layer near the membrane surface, thus more Ca^{2+} ions tend to diffuse through the membrane. Using this treatment increases TBT to 148ºC using NF, 160ºC using NF-GO and 166ºC using rGO membrane.

Future work should focus on studying membrane inorganic and organic fouling. Whereas, more intensive and critical investigations of synthesize 2rGO/PAM-PES membrane are required to improve and optimize the effectiveness of membrane. Additionally, investigate experimentally the 2rGO/PAM-PES as a pretreatment for MSF or MED. rGO-based pretreatments can provide the optimum feed water quality, which will make the desalting process more energy efficient and result in reduced costs of fresh water.

Reference

[1] "Desalination by the Numbers | IDA." [Online]. Available: http://idadesal.org/desalination-101/desalination-by-the-numbers/. [Accessed: 11-Mar-2017].

[2] H. T. El-Dessouky and H. M. Ettouney, *Fundamentals of Salt Water Desalination*, vol. 1. 2002.

[3] N. Voutchkov, *Desalination Engineering Planning and Design*, no. 9. 2013.

[4] J. Cotruvo, N. Voutchkov, J. Fawell, P. Payment, D. Cunliffe, and S. Lattemann, *Desalination Technology Health and Environmental impacts*. 2010.

[5] A. AlTaee, A. Mabrouk, and K. Bourouni, "A novel Forward osmosis membrane pretreatment of seawater for thermal desalination processes," *Desalination*, vol. 326, pp. 19–29, 2013.

[6] M.-H. E.Y., *Physical Chemistry (Book II). – M.: Foreign literature Press*. 1962.

[7] B. Zhu, Z. Hong, N. Milne, C. M. Doherty, L. Zou, Y. S. Lin, A. J. Hill, X. Gu, and M. Duke, "Desalination of seawater ion complexes by MFI-type zeolite membranes: Temperature and long term stability," *J. Memb. Sci.*, vol. 453, pp. 126–135, 2014.

[8] O. Bakajin, A. Noy, F. Fornasiero, H. G. Park, J. K. Holt, and S. Kim, "Membranes with functionalized carbon nanotube pores for selective transport," 2011.

[9] K. Xu, B. Feng, C. Zhou, and A. Huang, "Synthesis of highly stable graphene oxide membranes on polydopamine functionalized supports for seawater desalination,"

Chem. Eng. Sci., vol. 146, pp. 159–165, 2016.

[10] A. G. Volkov, S. Paula, and D. W. Deamer, "Two mechanisms of permeation of small neutral molecules and hydrated ions across phospholipid bilayers," *Bioelectrochemistry Bioenerg.*, vol. 42, no. 2, pp. 153–160, 1997.

[11] L. K. Wang, jiaping P. Chen, Y.-T. Hung, and N. K. Shammas, *Membrane and Desalination Technologies*, vol. 13, no. 9. 2011.

[12] WHO, "Total dissolved solids in Drinking-water Background document for development of," *Heal. criteria other Support. Inf.*, vol. 2, p. 8, 1996.

[13] H. Li, Z. Song, X. Zhang, Y. Huang, S. Li, Y. Mao, H. J. Ploehn, Y. Bao, and M. Yu, "Ultrathin, molecular-sieving graphene oxide membranes for selective hydrogen separation.," *Science*, vol. 342, no. 6154, pp. 95–8, Oct. 2013.

[14] C. Lee, X. Wei, J. W. Kysar, and J. Hone, "Measurement of the elastic properties and intrinsic strength of monolayer graphene.," *Science*, vol. 321, no. 5887, pp. 385–8, Jul. 2008.

[15] D. A. Dikin, S. Stankovich, E. J. Zimney, R. D. Piner, G. H. B. Dommett, G. Evmenenko, S. T. Nguyen, and R. S. Ruoff, "Preparation and characterization of graphene oxide paper.," *Nature*, vol. 448, no. 7152, pp. 457–60, Jul. 2007.

[16] S. Chen, L. Brown, M. Levendorf, W. Cai, S.-Y. Ju, J. Edgeworth, X. Li, C. W. Magnuson, A. Velamakanni, R. D. Piner, J. Kang, J. Park, and R. S. Ruoff, "Oxidation resistance of graphene-coated Cu and Cu/Ni alloy.," *ACS Nano*, vol. 5, no. 2, pp. 1321–7, Feb. 2011.

[17] S. Bano, A. Mahmood, S.-J. Kim, and K.-H. Lee, “Graphene oxide modified polyamide nanofiltration membrane with improved flux and antifouling properties,” *J. Mater. Chem. A*, vol. 3, no. 5, pp. 2065–2071, 2015.

[18] A. Altaee, G. Zaragoza, and H. R. van Tonningen, “Comparison between Forward Osmosis-Reverse Osmosis and Reverse Osmosis processes for seawater desalination,” *Desalination*, vol. 336, pp. 50–57, 2014.

[19] W. H. Jr and R. Offeman, “Preparation of graphitic oxide,” *J. Am. Chem.*, 1958.

[20] A. Aghigh, V. Alizadeh, H. Y. Wong, M. S. Islam, N. Amin, and M. Zaman, “Recent advances in utilization of graphene for filtration and desalination of water: A review,” *Desalination*, vol. 365, pp. 389–397, 2015.

[21] N. Hilal, H. Al-Zoubi, N. a. Darwish, a. W. Mohammad, and M. Abu Arabi, “A comprehensive review of nanofiltration membranes: Treatment, pretreatment, modelling, and atomic force microscopy,” *Desalination*, vol. 170, pp. 281–308, 2004.

[22] a. W. Mohammad, Y. H. Teow, W. L. Ang, Y. T. Chung, D. L. Oatley-Radcliffe, and N. Hilal, “Nanofiltration membranes review: Recent advances and future prospects,” *Desalination*, vol. 356, pp. 226–254, 2015.

[23] B. Van der Bruggen, M. Mänttäri, and M. Nyström, “Drawbacks of applying nanofiltration and how to avoid them: A review,” *Sep. Purif. Technol.*, vol. 63, pp. 251–263, 2008.

[24] J. Luo and Y. Wan, “Effects of pH and salt on nanofiltration-a critical review,” *J.*

Memb. Sci., vol. 438, pp. 18–28, 2013.

[25] D. Zhou, L. Zhu, Y. Fu, M. Zhu, and L. Xue, "Development of lower cost seawater desalination processes using nano filtration technologies — A review," *Desalination*, vol. 376, no. 1219, pp. 109–116, 2015.

[26] L. Llenas, X. Martínez-Lladó, A. Yaroshchuk, M. Rovira, and J. de Pablo, "Nanofiltration as pretreatment for scale prevention in seawater reverse osmosis desalination," *Desalin. Water Treat.*, vol. 36, no. September, pp. 310–318, 2011.

[27] L. Llenas, G. Ribera, X. Martínez-Lladó, M. Rovira, and J. de Pablo, "Selection of nanofiltration membranes as pretreatment for scaling prevention in SWRO using real seawater," *Desalin. Water Treat.*, vol. 51, no. September, pp. 930–935, 2013.

[28] N. Hilal, H. Al-Zoubi, a. W. Mohammad, and N. a. Darwish, "Nanofiltration of highly concentrated salt solutions up to seawater salinity," *Desalination*, vol. 184, no. May, pp. 315–326, 2005.

[29] B. E. Ryabchikov, a. a. Panteleev, and M. G. Gladush, "Performance testing of seawater desalination by nanofiltration," *Pet. Chem.*, vol. 52, no. 7, pp. 465–474, 2012.

[30] A. Pérez-González, R. Ibáñez, P. Gómez, a. M. Urtiaga, I. Ortiz, and J. a. Irabien, "Nanofiltration separation of polyvalent and monovalent anions in desalination brines," *J. Memb. Sci.*, vol. 473, pp. 16–27, 2015.

[31] A. A. Izadpanah and A. Javidnia, "The Ability of a Nanofiltration Membrane to Remove Hardness and Ions from Diluted Seawater," *Water*, vol. 4, pp. 283–294,

2012.

[32] C. J. Harrison, Y. a. Le Gouellec, R. C. Cheng, and A. E. Childress, "Bench-Scale Testing of Nanofiltration for Seawater Desalination," *J. Environ. Eng.*, vol. 133, no. November, pp. 1004–1014, 2007.

[33] J. Liu, L. Xie, Z. Wang, and J. Yuan, "Dual-stage nanofiltration seawater desalination: water quality, scaling and energy consumption," *Desalin. Water Treat.*, vol. 52, no. 1–3, pp. 134–144, 2014.

[34] J. Kaewsuk, D. Y. Lee, T. S. Lee, and G. T. Seo, "Effect of ion composition on nanofiltration rejection for desalination pretreatment," *Desalin. Water Treat.*, vol. 43, no. 1–3, pp. 260–266, 2012.

[35] J. Liu, J. Yuan, L. Xie, and Z. Ji, "Exergy analysis of dual-stage nanofiltration seawater desalination," *Energy*, vol. 62, pp. 248–254, 2013.

[36] A. AlTaee and A. O. Sharif, "Alternative design to dual stage NF seawater desalination using high rejection brackish water membranes," *Desalination*, vol. 273, no. 2–3, pp. 391–397, 2011.

[37] Diem Xuan Vuong, "Two stage nanofiltration seawater desalination system," 2006.

[38] A. Al-Rawajfeh, "Influence of nanofiltration pretreatment on scale deposition in multi-stage flash thermal desalination plants," *Therm. Sci.*, vol. 15, no. 1, pp. 55–65, 2011.

[39] Y. Song, B. Su, X. Gao, and C. Gao, "The performance of polyamide nano fi ltration membrane for long-term operation in an integrated membrane seawater pretreatment

system," *Desalination*, vol. 296, pp. 30–36, 2012.

[40] C. Kaya, G. Sert, N. Kabay, M. Arda, M. Yüksel, and Ö. Egemen, "Pre-treatment with nanofiltration (NF) in seawater desalination—Preliminary integrated membrane tests in Urla, Turkey," *Desalination*, vol. 369, pp. 10–17, 2015.

[41] Y. Song, X. Gao, and C. Gao, "Evaluation of scaling potential in a pilot-scale NF-SWRO integrated seawater desalination system," *J. Memb. Sci.*, vol. 443, pp. 201–209, 2013.

[42] Leon Awerbuch, "Water desalination process using ion selective membranes," 2006.

[43] M. a K. Al-Sofi, a M. Hassan, G. M. Mustafa, a G. I. Dalvi, and M. N. M. Kither, "Nanofiltration as a means of achieving higher TBT of >120°C in MSF," *Desalination*, vol. 118, no. September 1998, pp. 123–129, 1998.

[44] a M. Hassan, M. a K. Al-sofi, a M. Farooque, a. G. I. Dalvi, a T. M. Jamaluddin, N. M. Kither, a. S. Al-Amoudi, and I. a. R. Al-Tisan, "a Nano Filtration (Nf) Membrane Pretreatment of Swro Feed and Msf Make-Up," *Desalination*, vol. 118, pp. 35–51, 1998.

[45] a. M. Hassan, M. a K. Al-Sofi, a. S. Al-Amoudi, a. T. M. Jamaluddin, a. M. Farooque, a. Rowaili, a. G. I. Dalvi, N. M. Kither, G. M. Mustafa, and I. a R. Al-Tisan, "A new approach to membrane and thermal seawater desalination processes using nanofiltration membranes (Part 1)," *Desalination*, vol. 118, no. 1998, pp. 35–51, 1998.

[46] K. B.- Osman Ahmed Hamed, Ghulam M. Mustafa, Khalid Al-Shail, A. A.-R. Mardouf, Hamed Al-Washmi, Ata M. Hassan, and and S. Al-Sulami, "A Nanofiltration Membrane Pretreatment OF SWRO FEED & MSF MAKE-UP."

[47] O. a. Hamed, A. M. Hassan, K. Al-Shail, and M. a. Farooque, "Performance analysis of a trihybrid NF/RO/MSF desalination plant," *Desalin. Water Treat.*, vol. 1, no. October, pp. 215–222, 2009.

[48] A. M. Hassan, "Fully integrated NF-thermal seawater desalination process and equipment therefor," 2006.

[49] O. a. Hamed, "Overview of hybrid desalination systems - Current status and future prospects," *Desalination*, vol. 186, no. 1–3, pp. 207–214, 2005.

[50] "http://www.dow.com/en-us/water-and-process-solutions/products#q=%20," *Dow Chemicals Company*. .

[51] "http://www.kochmembrane.com/," *Koch Membrane*. .

[52] Hydranautics NITTO DENKO Company, "http://www.membranes.com/." .

[53] "http://www.alfalaval.com/," *Alfa Laval company*. .

[54] C. Company, "Product Specification Sheet / Model NE4040-90."

[55] B. Su, T. Wu, Z. Li, X. Cong, X. Gao, and C. Gao, "Pilot study of seawater nanofiltration softening technology based on integrated membrane system," *Desalination*, vol. 368, pp. 193–201, 2015.

[56] A. E. Al-Rawajfeh, "Hybrid salts precipitation-nanofiltration pretreatment of MSF

and RO seawater desalination feed," *Membr. Water Treat.*, vol. 3, no. 4, pp. 253–266, 2012.

[57] A. E. Al-rawajfeh and H. E. S. Fath, "Integrated Salts Precipitation and Nano-Filtration as Pretreatment of Multistage Flash Desalination System and Nano-Filtration as Pretreatment of Multistage Flash Desalination," *Heat Transf. Eng.*, no. October 2015, 2012.

[58] N. Hilal, V. Kochkodan, H. Al, S. Mandale, and S. A. Al-jlil, "A combined ion exchange – nano fi ltration process for water desalination : I . sulphate – chloride ion-exchange in saline solutions," *Desalination*, vol. 363, pp. 44–50, 2015.

[59] N. Hilal, V. Kochkodan, H. Al, and D. Johnson, "A combined ion exchange – nano fi ltration process for water desalination : II . Membrane selection," *Desalination*, vol. 363, pp. 51–57, 2015.

[60] N. Hilal, V. Kochkodan, H. Al, S. Mandale, and S. A. Al-jlil, "A combined ion exchange – nano fi ltration process for water desalination : III . Pilot scale studies," *Desalination*, vol. 363, pp. 58–63, 2015.

[61] S. Sarkar and A. K. SenGupta, "A new hybrid ion exchange-nanofiltration (HIX-NF) separation process for energy-efficient desalination: Process concept and laboratory evaluation," *J. Memb. Sci.*, vol. 324, no. 1–2, pp. 76–84, 2008.

[62] S. Sarkar and A. K. SenGupta, "A hybrid ion exchange-nanofiltration (HIX-NF) process for energy efficient desalination of brackish/seawater," *Water Sci. Technol. Water Supply*, vol. 9, no. 4, pp. 369–377, Oct. 2009.

[63] A. K. SenGupta and S. Sarkar, “United States Patent ,US 7,901,577 B2,” 2011.

[64] C. H. Tan and H. Y. Ng, “A novel hybrid forward osmosis - nanofiltration (FO-NF) process for seawater desalination: Draw solution selection and system configuration,” *Desalin. Water Treat.*, vol. 13, no. 1–3, pp. 356–361, 2010.

[65] S. Zhao, L. Zou, and D. Mulcahy, “Brackish water desalination by a hybrid forward osmosis–nanofiltration system using divalent draw solute,” *Desalination*, vol. 284, pp. 175–181, 2012.

[66] S. Phuntsho, S. Hong, M. Elimelech, and H. K. Shon, “Forward osmosis desalination of brackish groundwater: Meeting water quality requirements for fertigation by integrating nanofiltration,” *J. Memb. Sci.*, vol. 436, pp. 1–15, 2013.

[67] A. Altaee and N. Hilal, “High recovery rate NF-FO-RO hybrid system for inland brackish water treatment,” *Desalination*, vol. 363, pp. 19–25, 2015.

[68] A. A. Al-hajouri, A. S. Al-amoudi, A. M. Farooque, A. S. Al-amoudi, and A. M. Farooque, “Long term experience in the operation of nanofiltration pretreatment unit for seawater desalination at SWCC SWRO plant,” *Desalin. Water Treat.*, vol. 3994, no. September, 2015.

[69] “ROSA Software | Dow Water & Process Solutions.” [Online]. Available: http://www.dow.com/en-us/water-and-process-solutions/resources/design-software/rosa-software. [Accessed: 24-Feb-2017].

[70] E. Drioli, F. Laganà, a. Criscuoli, and G. Barbieri, “Integrated membrane operations in desalination processes,” *Desalination*, vol. 122, pp. 141–145, 1999.

[71] E. El-Zanati and K. M. El-Khatib, “Integrated membrane -based desalination system,” *Desalination*, vol. 205, no. May 2006, pp. 15–25, 2007.

[72] A. N. A. Mabrouk and H. E. S. Fath, “Experimental study of high-performance hybrid NF-MSF desalination pilot test unit driven by renewable energy,” *Desalin. Water Treat.*, vol. 51, no. 37–39, pp. 6895–6904, 2013.

[73] A. E. Al-Rawajfeh, “Nanofiltration pretreatment as CO2 deaerator of desalination feed: CO2 release reduction in MSF distillers,” *Desalination*, vol. 380, pp. 12–17, 2016.

[74] M. Turek and M. Chorazewska, “Nanofiltration process for seawater desalination-salt production integrated system,” *Desalin. Water Treat.*, vol. 7, no. November, p. 178–181 ST–Nanofiltration process for seawater, 2009.

[75] E. Curcio, X. Ji, A. M. Quazi, S. Barghi, G. Di Profio, E. Fontananova, T. Macleod, and E. Drioli, “Hybrid nanofiltration-membrane crystallization system for the treatment of sulfate wastes,” *J. Memb. Sci.*, vol. 360, no. 1–2, pp. 493–498, 2010.

[76] E. Drioli, E. Curcio, G. Di Profio, F. Macedonio, and A. Criscuoli, “Integrating Membrane Contactors Technology and Pressure-Driven Membrane Operations for Seawater Desalination,” *Chem. Eng. Res. Des.*, vol. 84, no. 3, pp. 209–220, 2006.

[77] A. Altaee and G. Zaragoza, “A conceptual design of low fouling and high recovery FO–MSF desalination plant,” *Desalination*, vol. 343, pp. 2–7, 2014.

[78] A. Altaee, A. Mabrouk, K. Bourouni, and P. Palenzuela, “Forward osmosis pretreatment of seawater to thermal desalination: High temperature FO-MSF/MED

hybrid system," *Desalination*, vol. 339, no. 1, pp. 18–25, 2014.

[79] M. Darwish, A. Hassan, A. N. Mabrouk, H. Abdulrahim, and A. Sharif, "Viability of integrating forward osmosis (FO) as pretreatment for existing MSF desalting unit," *Desalin. Water Treat.*, vol. 3994, no. November, pp. 1–11, 2015.

[80] A. E. Al-rawajfeh, "Prevention of scale deposits in desalination: pre-treatment of feed seawater by salts precipitation," pp. 1–4.

[81] G. M. Ayoub, R. M. Zayyat, and M. Al-hindi, "Precipitation softening : a pretreatment process for seawater desalination," *Env. Sci Pollut Res*, pp. 2876–2887, 2014.

[82] B. R. Constantz, K. Farsad, and M. Fernandez, "Desalination methods and systems that include carbonate compound precipitation," 2011.

[83] A. L. Ahmad, M. F. Chong, and S. Bhatia, "Mathematical modeling and simulation of the multiple solutes system for nanofiltration process," *J. Memb. Sci.*, vol. 253, no. 1–2, pp. 103–115, 2005.

[84] Z. V. P. Murthy and S. K. Gupta, "Estimation of mass transfer coefficient using a combined nonlinear membrane transport and film theory model," *Desalination*, vol. 109, no. 1, pp. 39–49, 1997.

[85] A. Nora'aini and M. A. Wahab, "The Development Of Predictive Modeling Of Nanofiltration Membrane Properties : A Review," *Reg. Symp. Membr. Sci. Technol.*, p. 15, 2004.

[86] D. L. Oatley-Radcliffe, S. R. Williams, M. S. Barrow, and P. M. Williams, "Critical

appraisal of current nanofiltration modelling strategies for seawater desalination and further insights on dielectric exclusion," *Desalination*, vol. 343, pp. 154–161, 2014.

[87] J. Garcia-Aleman and J. M. Dickson, "Mathematical modeling of nanofiltration membranes with mixed electrolyte solutions," *J. Memb. Sci.*, vol. 235, no. 1–2, pp. 1–13, 2004.

[88] A. W. Mohammad, L. Y. Pei, and A. A. H. Kadhum, "Characterization and identification of rejection mechanisms in nanofiltration membranes using extended Nernst – Planck model," *Clean Tech Env. Policy*, vol. 4, pp. 151–156, 2002.

[89] Y. Roy, M. H. Sharqawy, and J. H. Lienhard, "Modeling of flat-sheet and spiral-wound nanofiltration configurations and its application in seawater nanofiltration," *J. Memb. Sci.*, vol. 493, pp. 360–372, 2015.

[90] S. Bandini and D. Vezzani, "Nanofiltration modeling: The role of dielectric exclusion in membrane characterization," *Chem. Eng. Sci.*, vol. 58, no. 15, pp. 3303–3326, 2003.

[91] A. Szymczyk, C. Labbez, P. Fievet, A. Vidonne, A. Foissy, and J. Pagetti, "Contribution of convection, diffusion and migration to electrolyte transport through nanofiltration membranes," *Adv. Colloid Interface Sci.*, vol. 103, no. 1, pp. 77–94, 2003.

[92] N. M. Sidek, S. Fauziah, S. Draman, and I. Abdullah, "Prediction of Nanofiltration Membrane Performance : Analysis of Ion Transport Mechanisms," *Asian Res. Publ. Netw.*, vol. 10, no. 1, pp. 337–342, 2015.

[93] J. Fang and B. Deng, “Rejection and modeling of arsenate by nanofiltration: Contributions of convection, diffusion and electromigration to arsenic transport,” *J. Memb. Sci.*, vol. 453, pp. 42–51, 2014.

[94] J. F. Lapointe, S. F. Gauthier, Y. Pouliot, and C. Bouchard, “Fouling of a nanofiltration membrane by a Beta-lactoglobulin tryptic hydrolysate: Impact on the membrane sieving and electrostatic properties,” *J. Memb. Sci.*, vol. 253, no. 1–2, pp. 89–102, 2005.

[95] T. Thorsen, “Concentration polarisation by natural organic matter (NOM) in NF and UF,” *J. Memb. Sci.*, vol. 233, no. 1–2, pp. 79–91, 2004.

[96] F. Long, A. Zhu, X. L. Wang, and W. P. Zhu, “Membrane flux and CaCO3 crystallization in the unstirred dead-end nanofiltration of magnetic solution,” *Desalination*, vol. 186, no. 1–3, pp. 243–254, 2005.

[97] F. Beyer, B. M. Rietman, A. Zwijnenburg, P. van den Brink, J. S. Vrouwenvelder, M. Jarzembowska, J. Laurinonyte, A. J. M. Stams, and C. M. Plugge, “Long-term performance and fouling analysis of full-scale direct nanofiltration (NF) installations treating anoxic groundwater,” *J. Memb. Sci.*, vol. 468, pp. 339–348, 2014.

[98] A. M. Farooque, A. S. Al-amoudi, and A. M. Hassan, “Chemical Cleaning Experiments for Performance Restoration of Nf Membranes Operated on Seawater Feed 1.”

[99] J. R. V Flora, “Stochastic approach to modeling surface fouling of ultrafiltration

membranes," *J. Memb. Sci.*, vol. 76, pp. 85–88, 1993.

[100] A. S. Al-Amoudi and a. M. Farooque, "Performance restoration and autopsy of NF membranes used in seawater pretreatment," *Desalination*, vol. 178, no. 1–3 SPEC. ISS., pp. 261–271, 2005.

[101] A. Al-amoudi and R. W. Lovitt, "Fouling strategies and the cleaning system of NF membranes and factors affecting cleaning efficiency," *J. Memb. Sci.*, vol. 303, pp. 4–28, 2007.

[102] A. S. Al-Amoudi, "Factors affecting natural organic matter (NOM) and scaling fouling in NF membranes: A review," *Desalination*, vol. 259, no. 1–3, pp. 1–10, 2010.

[103] A. Matin, Z. Khan, S. M. J. Zaidi, and M. C. Boyce, "Biofouling in reverse osmosis membranes for seawater desalination: Phenomena and prevention," *Desalination*, vol. 281, no. 1, pp. 1–16, 2011.

[104] Q. Huang and W. Ma, "A model of estimating scaling potential in reverse osmosis and nanofiltration systems," *Desalination*, vol. 288, pp. 40–46, 2012.

[105] F. Faridirad, Z. Zourmand, N. Kasiri, M. Kazemi Moghaddam, and T. Mohammadi, "Modeling of suspension fouling in nanofiltration," *Desalination*, vol. 346, pp. 80–90, 2014.

[106] C.-J. Lin, S. Shirazi, P. Rao, and S. Agarwal, "Effects of operational parameters on cake formation of CaSO4 in nanofiltration," *Water Res.*, vol. 40, no. 4, pp. 806–816, 2006.

[107] S. Lee, J. Kim, and C. H. Lee, “Analysis of CaSO4 scale formation mechanism in various nanofiltration modules,” *J. Memb. Sci.*, vol. 163, no. 1, pp. 63–74, 1999.

[108] S. Lee and C. H. Lee, “Effect of operating conditions on CaSO4 scale formation mechanism in nanofiltration for water softening,” *Water Res.*, vol. 34, no. 15, pp. 3854–3866, 2000.

[109] E. M. Vrijenhoek, S. Hong, and M. Elimelech, “Influence of membrane surface properties on initial rate of colloidal fouling of reverse osmosis and nanofiltration membranes,” *J. Memb. Sci.*, vol. 188, no. 1, pp. 115–128, 2001.

[110] R. Sheikholeslami, “Mixed salts—scaling limits and propensity,” *Desalination*, vol. 154, no. 2, pp. 117–127, 2003.

[111] N. Her, G. Amy, and C. Jarusutthirak, “Seasonal variations of nanofiltration (NF) foulants: identification and control.,” *Desalination*, vol. 132, no. 1–3, pp. 143–160, 2000.

[112] N. Andritsos, M. Kontopoulou, A. J. Karabelas, and P. G. Koutsoukos, “Calcium carbonate deposit formation under isothermal conditions,” *Can. J. Chem. Eng.*, vol. 74, no. 6, pp. 911–919, 1996.

[113] C. Hobbs, S. Hong, and J. Taylor, “Effect of surface roughness on fouling of RO and NF membranes during filtration of a high organic surficial groundwater,” *J. Water Supply Res. Technol.*, vol. 55, pp. 559–570, 2006.

[114] M. E. A. Ali, L. Wang, X. Wang, and X. Feng, “Thin film composite membranes embedded with graphene oxide for water desalination,” *Desalination*, vol. 386, pp.

67–76, 2016.

[115] H. R. Chae, J. Lee, C. H. Lee, I. C. Kim, and P. K. Park, “Graphene oxide-embedded thin-film composite reverse osmosis membrane with high flux, anti-biofouling, and chlorine resistance,” *J. Memb. Sci.*, vol. 483, pp. 128–135, 2015.

[116] M. E. A. Ali, L. Wang, X. Wang, and X. Feng, “Thin film composite membranes embedded with graphene oxide for water desalination,” *Desalination*, vol. 386, pp. 67–76, 2016.

[117] S. G. S. H. Kim, D. H. Hyeon, J. H. Chun, and B.-H. Chun, “Novel thin nanocomposite RO membranes for chlorine resistance,” *Desalin. Water Treat.*, vol. 51, no. March 2015, pp. 6338–6345, 2013.

[118] S. Bano, A. Mahmood, S. J. Kim, and K. H. Lee, “Graphene oxide modified polyamide nanofiltration membrane with improved flux and antifouling properties,” *J. Mater. Chem. A*, vol. 3, no. 5, pp. 2065–2071, 2015.

[119] W. Choi, J. Choi, J. Bang, and J. Lee, “Layer-by-Layer Assembly of Graphene Oxide Nanosheets on Polyamide Membranes for Durable Reverse Osmosis Applications,” *ACS Appl. Mater. Interfaces*, p. Ahead of Print, 2013.

[120] M. Safarpour, A. Khataee, and V. Vatanpour, “Thin film nanocomposite reverse osmosis membrane modified by reduced graphene oxide/TiO<inf>2</inf> with improved desalination performance,” *J. Memb. Sci.*, vol. 489, pp. 43–54, 2015.

[121] “Sterlitech.” [Online]. Available: http://www.sterlitech.com/. [Accessed: 11-Mar-2017].

[122] “The DOW Chemical Company - Home.” [Online]. Available: http://www.dow.com/. [Accessed: 11-Mar-2017].

[123] “PolyScience | Remarkably Responsive Temperature Control Solutions.” [Online]. Available: https://www.polyscience.com/. [Accessed: 11-Mar-2017].

[124] “Laboratory Chemicals, Lab Chemicals, Analytical Reagents, Laboratory Reagents, Lab Reagents, and Fine Chemicals from Loba Chemie Pvt. Ltd., Mumbai, India.” [Online]. Available: http://www.lobachemie.com/. [Accessed: 11-Mar-2017].

[125] “Milli-Q® Integral Water Purification System for Ultrapure Water - Milli-Q.” [Online]. Available: http://www.merckmillipore.com/INTL/en/product/Sistema-de-purificación-de-agua-Milli-Q-Integral,MM_NF-C72876?ReferrerURL=https%3A%2F%2Fwww.google.com.sa%2F&bd=1. [Accessed: 11-Mar-2017].

[126] “G3 Spin Coater – Specialty Coating Systems.” [Online]. Available: https://scscoatings.com/equipment/spin-coating-systems/g3-spin-coaters/. [Accessed: 11-Mar-2017].

[127] “EP357 Conductivity isoPod^{TM}: eDAQ - Instruments for Electrochemistry Chromatography Electrophoresis Conductivity pH Biosensors.” [Online]. Available: https://www.edaq.com/EP357_Conductivity-isoPod^{TM}-. [Accessed: 17-Mar-2017].

[128] “Side-Bi-Side Cells - PermeGear.” [Online]. Available: http://permegear.com/side-bi-side-cells/. [Accessed: 17-Mar-2017].

[129] “Eldex Optos Series Pumps, Model 2 by Eldex Laboritories.” [Online]. Available: http://eldex.com/products/optos-series/model-2-high-pressure-liquid-metering-pump/. [Accessed: 17-Mar-2017].

[130] S. Yu, N. Li, D. Higgins, D. Li, Q. Li, H. Xu, J. Spendelow, and G. Wu, “Self-Assembled Reduced Graphene Oxide / Polyacrylamide Conductive Composite Films Self-Assembled Reduced Graphene Oxide / Polyacrylamide Conductive Composite Films,” 2014.

[131] O. A. O. Alameen, “Graphene Oxide based membrane for water purification,” KFUPM, 2017.

Vitae

Name	Bassel Alaa Awad Taha Abdelkader
Nationality	Egyptian
Date of Birth	15/05/1989
Email	abdelkaderbassel@gmail.com
Mobile Number	+201289122614
Permanent Address	240 District ¾, New Cairo, Cairo, Egypt
Academic Background	M.S. in Mechanical Engineering May, 2017 KFUPM, Saudi Arabia. B.S. in Aeronautical Engineering June, 2011 Institute of Aviation Engineering & Technology, Egypt